RAYLEIGH - BRILLOUIN LIGHT SCATTERING IN LIQUID SILICONES

Dissertation for the Degree of Ph. D.
MICHIGAN STATE UNIVERSITY
ANIL KUMAR
1973

LIBA.
Michigan Santa

This is to certify that the

thesis entitled

Rayleigh-Brillouin Light Scattering. in Liquid Silicones

presented by

Anil Kumar

has been accepted towards fulfillment of the requirements for

Ph.D. degree in Mechanics

Major pro

Date 9 Navi

0-7639

41:0414

Rayleid technique to chain and respond to the chain and the chain a

It was increased whad a tende

weights ran

different t

^{and} were in

Propagating

ABSTRACT

RAYLEIGH-BRILLOUIN LIGHT SCATTERING IN LIQUID SILICONES

by

ANIL KUMAR

Rayleigh and Brillouin light scattering was used as an experimental technique to determine light scattering and acoustical properties of chain and ring dimethylsiloxanes. The properties determined were the Brillouin shift, sound velocity, adiabatic compressibility, Brillouin linewidth, sonic absorption co-efficient, Landau-Placzek ratio and depolarization ratio. Fluctuation theory and the linearized hydrodynamical equations of Mountain were used to arrive at numerical values. Refractive indices were also measured where required. Nine silicones with molecular-weights ranging from 160 to 7,000, were examined spectrometrically at ten different temperatures falling between 20° and 80°C.

It was observed that, as molecular chains lengthened, sound velocity increased while adiabatic compressibility decreased. Sound velocities had a tendency to level off in the region of higher molecular weights, and were in good agreement with ultrasonic measurements in the MHz range. Propagating hypersonic waves died out in a distance of about 50,000 Å,

roughly ten
Values of th

The Lan

nolecular we ing temperat close to the liquids. Tr

D₅ was inve

Determi depolarized

more isotro;

roughly ten times the wavelength of the incident green light (5145 $\mathring{\text{A}}$). Values of the adiabatic compressibility were unusually high for all silicones.

The Landau-Placzek ratio was found always to increase with increasing molecular weight, but in every case to decrease monotonically with increasing temperature. These values were strikingly low (0.2 to 2.0) and were close to the values obtained for water and other low molecular weight liquids. The spectral distribution of the scattered light from MD₇M and D₅ was investigated in the frequency range 2 x 10^9 Hz to 5 x 10^9 Hz, but no sound velocity dispersion was detected.

Determination of the depolarization ratio, ρ_V , from polarized and depolarized measurements established that linear silicone samples were more isotropic than cyclic silicone samples at the same molecular weight.

RAYLEIGH-BRILLOUIN LIGHT SCATTERING IN LIQUID SILICONES

bу

Anil Kumar

A DISSERTATION

Submitted to
Michigan State University
in partial fulfillment of the requirements
for the degree of

DOCTOR OF PHILOSOPHY

Department of Metallurgy, Mechanics and Materials Science

G

TO MY PARENTS

Shri and Smt. H. Prasad

I want his counsel, acting as my tion to Pro-

at Michigan especially

the equipme

Appres

at Michigar

اد Beverl

The fi

ACKNOWLEDGEMENT

I want to express my deep appreciation to Professor T. Triffet for his counsel, patience and active interest in this work as well as for acting as my major Professor. I also want to extend my sincere appreciation to Professor J. B. Kinsinger, Chairman of the Chemistry Department at Michigan State University, for his guidance and encouragement, and especially for letting me make use of departmental facilities, including the equipment without which this work would not have been possible.

Appreciation is also extended to Professor D. J. Montgomery for valuable suggestions, Mrs. Shukla Sinha of the Department of Philosophy at Michigan State University for help in numerical calculations and Ms. Beverly Anderson for typing the thesis.

The financial support of the Department of Metallurgy, Mechanics and Materials Science, Michigan State University is greatly appreciated.

ACKNOALEDGE

LIST OF TABL

LIST OF FIG

I INTRODU

1.

2.

II THEORY

1.

2.

3.

4.

III EXPEPI

١.

2.

3

٨

TABLE OF CONTENTS

																					Page
ACKNO	WLI	EDGE	MENTS	S				•		•			•		•				•	•	iii
LIST	0F	TABI	LES .							•		•		•			•				vi
LIST	0F	FIG	URES.						•	•		•	•	•		•			•	•	x
I	IN	rodi	UCTIO	ON						•		•	•		•			•		•	1
		1.	Gene	eral B	ac kgrc	und		•		•					•			•		•	1
		2.	Purp	ose o	f Rese	earch				•										•	3
II	THI	EORY.								•					•	•		•			5
		1.	Gene	eral C	oncept	s.	•	•		•			•		•	•		•			5
		2.	Ther	modyn	amic T	heor	у.	•		•			•		•			•	•	•	6
		3.	Fluc	tuati	on The	eory		•	•	•			•		•	•			•	•	10
		4.	Cont	tinuum	Theor	ъ.			•						•					•	15
III	EXI	PERIN	MENTA	TION					•	•					•			•			24
		1.	Samp	ole Pr	eparat	ion		•		•					•					•	24
		2.	The	Brill	ouin S	Spect	rome	ete	er	•		•	•		•	•	•		•		26
			a.	Laser				•		•							•				26
			b.	Inter	ferome	ter		•	•			•	•								28
			c.	Optic:	s			•		•			•						•		29
			d.	Align	ment.			•	•	•			•	•			•	•			30
			e.	Detec	tion a	nd R	ecor	'd i	ng				•		•		•				30
		3.	The	Tempe	rature	Con	trol	C	el	1.		•		•			•		•		31
		4.	The	Scatt	ering	Ce11	and	i t	he	Но	old	er	•					•			36

5.

IV RESULTS

١.

2.

3.

4.

5.

6.

7.

V CONCL

A XIGHBOOK

APPENDIX E

XIGNEGET

	Page
5. Refractive-Index Measurements.	37
IV RESULTS AND DISCUSSION	40
1. Variation of the Refractive-Inc	dex with
Temperature and Molecular Weigh	nt 42
2. Variation of the Brillouin-shif	ft with
Temperature and Molecular Weigh	nt 49
3. Dispersion Measurements	70
4. Velocity of Sound and Adiabatic	Compressibility 74
5. Variation of the Brillouin Line	e Width and the
Sonic Absorption Co-efficient w	vith Temperature
and Molecular Weight	87
6. Variation of the Ratio of the I	Intensities of
the Central and Shifted Peaks w	with Temperature 95
7. Depolarization Measurements	105
V CONCLUSIONS	108
BIBLIOGRAPHY	111
APPENDIX A Calculation of the Refractive-I	ndex at 5145 Å 115
APPENDIX B Variation of J_V with Temperatur	re 131
APPENDIX C Laser-Brillouin-Velocimeter	137
The Experimental Set-up	138
Discussion	139

•

Cyclic

RefractLinear

3. Refract

Linear

4. Refrac

Cyclic

5. Observ

Tempor

and Sp Funct

6. Observ

Tempo

and S

Funct

7. _{Obser}

Tempo

and S

Funct

3. Obser

Tempo

LIST OF TABLES

Tabl	e	Page
1.	Measured and Corrected Temperature Obtained during	
	Brillouin Scattering Measurements for Linear and	
	Cyclic Polydimethylsiloxanes	34
2.	Refractive-index as a Function of Temperature for	
	Linear Silicones (MMMD $_3$ M and MD $_7$ M)	43
3.	Refractive-index as a Function of Temperature for	
	Linear Silicones (D.C. 200 fluids, 100 cts. and 10^5 cts	44
4.	Refractive-index as a Function of Temperature for	
	Cyclic Silicones	45
5.	Observed Brillouin Frequency Shifts (v_B), Velocities (V_S),	
	Temporal Attenuation Co-efficients (Γ_B), Life times ($1/\Gamma_B$)	
	and Spatial Attenuation Co-efficients (α) of MM as a	
	Function of Temperature	54
6.	Observed Brillouin Frequency Shifts (v_B), Velocities (V_S),	
	Temporal Attenuation Co-efficient (Γ_B), Life times ($1/\Gamma_B$)	
	and Spatial Attenuation Co-efficient (α) of MD $_3^{M}$ as a	
	Function of Temperature	55
7.	Observed Brillouin Frequency Shifts (v_B), Velocities (V_S),	
	Temporal Attenuation Co-efficient (Γ_B), Life times ($1/\Gamma_B$)	
	and Spatial Attenuation Co-efficient (α) of MD $_7$ M as a	
	Function of Temperature	56
8.	Observed Brillouin Frequency Shifts (v_B), Velocities (V_S),	
	Temporal Attenuation Co-efficient (Γ_B), Life times ($1/\Gamma_B$)	

Table

and Sp

fluid,

9. Observ Tempor

and S;

fluid,

10. Observ

Tempor and S

Funct:

11. Observ

Tempos and S

Funct

12. Obser

Tempo

and S

Funct

13. Obser

Tempo

and S

Funct

14. Inter

Tempe

15. Inter

Temper

Tabl	e	Page
	and Spatial Attenuation Co-efficient (α) of D.C. 200	
	fluid, 100 cts. as a Function of Temperature	57
9.	Observed Brillouin Frequency Shifts (${\bf v}_{\rm B}$), Velocities (${\bf V}_{\rm S}$),	
	Temporal Attenuation Co-efficient (r_B), Life times ($1/r_B$)	
	and Spatial Attenuation Co-efficient (α) of D.C. 200	
	fluid, 10 ⁵ cts. as a Function of Temperature	58
10.	Observed Brillouin Frequency Shifts (v_B), Velocities (V_S),	
	Temporal Attenuation Co-efficient (Γ_B), Life times ($1/\Gamma_B$) and Spatial Attenuation Co-efficient (α) of D $_5$ as a	
	Function of Temperature	5 9
11.	Observed Brillouin Frequency Shifts (v_B), Velocities (V_S),	
	Temporal Attenuation Co-efficient (Γ_B), Life times ($1/\Gamma_B$)	
	and Spatial Attenuation Co-efficient (α) of D $_3$ as a	
	Function of Temperature	59
12.	Observed Brillouin Frequency Shifts (v_B), Velocities (V_S),	
	Temporal Attenuation Co-efficient (Γ_B), Life times ($1/\Gamma_B$)	
	and Spatial Attenuation Co-efficient (α) of D $_{g}$ as a	
	Function of Temperature	60
13.	Observed Brillouin Frequency Shifts (v_B), Velocities (V_S),	
	Temporal Attenuation Co-efficient (\mathbb{F}_{B}), Life times ($1/\mathbb{F}_{B}$)	
	and Spatial Attenuation Co-efficient (α) of D $_{15}$ as a	
	Function of Temperature	61
14.	Intercept and Slope for the Brillouin Half-width (r_{B}) -	
	Temperature Relationship	62
15.	Intercept and Slope for the Absorption Co-efficient -	
	Temperature Relationship	62

17. Inter

Tempe

18. Inter

Tempe

Tempe 20. Inter

Tempe

21. Inter

Tempe 22. Varia

(V_S),

(1/r_B

Placz

23. Varia

(V_S),

Placz

24. Ultra 25. A.:

25. Adiab

26. Adiat

27. Obser

of Te

Table	e	Page
16.	Intercept and Slope for the Brillouin-shift-	
	Temperature Relationship	63
17.	Intercept and Slope for the Sound Velocity -	
	Temperature Relationship	63
18.	Intercept and Slope for the Brillouin-shift -	
	Temperature Relationship	64
19.	Intercept and Slope for the Sonic Velocity -	
	Temperature Relationship	64
20.	Intercept and Slope for the Brillouin Half-width -	
	Temperature Relationship	65
21.	Intercept and Slope for the Absorption Co-efficient -	
	Temperature Relationship	65
22.	Variations in Brillouin Frequency-shifts (v_B) , Velocities	
	(V_S), Temporal Attenuation Co-efficients (Γ_B), Life-times	
	(1/ Γ_B), Spatial Attenuation Co-efficient (α) and Landau-	
	Placzek Ratio (J_v) of MD_7M with Scattering angle θ	71
23.	Variations in Brillouin Frequency-shifts (v_B), Velocities	
	(V_S), Temporal Attenuation Co-efficients (Γ_B), Life-times	
	(1/ Γ_B), Spatial Attenuation Co-efficient (α) and Landau-	
	Placzek Ratio (J_v) of D_5 with Scattering angle θ	72
24.	Ultrasonic Data	74
25.	Adiabatic Compressibility of MM, MD ₃ M, MD ₇ M, D.C.200 fluid,	
	100 cts., D ₅ , and D ₁₅ at 22°C	77
26.	Adiabatic Compressibility as a Function of Temperature	78
27.	Observed Landau-Placzek Ratio (J_V) of MM as a Function	
	of Temperature	96

Table

28. Obser

Funct

29. Obser

100 c

30. Obser of Te

31. Obser

10⁵ c 32. Obser

Funct

33. Obser

Funct

34. Obser

Funct 35. Obser

Funct

36. Inter

Scatt

37. Obser

D.C.

æ. Obser

Table	e	Page
28.	Observed Landau-Placzek Ratio (J_v) of MD $_3$ M as a	
	Function of Temperature	96
29.	Observed Landau-Placzek Ratio (J _V) of D.C. 200 fluid,	
	100 cts. as a Function of Temperature	97
30.	Observed Landau-Placzek Ratio of MD ₇ M as a Function	
	of Temperature	97
31.	Observed Landau-Placzek Ratio (J _V) of D.C. 200 fluid,	
	10^5 cts. as a Function of Temperature	9 8
32.	Observed Landau-Placzek Ratio (J_v) of D_3 as a	
	Function of Temperature	99
33.	Observed Landau-Placzek Ratio (J_v) of D_5 as a	
	Function of Temperature	99
34.	Observed Landau-Placzek Ratio (J_v) of D_g as a	
	Function of Temperature	100
35.	Observed Landau-Placzek Ratio (J_v) of D_{15} as a	
	Function of Temperature	100
36.	Intercept and Slope for the Intensity Ratio of the	
	Scattered Light (J_v) -Temperature (T_C) Relationship	101
37.	Observed depolarization Ratios for MM, MD ₃ M, MD ₇ M,	
	D.C. 200 fluids, 100 cts. and 10 ⁵ cts	106
38.	Observed Depolarization Ratios for D_3 , D_5 , D_9 and D_{15}	. 107

Figures

- 1. Class
- 2. Spect
- 3. Filtr
- 4. Rayle
- 5. Picto
- 6. Cross
- 7. Calib
- 8. Cylin
- 9. Light
- 10. Refr.
 - D.C.
- 11. Refr
- 12. Refr
 - 18 CM
- 13. Spec
- 14. Spe
- 15. Spe
- 16. Spe
- 17. Br
 - D.
- is. Br
- 13. EL
 - 140

LIST OF FIGURES

Figu	ires	Page
1.	Classical Description of Brillouin Spectra	12
2.	Spectrum for MM at 40.0°C, θ = 90° and λ_0 = 5145 Å	21
3.	Filtration Apparatus	25
4.	Rayleigh-Brillouin Spectrometer	27
5.	Pictorial View of the Temperature Control Cell	32
6.	Cross-sectional View of the Temperature Control Cell	33
7.	Calibration Data for the Temperature Control Cell	35
8.	Cylindrical and Brewster Light Scattering Cell	38
9.	Light Scattering Cell Holder	39
10.	Refractive-Index Versus Temperature for MM, MD ₃ M, MD ₇ M,	
	D.C. 200 fluids, 100 cts. and 10^5 cts	46
11.	Refractive-Index Versus Temperature for $\mathrm{D_3}$, $\mathrm{D_5}$, $\mathrm{D_9}$ and $\mathrm{D_{15}}$.	47
12.	Refractive-Index Versus Temperature for $\mathrm{D_9}$, $\mathrm{MD_7M}$, $\mathrm{D_5}$ and	
	$MD_{3}M.$	4 8
13.	Spectrum for MM at 70°C, θ = 90° and λ_0 = 5145 \mathring{A}	50
14.	Spectrum for MD ₇ M at 40°C, θ = 90° and λ_0 = 5145 Å	51
15.	Spectrum for MD ₇ M at 50°C, θ = 90° and λ_0 = 5145 Å	52
16.	Spectrum for D ₅ at 45°C, θ = 90° and λ_0 = 5145 Å	53
17.	Brillouin-shift Versus Temperature for MM, $\mathrm{MD}_3\mathrm{M}$, $\mathrm{MD}_7\mathrm{M}$,	
	D.C. 200 fluid, 10^5 cts	66
18.	Brillouin-shift Versus Temperature for D_3 , D_5 , D_9 and D_{15}	67
19.	Brillouin-shift Versus Temperature for D^9 , D^5 , MD_7M and	
	MD ₂ M	6 8

21. Brill

22. Veloc Silic

23. Veloc Silic

24. Varia MM, M

25. Varia

03, [

26. Varia

D₉,

27. Temp Mo1 e

28. Adia Weig

29. Adia

30. Hal

MD 3

31. Hal

32. 5. E Si.

33. So:

5

Figu	ıre	Page
20.	avB/aTC Versus Molecular Weight for Linear and	
	Cyclic Silicones	. 69
21.	Brillouin-shift Versus $sin(\theta/2)$ for MD_7^M and D_5	. 73
22.	Velocity of Sound Versus Molecular Weight for Linear	
	Silicones at 29.32°C, 33.88°C, 48.60°C and 58.25°C	. 79
23.	Velocity of Sound Versus Molecular Weight for Cyclic	
	Silicones at 24.75°C, 34.21°C, 38.88°C and 52.83°C	. 80
24.	Variations of the Velocity of Sound with Temperature for	
	MM, MD_3M , MD_7M and D.C. 200 fluid, 10^5 cts	. 81
25.	Variation of the Velocity of Sound with Temperature for	
	D_3 , D_5 , D_9 and D_{15}	. 82
26.	Variation of the Velocity of Sound with Temperature for	٠
	D_9 , MD_7M , MD_3M and D_5	. 83
27.	Temperature Co-efficient of the Velocity of Sound Versus	
	Molecular Weight for Linear and Cyclic Silicones	. 84
28.	Adiabatic Compressibility as a Function of Molecular	
	Weight at Constant Temperature of 22°C	. 85
29.	Adiabatic Compressibility Versus Temperature for D_9 and D_{15}	. 86
30.	Half of Brillouin Line Width Versus Temperature for MM,	
	MD ₃ M, MD ₇ M and D.C. 200 fluid,100 cts	. 90
31.	Half of Brillouin Line Width Versus Temperature for	
	D ₅ , D ₉ and D ₁₅	. 91
32.		
	Silicones	. 92
33.	Sonic Absorption Co-efficient Versus Temperature for	
	D_5 , D_0 , MD_2M and MD_7M	. 93

Figu	re	Page
34.	∂α/∂T _C Versus Molecular Weight for Linear and	
	Cyclic Silicones	94
35.	J_V Versus Temperature for D_5 , D_9 , MD_3M and MD_7M	102

1. Historic

The s

ever since t and the redn theory in 18 His theory d

isotropic pa of the incid

No expl

particles. a real liqui

order of the

density abou

light scatte

developed a

interacting

ticularly us

that are lan

as in the "L

CHAPTER I

INTRODUCTION

1. <u>Historical Background</u>.

The scattering of light has challenged the understanding of men ever since the first attempt to explain the blueness of the daytime sky and the redness of the sunset. Lord Rayleigh [1,2] developed the basic theory in 1871 and 1881, identifying the process as one of diffraction. His theory dealt only with non-interacting, transparent, optically-isotropic particles with dimensions small compared with the wavelength of the incident radiation.

No explanation was provided for effects in liquids with interdependent particles. Smoluchowski [3] suggested that the density is not uniform in a real liquid; fluctuations in the density occur over a region of the order of the wavelengths of light. At each instant a different density distribution exists and light is scattered from the fluctuations of the density about its average value. Einstein [4] calculated the amount of light scattered from these density fluctuations, and in 1908 Mie [5] developed a general electromagnetic theory of light scattering for non-interacting, spherical particles of arbitrary size. His theory is particularly useful for analyzing scattering by particles width dimensions that are large compared with the wavelengths of the incident radiation, as in the "Laser Doppler Velocimeter" application [6,7,8].

Before with the ela light. Freq in 1922 inve time, and pr acoustical w Such sh velocity of difficult. ment was poor Were not avascattering co much attention extended elas molecular we Landau a the central A Brillouin pea Miller [15] 1 dynamic argum increase the cant only in The deve Tele it possi $^{\rm Since}$ the las

collimated th

wssible. Hi

Before 1922 the theoretical work on light scattering dealt only with the elastic case and emphasized the intensity of the scattered light. Frequency dependence was completely neglected. Brillouin [9] in 1922 investigated the problem of frequency dependence for the first time, and predicted that light would be inelastically scattered by acoustical waves in a liquid and should have two Doppler-shifted peaks.

Such shifts in frequency are small and directly related to the velocity of thermal waves in the liquid; hence spectral resolution was difficult. Gross [10] did verify them, but the accuracy of his experiment was poor owing to the fact that intense monochromatic light sources were not available. However, Raman's [11] discovery that inelastic scattering could also be caused by non-linear polarizability received much attention from scientists working in related areas. Debye [12,13] extended elastic scattering theory and used his results to predict the molecular weight of polymers.

Landau and Placzek [14] calculated the ratio of the intensity of the central Rayleigh peak (I_c) to the intensity of the Doppler-shifted Brillouin peaks ($2I_B$) from classical density-fluctuation theory, and Miller [15] later developed the same equation using strictly thermodynamic arguments. Miller also noticed that macromolecules significantly increase the amount of scattered light, but that the change was significant only in the intensity of the central peak [16,17].

The development of the laser by Maiman [18] and Javan [19] in 1961 made it possible to study the fine structure of the scattering spectrum. Since the laser beam is monochromatic, coherent, intense, and well-collimated the separation of the Rayleigh and Brillouin peaks became possible. High-resolution interferometers [20,21] could then be used to

Mountair
linearized hilliquids.
colleagues [2
scattering s;
at the incide
by heavily-da

2. <u>Purpose</u>

The 1

changes of changes with

present wor

by ultrason The pu

is to eluci Varied from

it is inten

1. Tc

di:

2. To

met

study the spectra of light scattered by density fluctuations.

Mountain [22-27], followed by Bhatia and Tong [28], introduced linearized hydrodynamic theory for describing the Brillouin spectra of liquids. Recently Volterra, Stoicheff, Stegeman, Cummins and their colleagues [29-33] have made high-resolution studies of depolarized light-scattering spectra of many molecular liquids, revealing a doublet centered at the incident frequency. This must be due to orientational motion caused by heavily-damped shear waves.

2. Purpose of Research.

The low intermolecular forces of silicones (linear and cyclic polymethylsiloxanes) lead to unusually high compressibilities and very small changes of viscosity with temperature [34,35]. The general structural changes with temperature and molecular weight that form the basis for these remarkable properties are the main features investigated in the present work. Some insight into such matters has previously been gained by ultrasonic measurements [36,37].

The purpose of the present Brillouin-scattering study of silicones is to elucidate physical and structural changes as the temeprature is varied from 20°C to 80°C for polymers of molecular weight 160 to 12,500. It is intended:

- To measure the index of refraction of silicones for wavelengths of 5145 Å and 5890 Å at varying temperatures. A more detailed discussion is given in Chapter IV.
- 2. To show that the dependence of certain light-scattering parameters (the Landau-Placzek ratio and the soundwave attenuation

co-€

def rela

giv∈

3. To r

ter:

lat∈

resp

the

sili

the

as i

4. To c

cone

data

5. To 0

Velo

- co-efficient) on molecular weight and temperature reflect well-defined structural changes. The Landau-Placzek ratio (J_v) is related to the ratio of specific heats; a brief derivation is given in the Section 2 of Chapter II.
- 3. To measure the velocity of sound in silicones as a function of temperature and molecular weight. This quantity can be calculated from the spectral positions of the Brillouin peaks with respect to the central Rayleigh peak. A brief discussion of the velocities, frequencies and wave lengths of sound waves in silicones is given in Section 3 of Chapter II. The widths of the Brillouin component give the life times of the sound waves, as is explained in Section 4 of Chapter II.
- 4. To calculate the adiabatic compressibilities of certain silicones from the above sound-velocity measurements and density data. Calculations are presented in Chapter IV.
- 5. To consider the feasibility of developing a Laser-Brillouin-Velocimeter. Conclusions are presented in Appendix C.

1. <u>General</u>

Ligh

inhomogene from inclu

tuations i In the lat

molecular Whene

the visib dipole moi

secondary Photon at

If the so

frequency

Rayl linear di

Wavelengt

of the so the incid

The

esplitude

CHAPTER II

THEORY

General Concepts.

Light passing through any medium is partially scattered by optical inhomogeneities in the medium. Such inhomogeneities may result either from inclusions of foreign particles, or from small-scale density fluctuations in the medium - even though the medium contains no inclusions. In the latter case the scattered light will carry information on the molecular structure of the medium.

Whenever electromagnetic radiation of a given incident frequency in the visible region interacts with a scattering molecule, it induces a dipole moment in the molecule, which will then oscillate and act as a secondary source of energy. If this secondary source scatters a light photon at the incident frequency, this process is said to be elastic. If the source scatters a photon at a frequency different from the incident frequency, this process is said to be inelastic.

Rayleigh scattering is an elastic process in which the maximum linear dimension of the scattering particles is small compared to the wavelength of the incident radiation. Where the corresponding dimension of the scattering particles is not small compared with the wavelength of the incident radiation, the process is called Mie scattering.

The induced dipole moment p_i of the particle is connected with the amplitude of the incident electromagnetic wave E_j by a polarizability

equation f
Eq. (1) in
used for di
A general e
be obtained

The inc

2. <u>Thermod</u>
In t

dynamical e

irto small tany molecu length of l

redium is h

tensor $\alpha_{i,j}$;

$$p_i = \alpha_{ij} \cdot E_j^{[38]}; i,j = 1,2,3$$
 (1)

where,

$$\alpha_{ij} = \begin{bmatrix} \alpha_{11} & \alpha_{12} & \alpha_{13} \\ \alpha_{21} & \alpha_{22} & \alpha_{23} \\ \alpha_{31} & \alpha_{32} & \alpha_{33} \end{bmatrix}$$
(2)

The induced dipole moment p_i is dependent upon the shape of the particle. In the case of a homogeneous medium the off-diagonal terms of Eq. (2) are zero and all diagonal elements are equal. The scattering equation for an independent particle can be obtained by substituting Eq. (1) in Maxwell's equations. But the resulting relation can only be used for dilute gases, because in liquids the particles are interdependent. A general equation for the intensity of light scattered from a liquid can be obtained by treating the liquid as a continuum and utilizing hydrodynamical equations. [22-28]

2. Thermodynamic Theory.

In the classical theory of light the sample volume V is divided into small elements of volume v. The latter is large enough to contain many molecules but its linear dimensions are small compared with the wavelength of light. The incident light wave induces a dipole moment in the volume element v which in turn, acts as a secondary source. If the medium is homogeneous, the induced polarization will be constant and the

scattered r
scattering
ever, this r
local dield
stant thro:
An equ
from Maxwel
each elemen

where I is

is 90°, I

scattering

light, and

about its

Einste

T, writing

He assumed

scattered radiation will act destructively in all directions producing no scattering except in the forward direction. Even in pure liquids, however, this does not occur. There is a small random fluctuation in the local dielectric constant ($\Delta \epsilon$) and the induced polarization is not constant throughout the medium.

An equation for the intensity of scattered light can be developed from Maxwell's equations [39,40]. The intensity of light scattered by each elemental volume φ is given by:

$$I = I_0 \frac{\pi^2 v^2}{R^2 \lambda_0^4} < (\Delta \varepsilon)^2 >$$
 (3)

Where I is the intensity of the scattered light when the scattering angle θ is 90°, I_0 the intensity of incident beam, R the distance between the scattering volume and the detector, λ_0 the wavelength of the incident light, and $<(\Delta\epsilon)^2>$ the mean-square fluctuation of the dielectric constant ϵ about its mean value in the elemental volume.

Einstein [4] expressed ϵ as a function of density ρ and temperature T, writing

$$\Delta \varepsilon = \left(\frac{\partial \varepsilon}{\partial \rho}\right)_{\mathsf{T}} \Delta \rho + \left(\frac{\partial \varepsilon}{\partial \mathsf{T}}\right)_{\rho} \Delta \mathsf{T} \qquad . \tag{4}$$

He assumed that

$$\frac{\Delta \rho}{\Delta T} \left(\frac{\partial \varepsilon}{\partial \rho} \right)_{T} >> \left(\frac{\partial \varepsilon}{\partial T} \right)_{\rho}$$

and from thermodynamic fluctuation theory

where k i

If or

pressure

or,

Landau and entropy flutherefore as pressur

^{spons}ible

$$\frac{\langle (\Delta \rho)^2 \rangle}{2} = \frac{\kappa T \beta_T}{2} \qquad , \tag{5}$$

where κ is Boltzmann's constant and β_T is the isothermal compressibility. Eq. (4) reduces to

$$\langle (\Delta \varepsilon)^2 \rangle = (\frac{\partial \varepsilon}{\partial \rho})_{\tau}^2 \langle (\Delta \rho)^2 \rangle = (\rho \frac{\partial \varepsilon}{\partial \rho})_{\tau}^2 \frac{\kappa T \partial_{\tau}}{\sigma} , \qquad (6)$$

and substituting Equation (6) in (3) gives

$$I = I_0 \frac{\pi^2 \kappa T \beta_T \sigma}{R^2 \lambda_0^4} \left(\rho \frac{\partial \epsilon}{\partial \rho}\right)_T^2 . \tag{7}$$

If on the other hand ε is chosen as a function of entropy (s) and pressure (p) it follows that

$$\Delta \varepsilon = \left(\frac{\partial \varepsilon}{\partial \mathbf{s}}\right)_{\mathbf{p}} \Delta \mathbf{s} + \left(\frac{\partial \varepsilon}{\partial \mathbf{p}}\right)_{\mathbf{s}} \Delta \mathbf{p} \tag{8}$$

or,

$$<(\Delta \varepsilon)^2> = (\frac{\partial \varepsilon}{\partial s})_p^2 <(\Delta s)^2> + (\frac{\partial \varepsilon}{\partial p})_s^2 <(\Delta p)^2> ,$$
 (9)

where the cross term vanishes since fluctuations in s and p are independent. Landau and Placzek [41,42] identified the first term of Equation (9) as entropy fluctuations at constant pressure which do not propagate and therefore give rise to the Rayleigh peak. The second term they identified as pressure fluctuation at constant entropy, which is the sound wave responsible for Brillouin doublets.

where c_p the adiab

Equation term giverial

Or

By making use of thermodynamic theory [33] Eq. (9) can be reduced to

$$<(\Delta \varepsilon)^2> = \left(\frac{\partial \varepsilon}{\partial T}\right)^2_p \frac{\kappa T^2}{c_p \rho v} + \left(\rho \frac{\partial T}{\partial p}\right)_s \frac{\kappa T \beta_s}{v} , \qquad (10)$$

where c_p is the specific heat per unit mass at constant volume and β_s is the adiabatic compressibility $(\beta_T/\beta_s = c_p/c_V)$. Equations (10) and (3) lead to:

$$I = I_0 \frac{\pi^2 \sigma}{R^2 \lambda_0^4} \left[\left(\frac{\partial \varepsilon}{\partial T} \right)^2_p \frac{\kappa T^2}{\rho c_p} + \left(\rho \frac{\partial \varepsilon}{\partial \rho} \right)^2 \kappa T \beta_s \right] . \tag{11}$$

$$(Rayleigh) \qquad (Brillouin)$$

Equation (7) gives the total intensity I and the first term of Equation (11) gives the intensity of the Rayleigh peak, I_c . The second term gives the intensity of the Brillouin peaks, $2I_B$. Hence (7) and (11) yield

$$\frac{I}{2I_B} = \frac{I_c + 2I_B}{2I_B} = \frac{\beta_T}{\beta_S}$$
 (12)

or

$$\frac{I_c}{2I_B} = \frac{\beta_T}{\beta_S} - 1 \quad , \quad \text{and}$$
 (13)

$$\frac{I_c}{2I_B} = R_{Lp} = \gamma - 1 \tag{14}$$

where Y =
and specif

This
liquids be
like Cy.
calculated
frequency.
above ment

3. Fluctu

The fluctuation constant.

homogeneit dielectric

Let $u^{ ext{decomposed}}$ stant 4ε ij

the optica

The for the die.

where $\gamma = C_p/C_V$, the ratio of the specific heat at constant pressure and specific heat at constant volume.

This thermodynamic derivation is not entirely accurate for all liquids because of the frequency dependence of thermodynamic parameters like C_V. The measured Landau-Placzek ratio is generally greater than its calculated value, and the velocity of sound increases with increasing frequency. A theory is needed which will account for dispersion in the above mentioned quantities.

3. Fluctuation Theory.

Thermal motion of the molecules in a liquid produces density fluctuations which, in turn, cause fluctuations of the optical dielectric constant. Light passing through the liquid will be scattered by these inhomogeneities and its intensity will depend upon the extent to which the dielectric constant is coupled with the density fluctuations.

Let us assume that the dielectric constant of the liquid ε , can be decomposed into an average dielectric constant, ε_0 , and dielectric constant $\Delta \varepsilon_{ij}$ [43] due to the density fluctuations. Thus, $\Delta \varepsilon_{ij}$ reflects the optical inhomogeneity in the liquid. We write

$$\epsilon_{ij} = \epsilon_0 \delta_{ij} + \Delta \epsilon_{ij} \tag{15}$$

where $\delta_{i,j}$ is Kronecker's delta and i, j = 1,2,3.

The first term on the right-hand side of Eq. (15) gives the value of the dielectric constant in a homogeneous medium in which there is no light scattering. The second term can be divided into two terms, a

symmetric as follow

where

The fluctuatic

independer

fluctuation The s

of the med

^{nclecules}

obi ed ton

sent in th

in the liq

As in

cuencies (

when the v

symmetric (or, isotropic) and a skew-symmetric (or, anisotropic) part, as follows;

$$\Delta \varepsilon_{ij} = \Delta \varepsilon \cdot \delta_{ij} + \Delta \varepsilon'_{ij}$$
 (16)

where

$$\sum_{i=1}^{3} \Delta \varepsilon'_{ii} = 0 .$$

The first term on the right hand side of (16) represents isotropic fluctuations in the liquid and can be determined by the fluctuations in pressure and entropy, or density and temperature, or any other pair of independent thermodynamic variables. The light scattered by the fluctuations represented by $\Delta \varepsilon$ will be completely polarized.

The second term on the right hand side, $\Delta \varepsilon^{\prime}_{ij}$ reflects the anisotropy of the medium resulting from thermal motion, but $\Delta \varepsilon^{\prime}_{ij}$ also appears to result in part from fluctuations in the orientation of the anistropic molecules [43]. Light scattered by $\Delta \varepsilon^{\prime}_{ij}$ will be depolarized.

The frequency distribution of the scattered light from a liquid will not be identical to that of the incident light since the fluctuations present in the liquid are not static. Measurements of the scattered spectrum make it possible to study the temporal behavior of the thermal fluctuations in the liquid.

As in a crystal, longitudinal and transverse waves of different frequencies (thermally excited sound waves) may be present in a viscous liquid.

When the viscosity of the liquid is small, transverse waves will not be

present, t available needed to The wave in a

By t

The light, so mation material

present, but the longitudinal waves are easily excited. The energy available as heat (kT) is much more than the energy per phonon ($h\Omega$) needed to excite longitudinal waves.

The incident light wave of wave vector \vec{k}_i is scattered by the sound wave in a direction \vec{k}_i satisfying Bragg's Law.

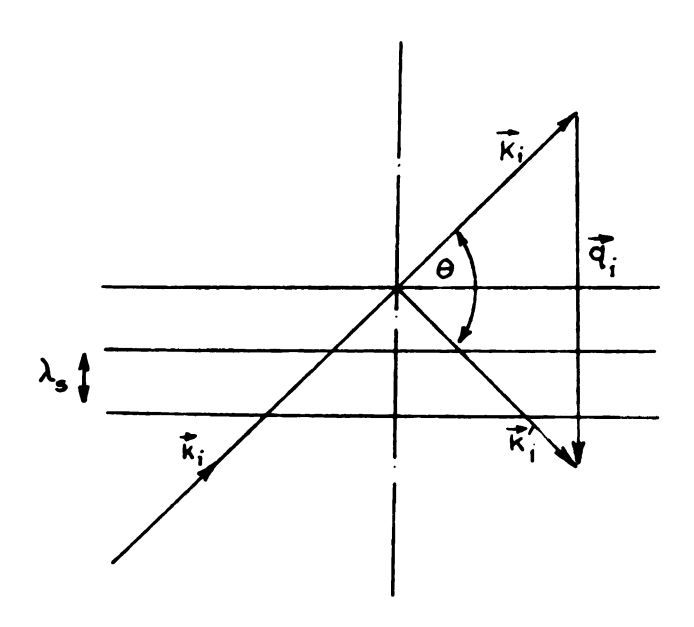


Figure 1.

By this, the sum of the vectors for the incident wave, scattered wave and sound wave must be equal to zero, whence

$$\vec{k}_{i} = \vec{k}_{i} + \vec{q}_{i} \tag{17}$$

The velocity of the sound wave is much smaller than the velocity of light, so we can make the approximation that $|k_i| \approx |k_i'|$. This approximation makes the vector triangle isosceles; therefore,

$$q_i = 2k_i \sin \frac{\theta}{2} \tag{18}$$

where 0 mentation

length of V_s the so scatterin

where λ i

Fro is depen

of the w

^{cal}culat Shift (v

waveleng

the medi the ligh

Deasure

where θ is the scattering angle which can be controlled during experimentation. Using the relations

$$k_i = 2\pi/\lambda$$
 and $q_i = 2\pi/\lambda_s$ (19)

where λ is the wave length of the incident light and λ_S is the wave length of the sound wave in the liquid, let v_S be the sound frequency, V_S the sound velocity and $\lambda = \lambda_O/n$, with n the refractive index of the scattering medium. Substituting (19) in (18) we get,

$$\lambda_{S} = \frac{\lambda_{O}}{2n \operatorname{Sin}(\frac{\theta}{2})}$$
 (20)

$$V_{S} = \frac{v_{S} \cdot \lambda_{O}}{2n \cdot Sin(\frac{\theta}{2})} \qquad (21)$$

$$v_{B} = v_{s} = \frac{V_{s} \cdot 2n \sin \frac{\theta}{2}}{\lambda_{0}}$$
 (22)

From Eq. (20) it can be seen that the wave-length of the sound wave is dependent upon the scattering angle, and is of the order of magnitude of the wave-length of the incident light. Eq. (21) shows that we can calculate the velocity of sound in the medium by measuring the frequency shift (v_s) of the Brillouin peaks, then inserting known values - the wavelength of the incident light in vacuum (λ_0) , the refractive index of the medium (n), and the scattering angle (θ). If we increase the angle θ the light scatters from sound waves of increasing frequency; thus we can measure the dispersion in the velocity of sound by changing the scattering

angle. Flated, bu
Eq.
measured

the incid

for λ_0 =

It for the original physical molecular from coher fluctuation propagate being relatine of er the at at contact the contact th

central pe

angle. From Eq. (22) the ultra-high acoustic frequencies can be calculated, but these can also be measured directly from the spectrum.

Eq. (20) shows that the shortest pressure fluctuation which can be measured from Brillouin scattering is dependent upon the wave-length of the incident light,

$$\lambda_{\text{s min}} = \lambda_{\text{o}}/2n \quad , \tag{23}$$

for λ_0 = 5145 Å and n = 1.40 , $\lambda_{s min}$ = 1.62 x 10⁻⁵ cm .

It follows that the shortest pressure fluctuation has a wave length of the order of 10^{-5} cm, and a frequency of the order of 10^{10} Hz. The physical length of these pressure fluctuations is very long compared with molecular sizes. Hence, the scattered light can be assumed to emanate from coherent density fluctuations. In addition to propagating pressure fluctuations, entropy fluctuations occur in the liquid; but these do not propagate. They occur only over extremely short time intervals, and being related to thermal-diffusion processes, are incoherent. The lifetime of entropy fluctuations is determined by the thermal diffusivity $\alpha = \lambda^2/\rho c_p$, where λ^2 is the thermal conductivity and c_p is the specific heat at constant pressure per unit mass. Therefore, the width of the central peak is proportional to the thermal diffusivity α .

4. Conti

produced describin

An and frequence developed principle scattered cm.). Cd hydrodyna higher theory [2]

scatter p the scatt measured

reciproca

degrees c

This

The a small v

fluids (s

4. Continuum Theory.

According to Onsager's hypothesis, the relaxation of thermallyproduced fluctuations can be described by the same equations as those describing deviations from equilibrium resulting from external causes.

An approximate theory yielding intensity as a function of magnitude and frequency for the various components of the Brillouin spectrum was developed by Mountain et al. [22-27] from thermodynamic and hydrodynamic principles. Eq. (23) establishes that the wave-length of the scattered light is large in relation to molecular sizes $(10^{-5} \text{ vs. } 10^{-7} \text{ cm.})$. Consequently the medium can be treated as a continuum and hydrodynamic theory can be applied. The frequency of 10^{10} Hz is higher than is usually encountered in hydrodynamics but Mountain's theory [23] should be applicable up to frequencies approximating the reciprocal of the collision time, 10^{12} to 10^{14} Hz [45].

This theory assumes a model in which the fluid possesses internal degrees of freedom for the molecules which are weakly coupled to the translational degrees of freedom of the fluid. Fluctuations in the density scatter polarized light, and the weak coupling of modes serve to modify the scattered frequency spectrum. This modification explains why the measured Landau-Placzek ratio is found to differ from γ - 1 for relaxing fluids (see Eq. 14).

The intensity of the light scattered from density fluctuations within a small volume element containing N molecules of the scattering fluid is given by

$$I(\vec{R},\omega) = I_0 \frac{N}{16\pi^2 R^2} K_i^4 \sin^2 \phi < [\Delta \epsilon(K,\omega)]^2 > \qquad (24)$$

Where I_0 vector \vec{k} , $u(\vec{k}, \omega)$, \vec{k} is the angle be is the F. and ω is tude of

where n

over the

in the

erature

With

Eq. (24

Where I_0 is the intensity of the incident plane-polarized light of wave vector \vec{k}_i , \vec{k} is the point of observation of the scattered light intensity $I(\vec{k}, \omega)$, and scattering is considered to have taken place at the origin. \vec{k} is the vectorial sum of the scattered and incident wave vectors. The angle between the electric vector of the incident wave and \vec{k} is ϕ , $\Delta \epsilon(R, \omega)$ is the Fourier component of the fluctuation in the dielectric constant, and ω is the shift in angular frequency of the scattered light. The magnitude of the wave vector K can be defined as

$$K = 2nK_{i} Sin(\frac{\theta}{2})$$
 (25)

where n is the index of refraction of the scattering fluid and θ is the scattering angle. The angular brackets < > indicate an ensemble average over the initial states of the system.

To calculate $\Delta \varepsilon$ (K, ω) in Eq. (24) it is assumed that the fluctuations in the dielectric constant are due to fluctuations in the density and temperature, e.g., $\varepsilon = \varepsilon(\rho, T)$. Then

$$\Delta \varepsilon = \left(\frac{\partial \varepsilon}{\partial \rho}\right)_{T} \Delta \rho + \left(\frac{\partial \varepsilon}{\partial T}\right)_{\rho} \Delta T \qquad . \tag{26}$$

With

$$\frac{\Delta \rho}{\Delta T} (\frac{\partial \varepsilon}{\partial \rho})_{T} >> (\frac{\partial \varepsilon}{\partial T})_{\rho}$$

Eq. (24) can be rewritten in the form

$$I(\vec{R},\omega) = \frac{I_0 N}{16\pi^2 p^2} K_i^4 \sin^2 \phi \left(\frac{3\varepsilon}{3\rho}\right)_T^2 \langle [\rho(K,\omega)]^2 \rangle$$
 (27)

where a the eval fluctuat irrevers in terms adapting assumed to the t the hydr

The

be expar

Con

Nav

where $\rho(K,\omega)$ is a Fourier component of the density fluctuation. For the evaluation of the mean square Fourier component of the density fluctuation, Mountain utilizes the linearized hydrodynamic equations of irreversible thermodynamics. These equations must be solved for $\rho(K,\omega)$ in terms of an initial fluctuation $\rho(K)$, which can be accomplished by adapting Van Hove's [47] method. In our present analysis it will be assumed that the transfer of energy from the internal degrees of freedom to the translational degrees occurs by a single relaxational process. In the hydrodynamic and energy equations the deviation from equilibrium is assumed to be small so that the mass density ρ , and the temperature T can be expanded about their equilibrium values (ρ_0 and T_0 , respectively),

$$\rho = \rho_0 + \rho_1$$

$$T = T_0 + T_1$$
(28)

The linearized hydrodynamic and energy equations are:
Continuity

$$\frac{\partial \rho_{1}}{\partial t} + \rho_{0} \operatorname{div} \vec{V} = 0 \tag{29}$$

Navier-Stokes:

$$\rho_{0} \frac{\partial \vec{V}}{\partial t} = -\frac{V_{0}^{2}}{\gamma} \operatorname{grad} \rho_{1} - \frac{V_{0}^{2} \beta \rho_{0}}{\gamma} \operatorname{grad} T_{1} + (\frac{4}{3} \eta_{s} + \eta_{V}) \operatorname{grad} \operatorname{div} \vec{V}$$

$$+ \int_{0}^{t} \eta'_{V}(t - t') \operatorname{grad} \operatorname{div} \vec{V} (t') dt' ; \qquad (30)$$

In these the ther is the 1:
The bulk

Acco scattered ability,

7_V(t)

where S(

The ord; Eq. (33)

Energy Transport:

$$\rho_{0}C_{v}(\frac{\partial T_{1}}{\partial t}) - [C_{v}(\gamma-1)/\beta] \frac{\partial \rho_{1}}{\partial t} - \lambda \nabla^{2}T_{1} = 0 \qquad (31)$$

In these three equations β is the thermal expansion co-efficient, λ' is the thermal conductivity, $\gamma = C_p/C_V$ is the ratio of specific heats, V_o is the low-frequency sound velocity, and the shear viscosity γ_s . The bulk visocsity consists of two terms, a frequency-independent term γ_V , and a frequency-dependent term which is the Fourier transform of $\gamma_V'(t)$ where t is the time.

According to Komarov and Fisher, [48] the intensity of the light scattered by N molecules of a fluid with effective molecular polarizability, α , is

$$I(\vec{R},\omega) = \frac{I_0 N}{2\pi R^2} \alpha^2 K_i^4 \sin^2 \phi S(K,\omega)$$
 (32)

where $S(K, \omega)$ is the generalized structure factor, related to the Fourier component of the density fluctuations by

$$S(K,\omega) = \langle \rho(K,\omega) | \rho(-K) \rangle \qquad . \tag{33}$$

The ordinary structure factor S(k) can be calculated by integrating Eq. (33) over all possible angular frequencies in the liquid. Hence,

$$S(K) = \frac{1}{2\pi} \int_{-\infty}^{\infty} S(K,\omega)d\omega = \langle \rho(K) \rho(-K) \rangle \qquad (34)$$

The gene tions by scattere

where

Her**e s i**s Eqs.

fluctuati

to the fo

+[

X

+[

χ

The generalized structure factor is related to initial density fluctuations by a function $\sigma(K, \omega)$, which is the frequency distribution of the scattered light:

$$S(K,\omega) = \langle \rho(K) | \rho(-K) \rangle \sigma(K,\omega)$$
 (35)

where

$$\sigma(K,\omega) = 2 \operatorname{Re} \left[\frac{\langle \rho(K,s) \rho(-K) \rangle}{\langle \rho(K) \rho(-K) \rangle} \right] \quad s = i\omega \quad . \tag{36}$$

Here s is a dummy variable utilizing Fourier and Laplace transforms.

Eqs. (29)-(31) are solved for the time-dependence of the density fluctuations by eliminating the velocity and obtaining two equations in the density and the temperature. Approximate transformations then lead to the following result:

$$\sigma(K,\omega) \simeq (1 - 1/\gamma) \left[\frac{2\lambda^{2} K^{2}/\rho_{o} C_{p}}{(\lambda^{2} K^{2}/\rho_{o} C_{p})^{2} + \omega^{2}} \right] + \left[\frac{(V_{\infty}^{2} - {}_{o}^{2}) K^{2} - (V^{2}/V_{o}^{2} - 1) (V_{o}^{4}/V^{2} \tau^{2} + V_{o}^{2} K^{2} (1 - 1/\gamma))}{(V_{o}^{4}/V^{4} \tau^{2} + V^{2} K^{2})} \right] \times \left[\frac{V^{2}/V^{2} \tau}{V_{o}^{4}/V^{4} \tau^{2} + \omega^{2}} \right] + \left[\frac{[1 - V_{o}^{2}/V^{2} (1 - 1/\gamma)] [V^{2} K^{2} + V_{o}^{2}/V^{2} \tau^{2}] - (V_{\infty}^{2} - V_{o}^{2}) K^{2}}{V_{o}^{4}/V^{4} \tau^{2} + V^{2} K^{2}} \right] \times \left[\frac{V^{2}/V^{2} \tau}{V_{o}^{4}/V^{4} \tau^{2} + V^{2} K^{2}} \right] \times \left[\frac{V^{2}/V^{2} \tau}{V_{o}^{4}/V^{4} \tau^{2} + V^{2} K^{2}} \right] \times \left[\frac{V^{2}/V^{2} \tau}{V_{o}^{4}/V^{4} \tau^{2} + V^{2} K^{2}} \right] \times \left[\frac{V^{2}/V^{2} \tau}{V_{o}^{4}/V^{4} \tau^{2} + V^{2} K^{2}} \right] \times \left[\frac{V^{2}/V^{2} \tau}{V_{o}^{4}/V^{4} \tau^{2} + V^{2} K^{2}} \right] \times \left[\frac{V^{2}/V^{2} \tau}{V_{o}^{4}/V^{4} \tau^{2} + V^{2} K^{2}} \right] \times \left[\frac{V^{2}/V^{2} \tau}{V_{o}^{4}/V^{4} \tau^{2} + V^{2} K^{2}} \right] \times \left[\frac{V^{2}/V^{2} \tau}{V_{o}^{4}/V^{4} \tau^{2} + V^{2} K^{2}} \right] \times \left[\frac{V^{2}/V^{2} \tau}{V_{o}^{4}/V^{4} \tau^{2} + V^{2} K^{2}} \right] \times \left[\frac{V^{2}/V^{2} \tau}{V_{o}^{4}/V^{4} \tau^{2} + V^{2} K^{2}} \right] \times \left[\frac{V^{2}/V^{2} \tau}{V_{o}^{4}/V^{4} \tau^{2} + V^{2} K^{2}} \right] \times \left[\frac{V^{2}/V^{2} \tau}{V_{o}^{4}/V^{4} \tau^{2} + V^{2} K^{2}} \right] \times \left[\frac{V^{2}/V^{2} \tau}{V_{o}^{4}/V^{4} \tau^{2} + V^{2} K^{2}} \right] \times \left[\frac{V^{2}/V^{2} \tau}{V_{o}^{4}/V^{4} \tau^{2} + V^{2} K^{2}} \right] \times \left[\frac{V^{2}/V^{2} \tau}{V_{o}^{4}/V^{4} \tau^{2} + V^{2} K^{2}} \right] \times \left[\frac{V^{2}/V^{2} \tau}{V_{o}^{4}/V^{4} \tau^{2} + V^{2} K^{2}} \right] \times \left[\frac{V^{2}/V^{2} \tau}{V_{o}^{4}/V^{4} \tau^{2} + V^{2} K^{2}} \right] \times \left[\frac{V^{2}/V^{2} \tau}{V_{o}^{4}/V^{4} \tau^{2} + V^{2} K^{2}} \right] \times \left[\frac{V^{2}/V^{2} \tau}{V_{o}^{4}/V^{4} \tau^{2} + V^{2} K^{2}} \right] \times \left[\frac{V^{2}/V^{2} \tau}{V_{o}^{4}/V^{4} \tau^{2} + V^{2} K^{2}} \right] \times \left[\frac{V^{2}/V^{2} \tau}{V_{o}^{4}/V^{4} \tau^{2} + V^{2} K^{2}} \right] \times \left[\frac{V^{2}/V^{2} \tau}{V_{o}^{4}/V^{4} \tau^{2} + V^{2} K^{2}} \right] \times \left[\frac{V^{2}/V^{2} \tau}{V_{o}^{4}/V^{4} \tau^{2} + V^{2} K^{2}} \right] \times \left[\frac{V^{2}/V^{2} \tau}{V_{o}^{4}/V^{4} \tau^{2} + V^{2} K^{2}} \right] \times \left[\frac{V^{2}/V^{2} \tau}{V_{o}^{4}/V^{4} \tau^{2} + V^{2} K^{2}} \right] \times \left[\frac{V^{2}/V^{2} \tau}{V^{2}/V^{2} + V^{$$

$$X \left[\frac{r_B}{r_B^2 + (\omega - v_K)^2} + \frac{r_B}{r_B^2 + (\omega + v_K)^2} \right]$$
 (37)

 r_B is the phonon spin the in

the them

internal

In
The first
sents dec

where

Therefore

The decay and This peak

^{Consequen}.

on the ci

 r_B is the half-width at half-height of a Brillouin peak, V is the phonon speed calculated from the Brillouin shift v_B (see Figure 2), V_∞ is the infinite-frequency phonon speed, and τ is the relaxation time of the thermal-diffusion process responsible for the weak coupling of the internal to the translational degrees of freedom.

In Eq. (37) all four terms are Lorentzian in character ($I^{-1} = A + B\omega^2$). The first term corresponds to the non-propagating Rayleigh peak, and represents decay of a density fluctuation by thermal-diffusion processes. Its half-width at half-height is given by

$$\Gamma_{R} = \frac{\lambda \Gamma K^{2}}{\rho_{o}C_{p}} \tag{38}$$

where

$$K^{2} = \frac{8\pi^{2}n^{2}}{\lambda_{0}^{2}} (1 - \cos \theta) . \tag{39}$$

Therefore Γ_R for the Rayleigh peak should increase when the scattering angle θ increases.

The second term corresponds to a non-propagating density fluctuation decay and is related to the internal degrees of freedom of the molecules.

This peak is call the "Mountain line", and its half-width at half-height is

$$\Gamma_{\mathsf{M}} = \frac{\mathsf{V}_{\mathsf{O}}^{2}}{\mathsf{V}_{\mathsf{T}}^{2}} \qquad . \tag{40}$$

Consequently, r_M depends on the dispersion of the velocity of sound and on the single relaxation time (τ) of the liquid.

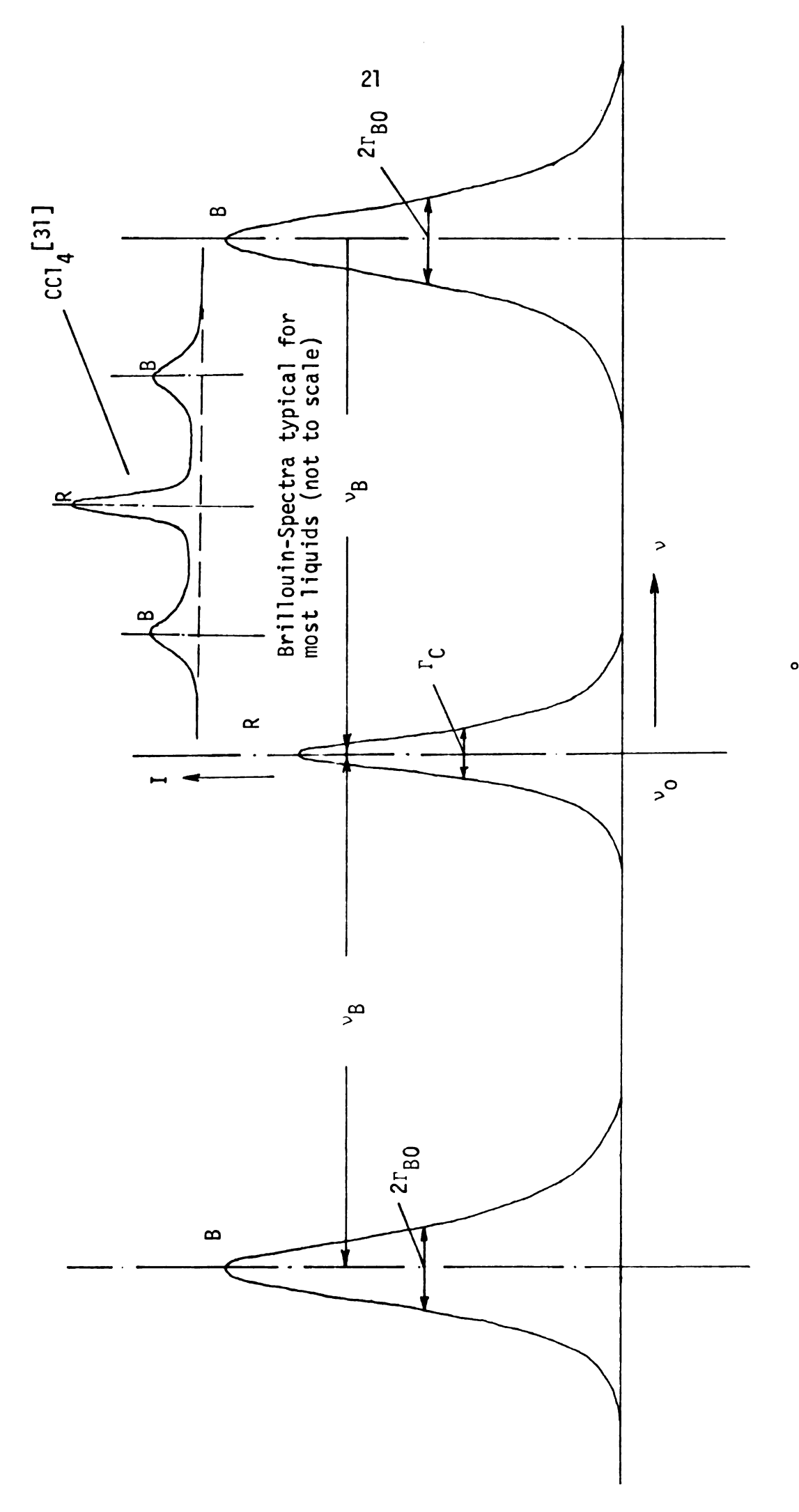


Fig. 2. Spectrum for MM at 40.0° C,0 = 90° and λ_0 = 5145 Å.

fluctua frequen

where

Eq. ing scatt Brillouir

in the sc The Ponding t The last term corresponds to the decay of the propagating density fluctuation (Brillouin peaks), and the frequency shift from the incident frequency ω_0 is given by

$$\Delta \omega = V \cdot K$$
 (41)

where

$$K = \frac{2\pi n}{\lambda_0} \operatorname{Sin}(\frac{\theta}{2}) \qquad . \tag{42}$$

Eq. (42) shows that the frequency shift ($\Delta\omega$) decreases with decreasing scattering angle θ . The half-width at half-height of the shifted Brillouin peak is:

$$r_{B} = \{ \frac{1}{\rho_{o}} \left[\frac{4}{3} \eta_{s} + \eta_{V} + \frac{\lambda^{2}}{C_{p}} \left(\gamma - \frac{V_{o}^{2}}{V^{2}} \right) \right] \} K^{2} + \left(\frac{V_{\infty}^{2} - V_{o}^{2}}{1 + V^{2} \tau^{2} K^{2}} \right) \left(1 - \frac{\lambda^{2} \tau K^{2}}{\rho_{o} C_{V}} \right) K^{2}$$

$$(43)$$

 Γ_B is strongly dependent upon K^2 and, therefore, decreases with a decrease in the scattering angle θ .

The ratio of the intensities of the central and shifted peaks, corresponding to the Landau-Placzek ratio R_{LP} in the absence of relaxation, is called J_{v} . From Eq. (37) it follows that

.1 = -

for low Landau-

and for

$$J_{V} = \frac{(1-1/\gamma)(\frac{V_{o}^{4}}{V_{o}^{4}} + V^{2}K^{2}) + (V_{\infty}^{2} - V_{o}^{2}) - (\frac{V^{2}}{V_{o}^{2}} - 1)[\frac{V_{o}^{4}}{V_{o}^{4}} + V_{o}^{2}K^{2}(1 - \frac{1}{\gamma})]}{[1 - \frac{V_{o}^{2}}{V^{2}}(1 - 1/\gamma)][V^{2}K^{2} + \frac{V_{o}^{2}}{V_{o}^{2}}] - (V_{\infty}^{2} - V_{o}^{2})K^{2}} . (44)$$

For low phonon frequencies (VK_{τ} <<1), this equation simplifies to the Landau-Placzek ratio (13),

$$J_{V} = \frac{Ic}{2I_{B}} = R_{LP} = \gamma - 1 \quad ,$$

and for large phonon frequencies ($VK_{\tau} >> 1$) it reduces to the simpler form

$$J_{V} = (\frac{V_{\infty}^{2}}{V_{0}^{2}}) Y - 1 . (45)$$

1. <u>Samp</u>

filtered mounting

^{obtain} q Th

with the

and dust

filter i

millipor.

^{ing} cell

and a te

^{pressure}

dependin:

A vacuum

vacuum se

was not s

CHAPTER III

EXPERIMENTATION

1. Sample Preparation.

Silicone samples were obtained from Dow Corning Co. and were filtered by an apparatus, designed primarily by Yuen, [53] before mounting on the instrument. The liquid must be dust free in order to obtain quantitative information from the calculations.

The apparatus consists of two filters arranged in series along with the sample cell, as is shown in Figure 3. Any contact with air and dust is eliminated while the sample is being filtered. The first filter is an ultrafine pyrex sintered glass filter with a solvenert millipore filter with a pore size of 0.25 µ. The cylindrical scattering cell was connected to the apparatus with two Fisher-Porter joints and a teflon gasket, making a completely sealed system. A hydrogen pressure of about 20 psi was applied on the top of the silicone to force it through the filters. This was repeated at least four times, depending upon the silicones, until the sample was completely dust free. A vacuum pump was connected to the vacuum manifold; the cell was then vacuum sealed and could be used repeatedly. The Brewster angle cell was not sealed.

Purifie Nitrogé

To Vacuum Manifol

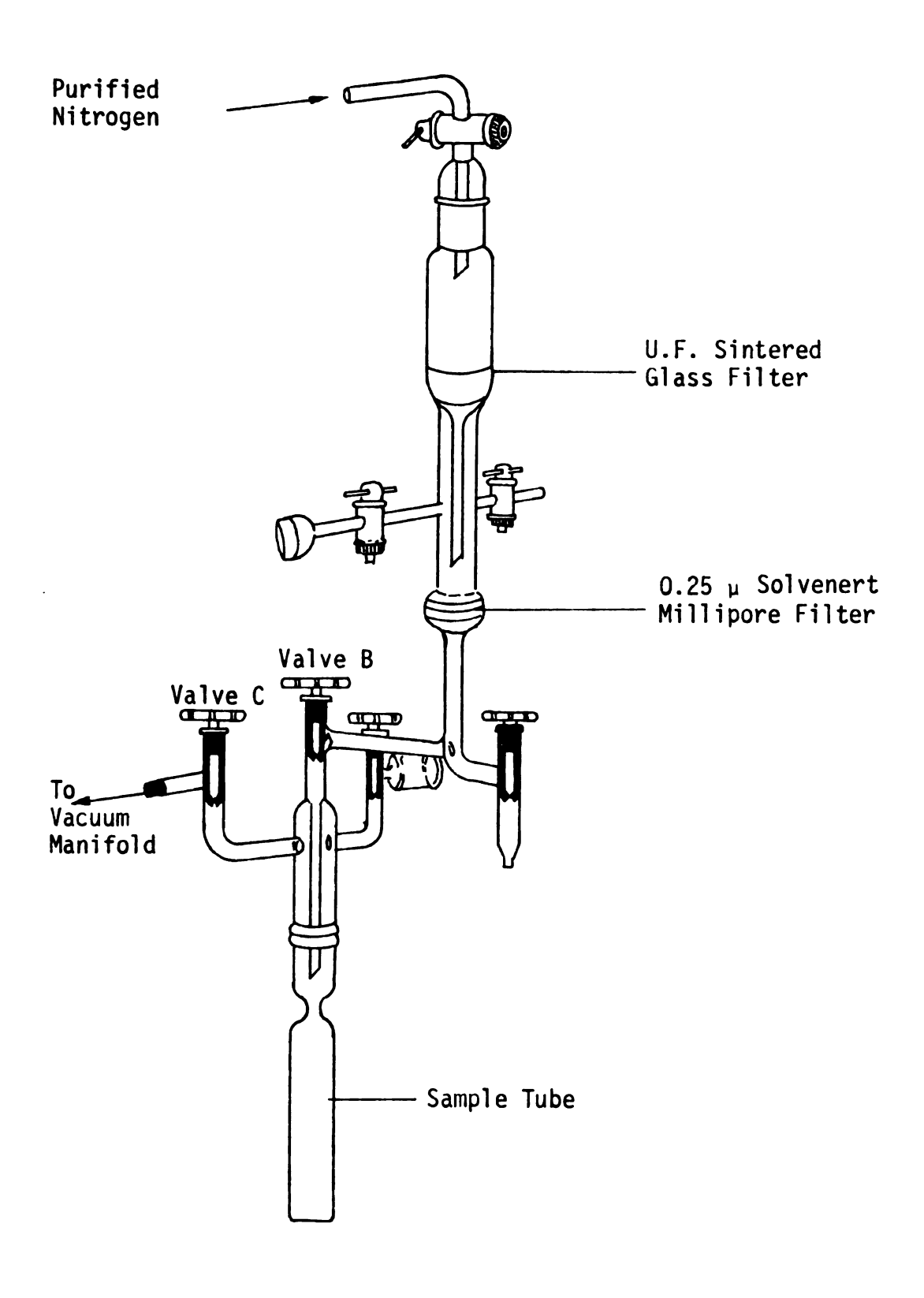


Fig. 3. Filtration Apparatus.

2. <u>The</u>

ing was :
State Uninstrume:
laser, r:
tube, pic
a large,
ternal vi
keep dus:
tion of t

a. <u>Laser</u>

laser, Mo

cussion o

(intensi:
Polarized
light sca
4579 Å) r
measureme

of 250 mm hence a g

Ver nowever, -

^{rota}ted Ł

2. The Brillouin Spectrometer.

The Brillouin spectrometer for measuring Brillouin light scattering was designed and constructed in the Chemistry laboratory at Michigan State University [50]. A diagrammatic sketch and pictorial view of the instrument is given in Figure 4. The spectrometer consists mainly of a laser, rotating table, optic housing, collecting lenses, photomultiplier tube, picoammeter and recorder. The whole optical system is mounted on a large, flat, acoustically-isolated table in order to eliminate any external vibrations. The incoming room air is also filtered in order to keep dust particles at a minimum level inside the room. A brief description of the equipment is given in this chapter and a more complete discussion can be found in Reference 50.

a. Laser

The source of light is a commercial Spectra Physics argon-ion laser, Model 165-03. The light coming out of this laser is very intense (intensity up to 800 mw), monochromatic (single frequency) and fully-polarized. There are eight different wavelengths which can be used for light scattering measurements, five of which (5145 Å, 4965 Å, 4765 Å and 4579 Å) have sufficient intensity to provide good spectra. In the present measurements a wavelength of 5145 Å was used with the single mode intensity of 250 mw. This intensity gives better stability of the light output and hence a good spectrum.

Vertically polarized light was used for most of the measurements; however, - for the depolarization measurements, the electric vector was rotated by 90° in order to obtain horizontally polarized light.

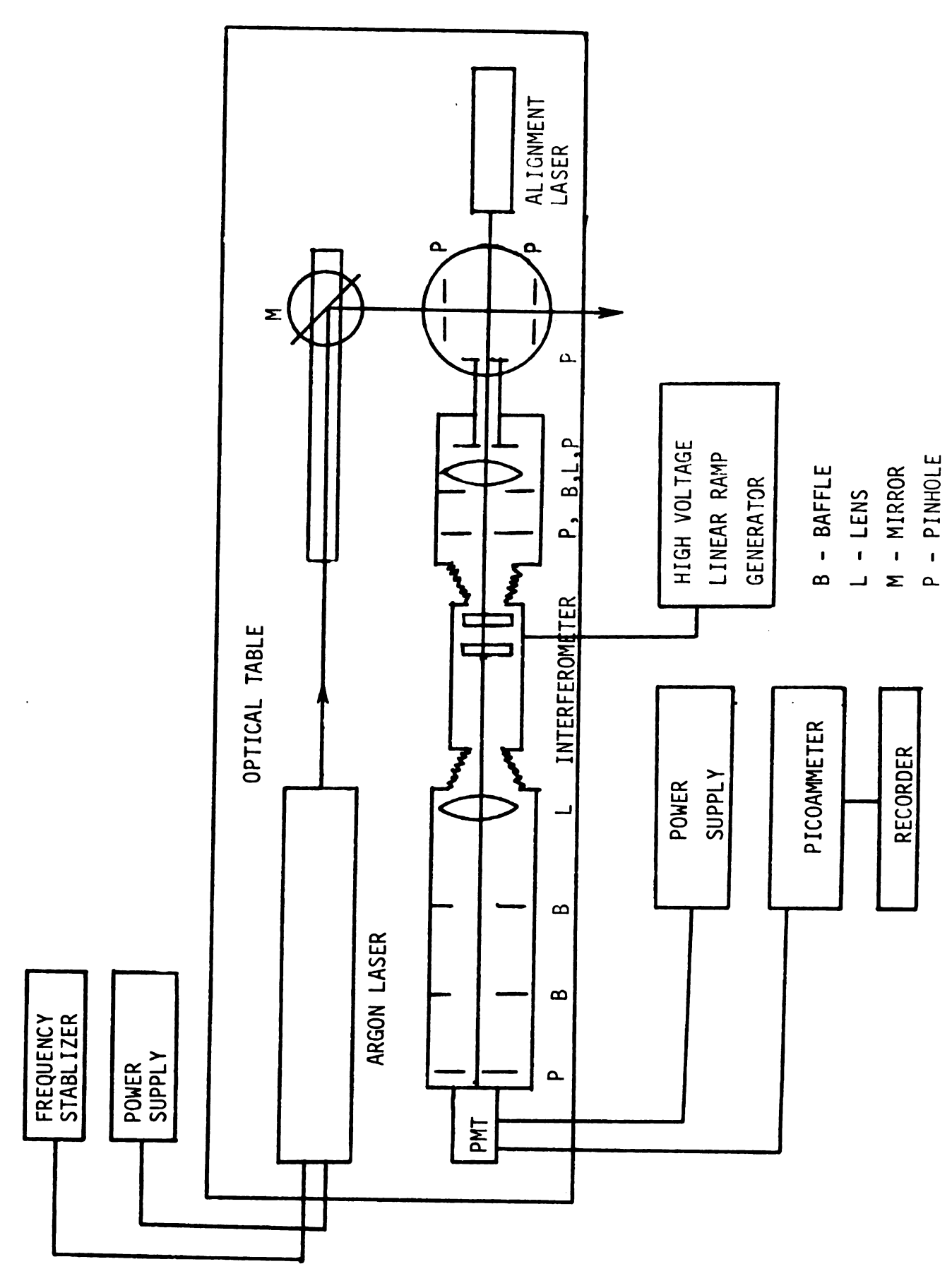


Fig. 4. Rayleigh-Brillouin Spectrometer

b. <u>Int</u>

of the ometer,
of the o

Ti [51,56]

of freq.

where a the incfor the

a Brills index of

the ang:

feromete

0 to 160

to one c

Lansing expanded

b. Interferometer

The interferometer is the most sensitive component of the entire instrument. Its alignment and operation is very critical to the quality of the Brillouin spectrum. A commercial Fabry-Perot scanning interferometer, Lansing Research Model 30.205, was used for resolving frequencies of the order of 10^9 Hz from the incident frequency of 10^{14} Hz. The interferometer consists of two, one-inch diameter mirrors which have inside surfaces polished to $\lambda/100$ flatness. It allows a very narrow frequency distribution to pass at one time, but can be scanned-over a small range of frequencies by varying the optical path length between the two mirrors.

The intensity of the light transmitted by the mirrors is given by [51,56]

$$I_{\text{trans}} = \frac{I_{\text{incident}}}{1 + \frac{4R}{(1-R)^2} \sin^2 \frac{\delta}{\lambda_0}}$$
 (46)

where δ = $2\pi n \ell$ Cos ϕ . It can be seen from Eq. (46) that I trans depends on the incident intensity, I incident, the reflection co-efficient R(R=98.5% for the mirrors used), and the optical path length δ . In order to obtain a Brillouin spectrum the optical length δ can be changed by varying the index of refraction n between the mirrors, the mirror separation ℓ , and the angle of refraction in the material ϕ . For scanning through the interferometer, the mirror separation ℓ was changed by varying the voltage from 0 to 1600 across two opposite faces of the piezoelectric crystal attached to one of the mirrors. This voltage was linearly increased with time by a Lansing Research Model 80.010 power supply. The applied voltage gradually expanded the crystal, decreasing the mirror separation, and almost five

spectra were av

Th

the Fre

(1.3 cm

Th

n(n = 1

in orde

and yet

Brillou

and ref

Th

(about

of the

quantit

c. 3£;

Th. directi

^{mount}ed

light i

a varia;

determin

apertur,

Th. length spectral orders could be obtained. Only the three most accurate orders were averaged in the final analysis in order to secure better accuracy.

The total frequency range scanned in one spectral order is called the Free Spectral Range and is defined as

$$f = \frac{C}{2nt} \quad . \tag{47}$$

This quantity is inversely proportional to the mirrors separation £

(1.3 cm to 1.4 cm for the present measurements) and the index of refractions n(n = 1 for air). Care was taken in choosing the correct mirror separation in order to eliminate the overlap of Brillouin peaks from adjacent orders, and yet identify the correct central Rayleigh peak associated with each Brillouin peak.

The instrumental band width v_{BW} is dependent upon the transmissivity and reflectivity of the mirrors and appears as an instrumental constant (about 300 MHz for the instrument used). It is the full width at half-height of the Rayleigh peak when perfectly monochromatic light is passed, a quantity which depends very much upon the alignment of the instrument.

c. <u>Optics</u>

There are two achromatic lenses and three pinholes for defining the direction of the scattered light, as illustrated in Figure 4. These are mounted on an optical rail inside two light-tight boxes. The scattered light is collected by a collimating tube near the scattering cell, which has a variable aperature at each end. The first aperture (1.0 mm in diameter) determines the acceptance angle of the scattered light, while the second aperture (3.0 mm in diameter) determines the core angle.

The scattered light is then collected by an achromatic lens of focal length 50 cms before entering the interferometer. The focal point of this

lens fall the from beam par of the

ometer a thus all fineness width at

tween th

d. Alia

alignmen

ment. I

instrume

alignmen

. Deci

scattere used for

was cont refriger

with a v

lens falls within the scattering cell. To reduce the light reflected off the front surface of the front mirror and prevent it from re-entering the beam path, a 1.5 cm aperture is placed between the first lens and the front of the interferometer.

The second lens of focal length 100 cm is placed behind the interferometer and this focuses on a pinhole in front of the photomultiplier tube, thus allowing detection of a central spot of the ring and increasing the fineness by about a factor of two. Fineness is defined as the ratio of the width at the half-height of the central Rayleigh peak to the separation between the central Rayleigh peaks of consecutive orders. Hence, the higher the fineness, the better the alignment.

d. Alignment

A Spectra-Physics Model 125 helium-neon laser was used for initial alignment; an oscilloscope was then used to improve upon the initial alignment. It was essential that the alignment be good in order to obtain reproducible spectra. Maximum care was taken with these procedures, the instrument being aligned after every run. A more detailed discussion of alignment procedures can be found in Reference [62].

e. Dectection and Recording

An EMI 9558 B photomultiplier tube was utilized to detect the scattered light. A regulated high voltage power supply from KEPCO was used for supplying 1100 volts to the photomultiplier tube. Its cathode was continuously cooled to -10° C with a Products for Research Model TE-104TS refrigerated chamber. The detector signal was then fed into a preamplifier with a variable current range (typically $0 - 10^{-9}$ amps). The damping

control was set at about 25% of the maximum value. The signal was then fed into a Keithly Model 417 picoamplifier, and finally to a Sargent Model SRC Strip Chart Recorder for a read out of the final spectrum.

3. The Temperature Control Cell.

A pictorial view of the temperature control cell is given in Figure 5 and a simplified cross-sectional view appears in Figure 6. This cell consists of a hollow copper cylinder thermostat, insulated on the outside, and with a calibrating cell inside. (Glycerin was used for the calibration of the temperature control cell.) The cylinder is 4 3/4 inches long and 3 1/4 inches in diameter. The inside cavity which houses the sample cell is 3 inches long and 2 inches in diameter. The copper base plate (1/4 inch thick) is discussed later in Section 3. A cooling coil is bihelically wound outside the copper cylinder and projects at the top for connection to an external coolant supply.

An epoxy resin shell 7/8 inch thick fits over the copper cylinder and is bolted to it at the top, so that the entire temperature control cell can be conveniently lifted on and off, leaving the sample and the sample-holder in place. A 180° viewing slot is provided in both the epoxy jacket and the copper cylinder. The thermometer and thermocouple locations are clearly shown in the sketch. For more details see Reference [52].

A YSI Model 72 temperature controller was used for applying voltage to the nichrome wire in order to heat the copper cylinder. A band width of 0.1°C was set on the controller while the temperatures could be set to the nearest tenth of a degree.

The controller was set at a temperature ranging from 25°C to 80°C

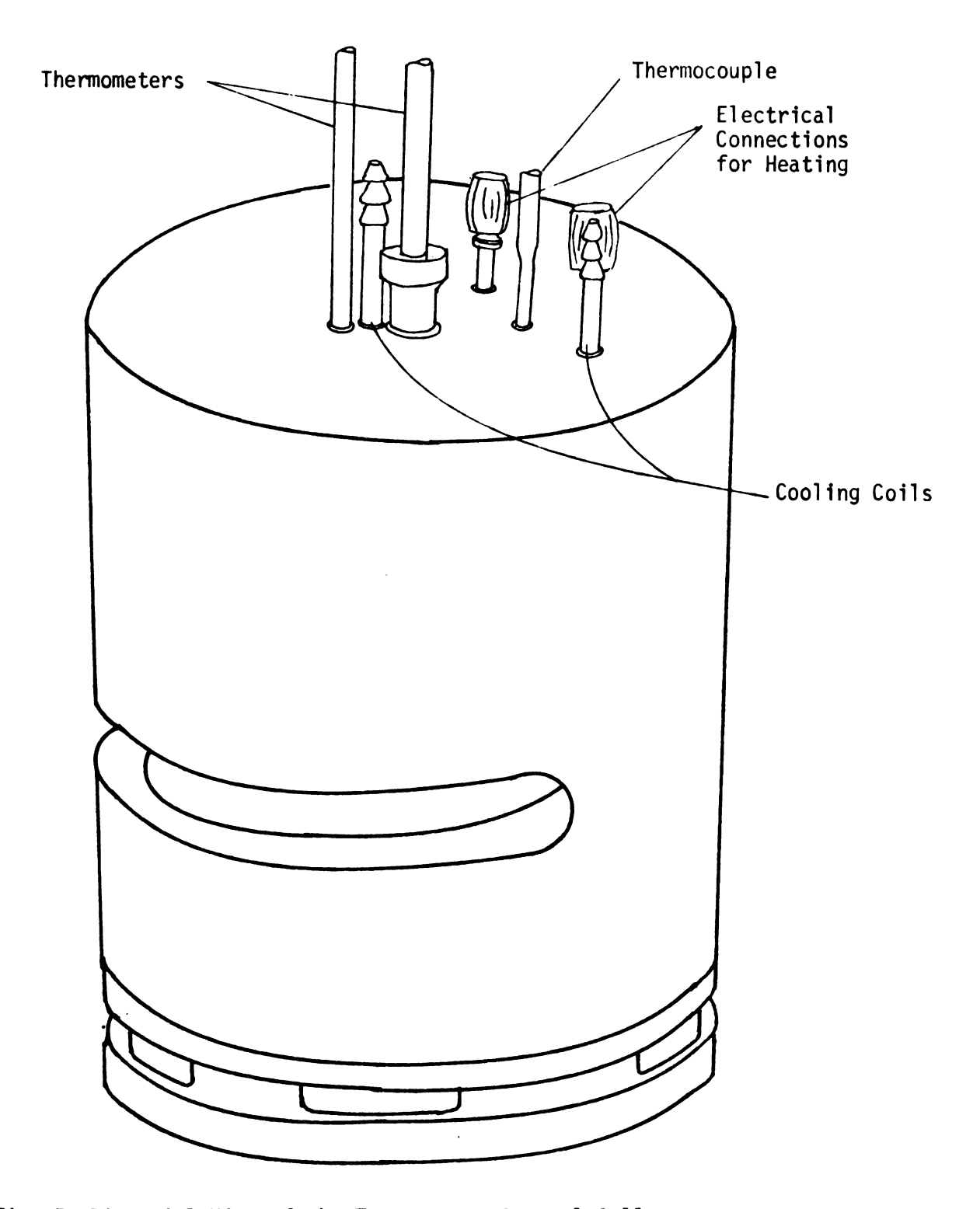


Fig. 5 Pictorial View of the Temperature Control Cell.

Epo Jaq

Sam Cel

Gly

180 Vie Por

Insu Base Plat

Fig. €

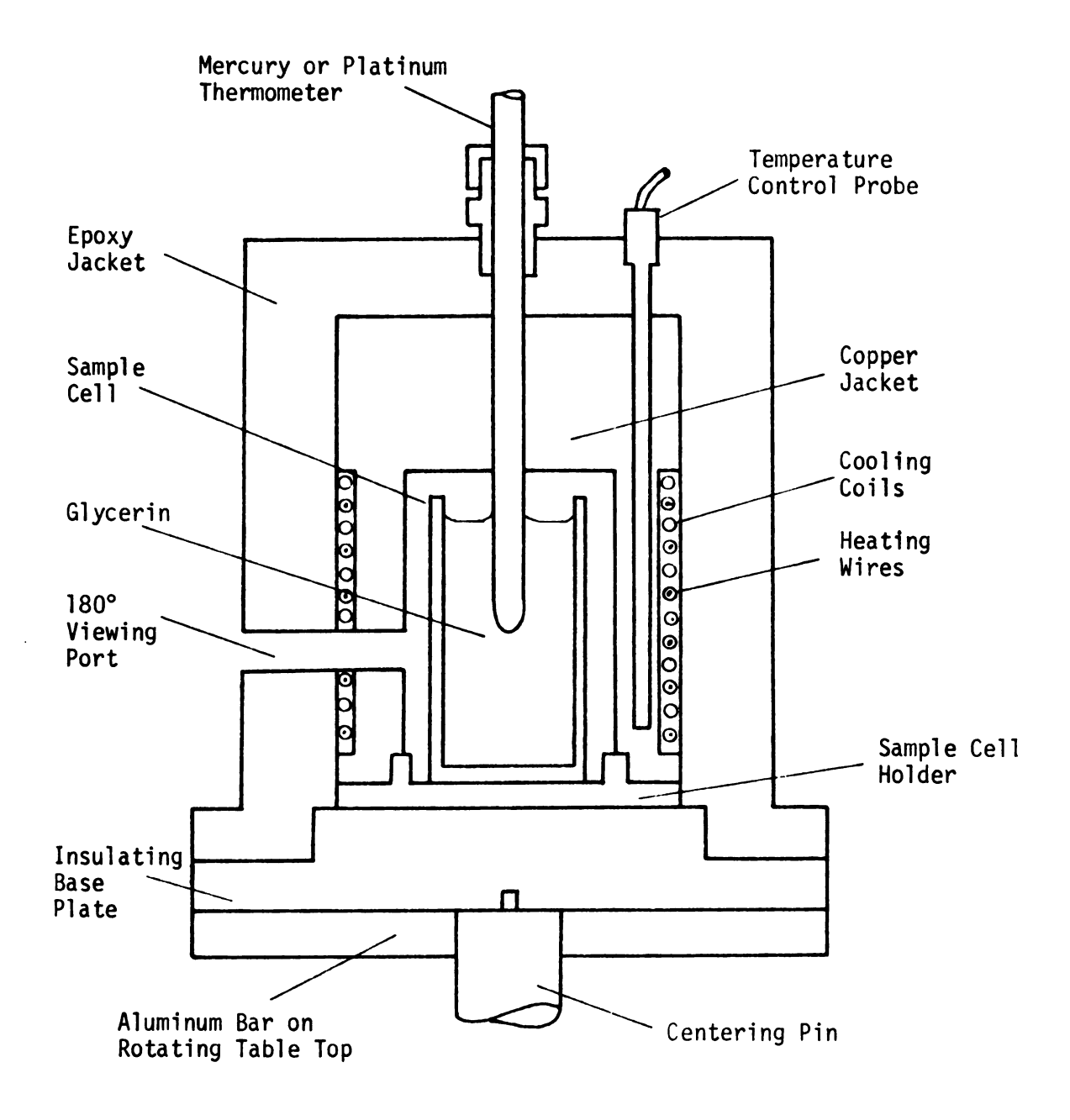


Fig. 6. Cross-sectional View of Temperature Control Cell

TABLE I

Measured and Corrected Temperatures Obtained During

Brillouin Scattering Measurements for Linear

and Cyclic Polydimethylsiloxanes.

Measured Temp.	Corrected Temp.
T _B (°C)	T _c (°C)
25.00	24.75
29.60	29.32
34.70	34.21
39.60	38.88
44.60	43.84
49.60	48.60
54.50	53.30
59.30	58.25
64.30	62.90
69.20	67.80
79.20	77.60

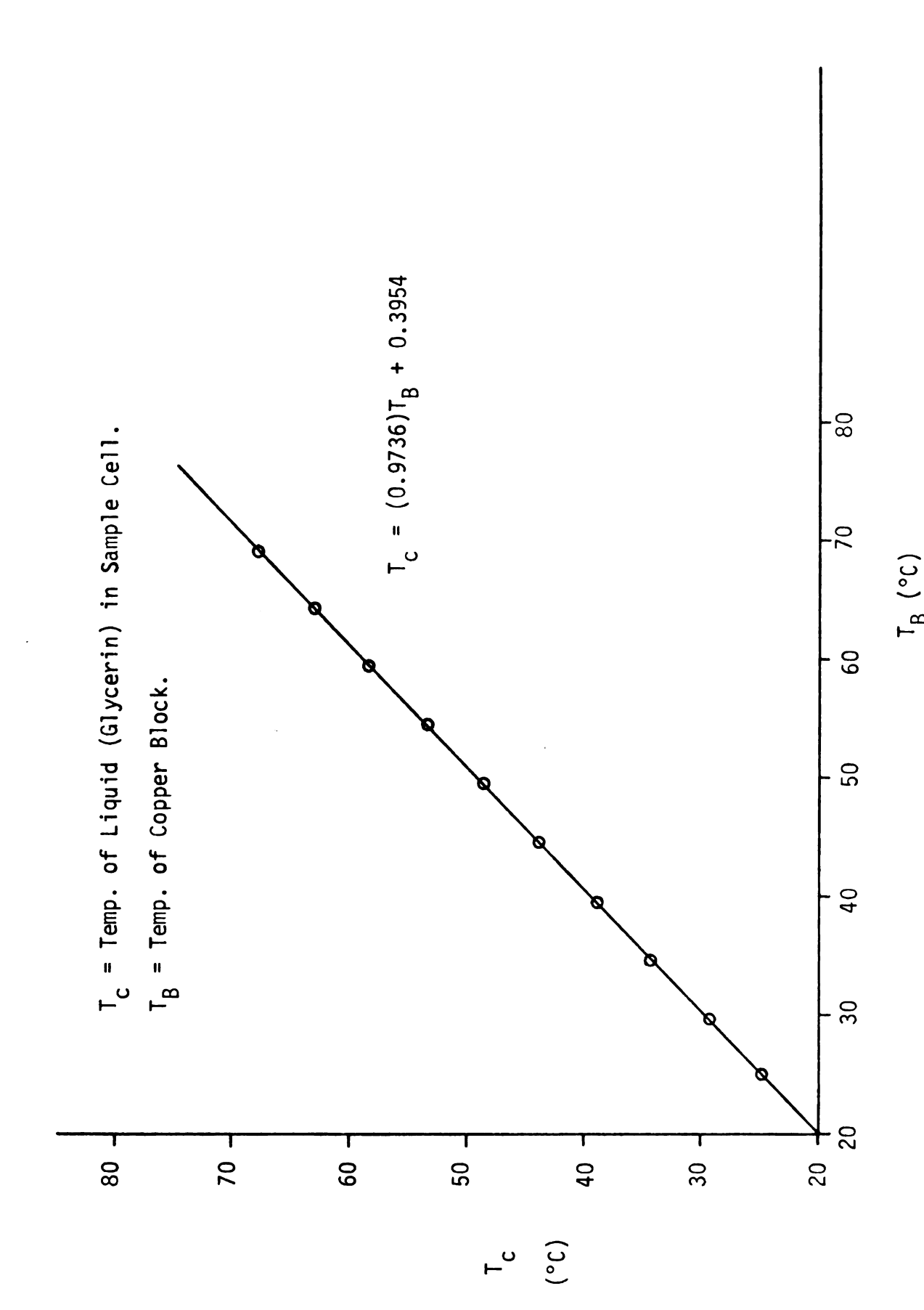


Figure 7. Calibration Data for the Temp. Control Cell.

using
allower
change
Model
the gl
corre
varia

4. <u>Th</u>

diamet

5 inch Figure

joint.

the fi

air in light

angle

To avo

light

using an interval of 5°C for temperature calibration. Two hours were allowed for the glycerin sample to attain thermal equilibrium after every change in temperature. In Table 1, T_A is the temperature set on the YSI Model 72, T_B the temperature of the copper box, and T_C the temperature of the glycerin sample. The precision of the measured temperature, T_B and the corrected temperature T_C is \pm 0.1°C. A linear relationship between these variables was established, as illustrated in Figure 7.

4. The Scattering Cell and the Holder.

The scattering cell consists of a precision-bore tube one inch in diameter, sealed to a 15mm Fisher-Porter joint. The total height is about 5 inches with the bottom sealed and flattened for a base, as shown in Figure 8. A neck was formed about 1 1/2 inches below the Fisher-Porter joint. This cell was then attached to a similar Fisher-Porter joint on the filtration apparatus with a teflon gasket, making an air-tight system.

A small amount of the incident beam is reflected back from the glassair interface where the incident beam exits from the cell. This reflectedlight causes a very weak Brillouin peak when scattering is measured at some angle other than 90°,

$$v_{\text{B reflected}} = \frac{2V_{\text{S}}^{\text{n}}}{\lambda_{\text{O}}} \text{ Sin } \left(\frac{180 - \theta}{2}\right)$$
 (48)

To avoid effects due to back-reflection for angular measurements, a

Brewster angle cell was used. At the Brewster angle, vertically-polarized

light will be reflected. The incident light used for Brillouin scattering

the Brewin the sa 5° and

secured

and can

secure t

sample is

the cyli

Α

5. Refra

Bausch an for all n

prism was

The Tation gi

measurements is vertically-polarized. Hence all light will pass through the Brewster angle. Some refraction will also occur if there are bends in the scattering cell. It was found that at the silicone-glass interface a 5° angle of the exit plane with the vertical was sufficient to cut out the effects of back reflection. To avoid any undesirable light reflections, the cylindrical and the Brewster angle cells were painted black.

A sample cell holder is shown in Figure 9. The sample cell is secured to the holder with an "0" ring which is located between two plates and can be tightened by the three small screws shown in the figure to secure the sample in place. The height and vertical alignment of the sample is adjusted with the three supporting screws indicated.

5. Refractive-Index Measurements.

The refractive-indices of the liquid silicones were measured by a Bausch and Lomb Abbe 3-L Refractometer at a wavelength of 5890 Å. Indices for all nine silicones were measured at five different temperatures (26°C, 35°C, 45°C, 55°C and 70°C). Temperature control for the refractometer prism was provided by a Haake circulating-bath temperature control unit.

The refractive indices for λ = 5145 Å were calculated from the information given in the dispersion table series 516 provided by the Bausch and Lomb Company. A more detailed discussion is given in Appendix A.

- Fisher-Porter Joint

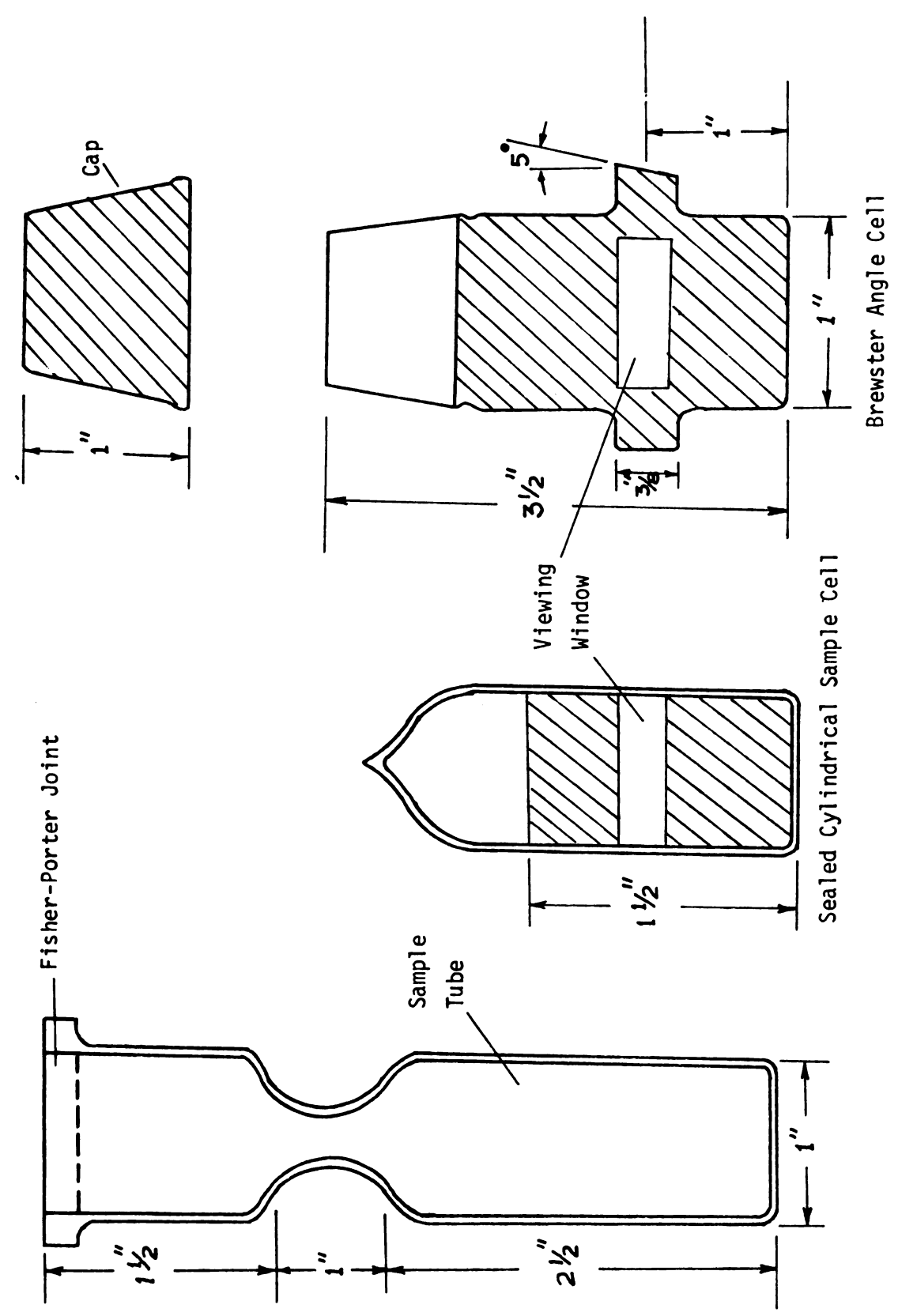


Fig. 8. Cylindrical and Brewster Light Scattering Cell.

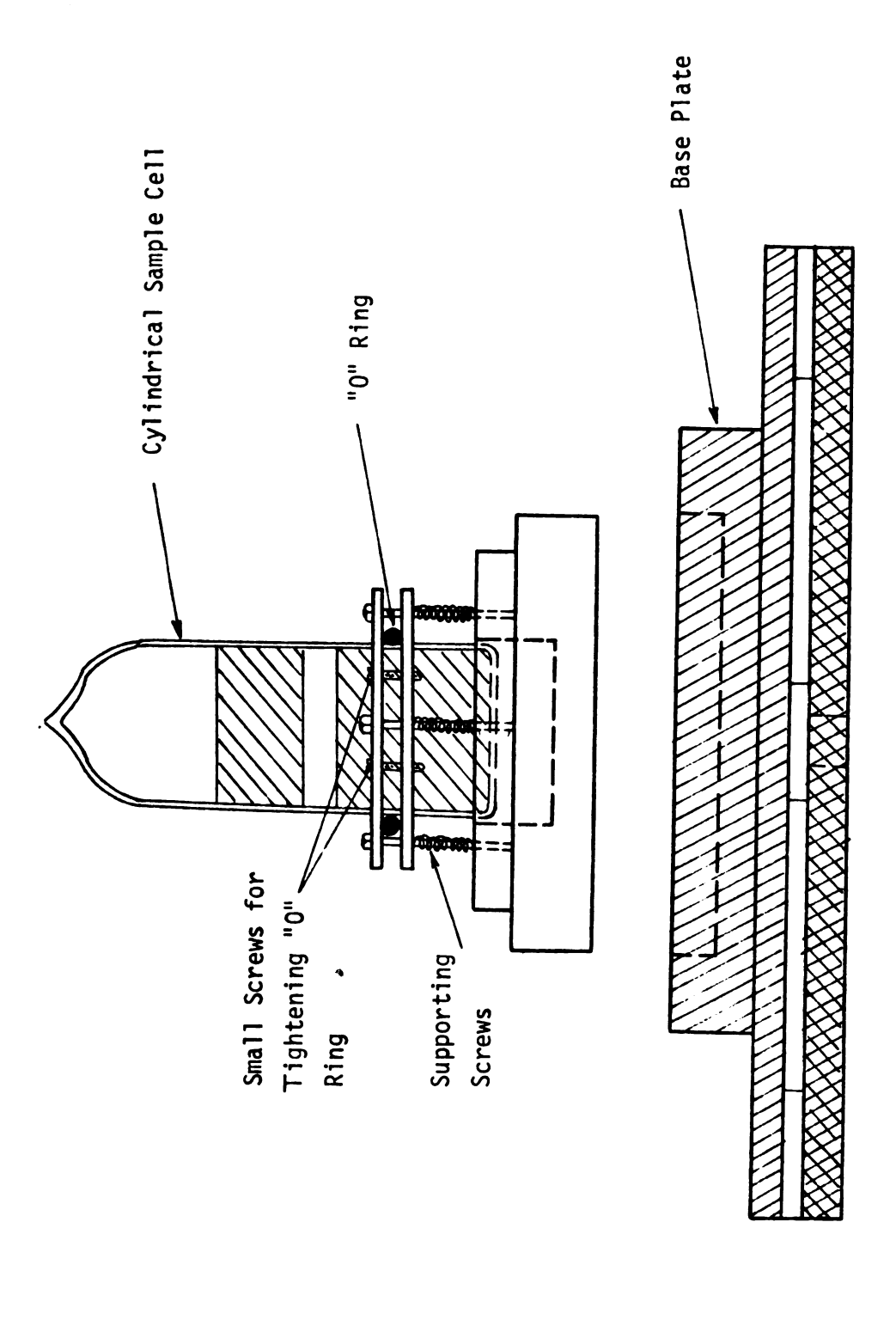


Fig. 9. Light Scattering Cell Holder.

The polydime

and cycl

Where 2: 10⁵ Cts.

and D =

The ^{eşpec}ia]

a result

siloxane

The ^{adi}abati

ratio of

CHAPTER IV

RESULTS AND DISCUSSION

The liquids studied in the present work are linear silicones (linear polydimethyl-siloxanes)

$$MD_{2}M = (CH_{3})_{3} Si - \begin{bmatrix} CH_{3} \\ 0 - Si - \\ CH_{3} \end{bmatrix}_{4} - 0 - Si(CH_{3})_{3}$$

and cyclic dimethylsiloxanes

$$D_{m} = \begin{bmatrix} CH_{3} \\ Si - 0 \\ CH_{3} \end{bmatrix}_{m}$$

where £ = 0,3,7 and m = 3, 5,9 and 15. Dow Corning 200 fluids, 100 cts. and 10^5 Cts. were also studied. In the above chemical equations M = $(CH_3)_3SiO_{1/2}$ and D = $(CH_3)_2SiO_3$.

The siloxane bond flexes and rotates fairly freely about the SiO axis especially with small substituents, such as methyl on the silicon atom. As a result of this freedom of motion, intermolecular distances between methyl-siloxane chains are greater and intermolecular forces are smaller.

The present objective is to calculate the velocity of sound, V_s , the adiabatic compressibility β_s , the sonic absorption co-efficient α and the ratio of the scattered light intensities J_V , all as a function of temperature

and mole

The

where, (
incident
investitions
sound wa

from the

as shown

Where c

The

obtainec

Wni culation perature

Prior to

and molecular weight for linear and cyclic silicones.

The velocity of sound V_s , is given by Eq. (21), with $\lambda_0 = \frac{c}{v_0}$,

$$V_s = \frac{Cv_B}{2nv_0 \sin \frac{\theta}{2}}$$

where, C is the velocity of light in a vacuum, v_0 is the frequency of the incident light wave, n is the index of refraction of the silicone under investigation, θ is the scattering angle and v_B is the frequency of the sound wave — which can be measured directly from the Brillouin spectrum as shown in Figure 2. The adiabatic compressibility β_S can be calculated from the velocity of sound V_S and density data, using the relationship

$$\beta_{S} = \frac{1}{\rho V_{S}^{2}} \tag{49}$$

where ρ is the density of the liquid.

The sonic absorption co-efficient is defined as

$$\alpha = \Gamma_{\mathsf{B}}/\mathsf{V}_{\mathsf{S}} \tag{50}$$

where Γ_B is the half-width at half-height of the Brillouin peak and can be obtained from the spectrum, also as illustrated in Figure 2.

While ν_B and Γ_B come from the spectrum, separate measurements and calculations were required for the index of refraction as a function of temperature and molecular weight. These are described in the following section, prior to the discussion of spectral measurements and related results.

nonexis

ľ

crease remaine

1. Var

0.0. 20 at the

peratur

ing obs

refract

value (

differe

Dà

in Tabl.

ⁿ5145 Å It is c:

tween re

uo anor i

25°C to

Perature

is also

ระกอ_{ยสก}ร

^{o€}3^M ar

It should also be noted that velocity dispersion was proved to be nonexistent at several different frequencies by varying the scattering angle θ , and that the vertical polarization ratio, ρ_V , was shown to decrease with temperature, while the horizontal polarization ratio, ρ_h , remained constant at all temperatures for every silicone studied.

Variation of the Refractive Index n with Temperature T_c and Molecular Weight.

Refractive indices of all the silicones studied (MM, MD₃M, MD₇M, D.C. 200 fluids of 100 Cts. and 10^5 Cts., D₃, D₅, and D₁₅) were measured at the wavelength of 5890 Å (the sodium D line) for five different temperatures (26°C, 35.1°C, 45°C, 55°C and 70.5°C). Since the light scattering observations were made using incident light of 5145 Å wave-length, the refractive indices were calculated for $\lambda = 5145$ Å from the $\lambda = 5890$ Å value (See Eq. A-1). Details of calculations and values of n_{5145} Å at the different temperatures are presented in the Appendix A.

Data for n_{5890} Å and n_{5145} Å at different temperatures are provided in Tables 2 - 4. Typical graphs of the calculated refractive index, n_{5145} Å, versus temperature for all silicones are shown in Figures 10 - 12. It is obvious from Figures 10 - 12 that there is a linear relationship between refractive index and temperature for all silicones, and that there is no anomaly in the refractive index behavior in the temperature range of 25°C to 70°C. It can be observed from Tables 2 - 4 that at constant temperature, refractive index increases as molecular weight is increased. It is also clear from Figure 12 that, for the same molecular weight, cyclic compounds (D_5 and D_9) have a higher refractive index than the linear compounds (MD_3M and MD_7M).

TABLE 2 Refractive Index as a Function of Temperature at $\lambda = 5890 \mathring{\text{A}} \text{ and } 5145 \mathring{\text{A}}$

Liquid	T(°C)	ⁿ 58 90 Å	ⁿ 5145Å
MM	26.0°C	1.3750	1.3778
	35.0°C	1.3700	1.3730
	45.0°C	1.3645	1.3673
	55.0°C	1.3584	1.3605
	70.5°C	1.3496	1.3524
Liquid	T(°C)	ⁿ 5890Å	ⁿ 5145Å
•	, ,	5890A	5145A
MD ₃ M	26.0°C	1.3905	1.3936
	35.0°C	1.3860	1.3893
	45.0°C	1.3816	1.3847
	55.0°C	1.3771	1.3801
	70.0°C	1.3705	1.3733
Liquid	T(°C)	n °	n °
Liquia	1(0)	ⁿ 5890Å	ⁿ 15145Å
MD_7M	26.0°C	1.3950	1.3989
,	35.0°C	1.3924	1.3955
	45.0° C	1.3886	1.3915
	55.0°C	1.3840	1.3870
	70.0°C	1.3778	1.3806

TABLE 3 Refractive Index as a Function of Temperature at $\lambda = 5890 \mathring{\text{A}}$ and $5145 \mathring{\text{A}}$

Liquid	T(°C)	ⁿ 5890Å	ⁿ 5145Å
D.C. fluid, 100 cts.	26.0°C 35.1°C 45.0°C	1.4030 1.3992 1.3955	1.4055 1.4025 1.3988
	55.0°C 70.5°C	1.3916 1.3859	1.3945 1.3888
Liquid	T(°C)	n ₅₈₉₀ Å	ⁿ 5145Å
D.C. fluid, 10 ⁵ cts.	26.0°C 35.1°C 45.0°C 55.0°C 70.5°C	1.4036 1.4000 1.3965 1.3926 1.3870	1.4053 1.4033 1.3998 1.3959 1.3901
	80.0°C	1.3831	1.3859

TABLE 4

Refractive Index as a Function of Temperature at

	$\lambda = 5890\text{\AA}$ a	and 5145Å	
Liquid	T(°C)	ⁿ 5890Å	ⁿ 5145Å
D_3	70.1°C	1.3602	1.3633
J	80.1°C	1.3550	1.3578
Liquid	T(°C)	ⁿ 5890Å	ⁿ 5145Å
D ₅	26.0°C	1.3960	1.3989
J	35.1°C	1.3917	1.3945
	45.0°C	1.3873	1.3905
	55.0°C	1.3825	1.3 854
	70.5°C	1.3753	1.3782
Liquid	T(°C)	n ₅₈₉₀ Å	ⁿ 5145Å
D_{9}	26.0°C	1.4050	1.4082
•	35.0°C	1.4016	1.4047
	45.0°C	1.3980	1.4008
	55.1°C	1.3936	1.3970
	70.2°C	1.3878	1.3819
Liquid	T(°C)	ⁿ 5890Å	ⁿ 5145Å
D ₁₅	26.0°C	1.4045	1.4080
	35.1°C	1.4015	1.4067
	45.0°C	1.3979	1.4007
	55.0°C	1.3939	1.3971
	70.5°C	1.3878	1.3908

Figure

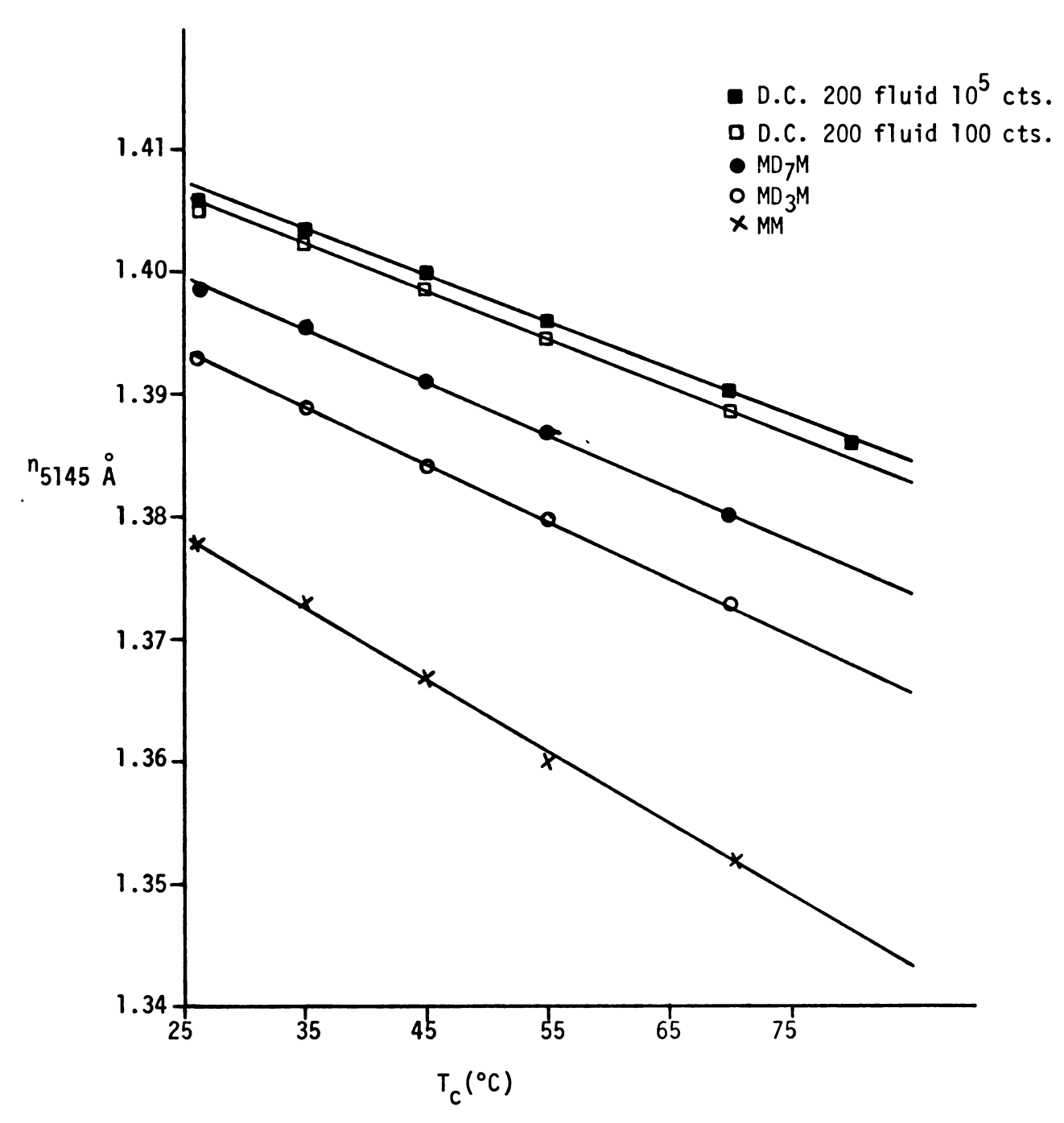


Figure 10. Refractive Index Versus Temperature for MM , MD $_3$ M, MD $_7$ M, D.C. 200 fluids, 100 cts. and 10^5 cts.

ⁿ5145

Figura

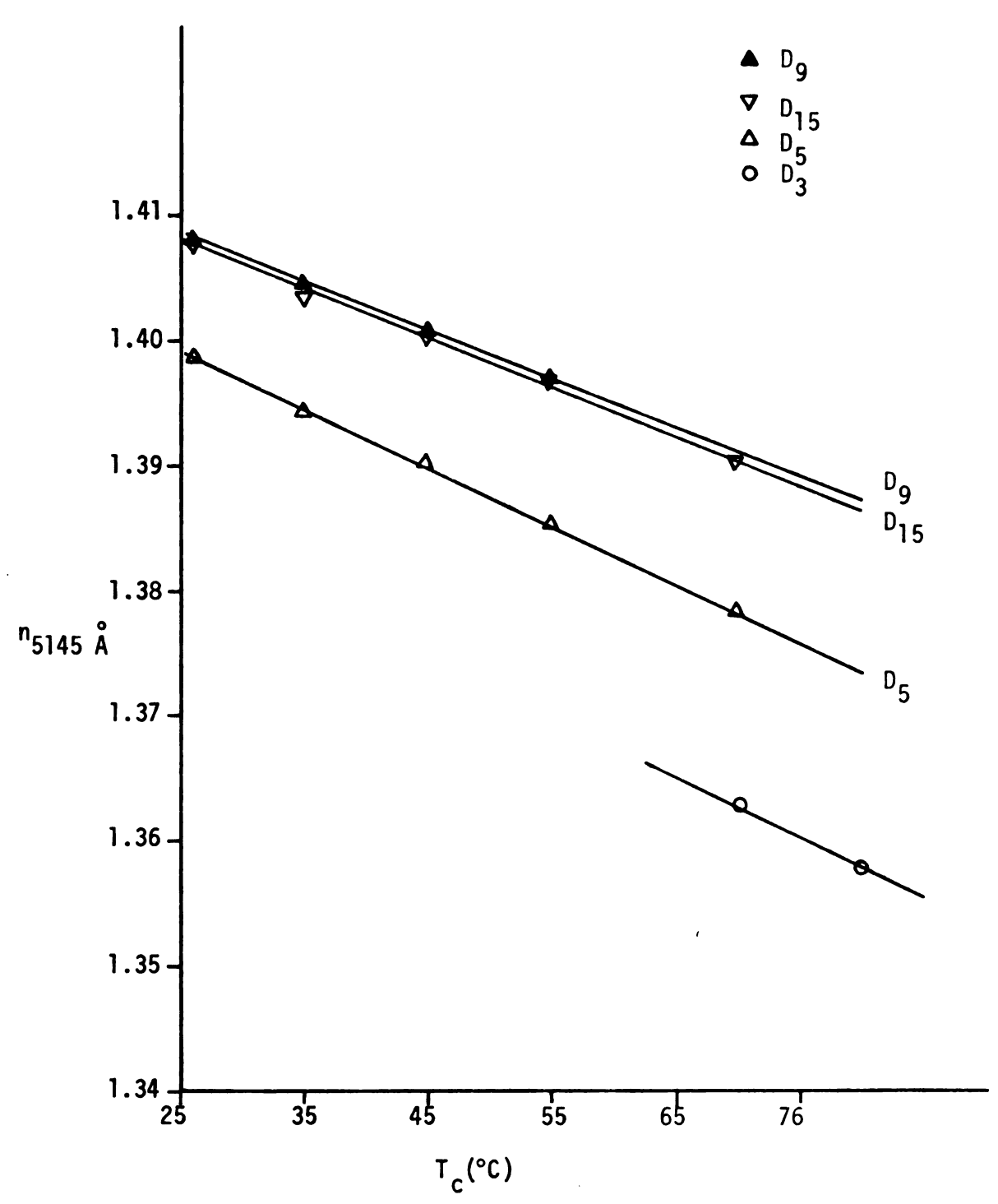


Figure 11. Refractive Index versus Temeprature for D_3 , D_5 , D_9 and D_{15} .

"5]

10 miles

F.

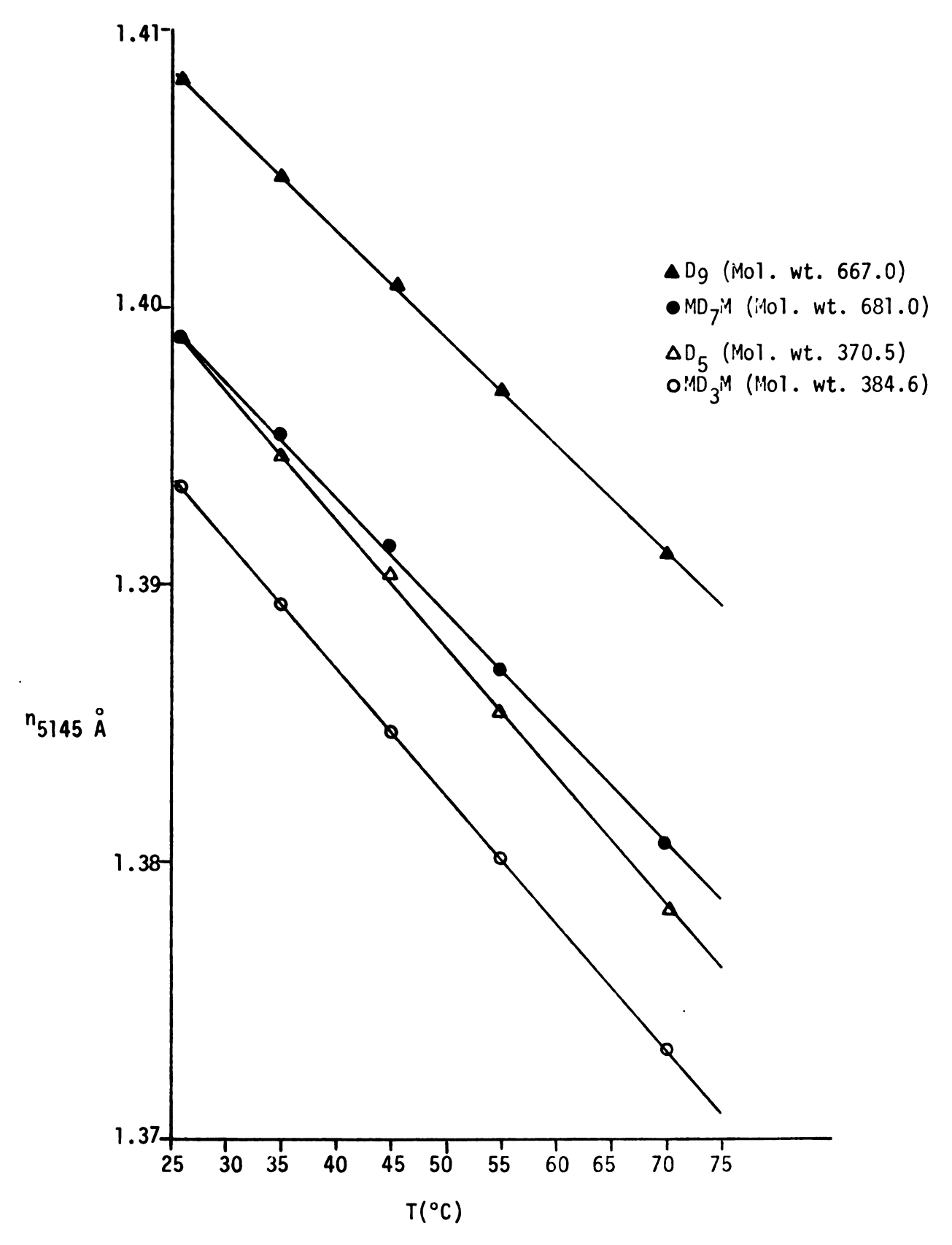


Figure 12. Refractive Index Versus Temperature for D_9 , $\mathrm{MD}_7\mathrm{M}$, D_5 and $\mathrm{MD}_3\mathrm{M}$.

re

ill tr

jur

sh :ed

lec

e,

. v

ue

B

ļ

re

ll at:

re:

lin

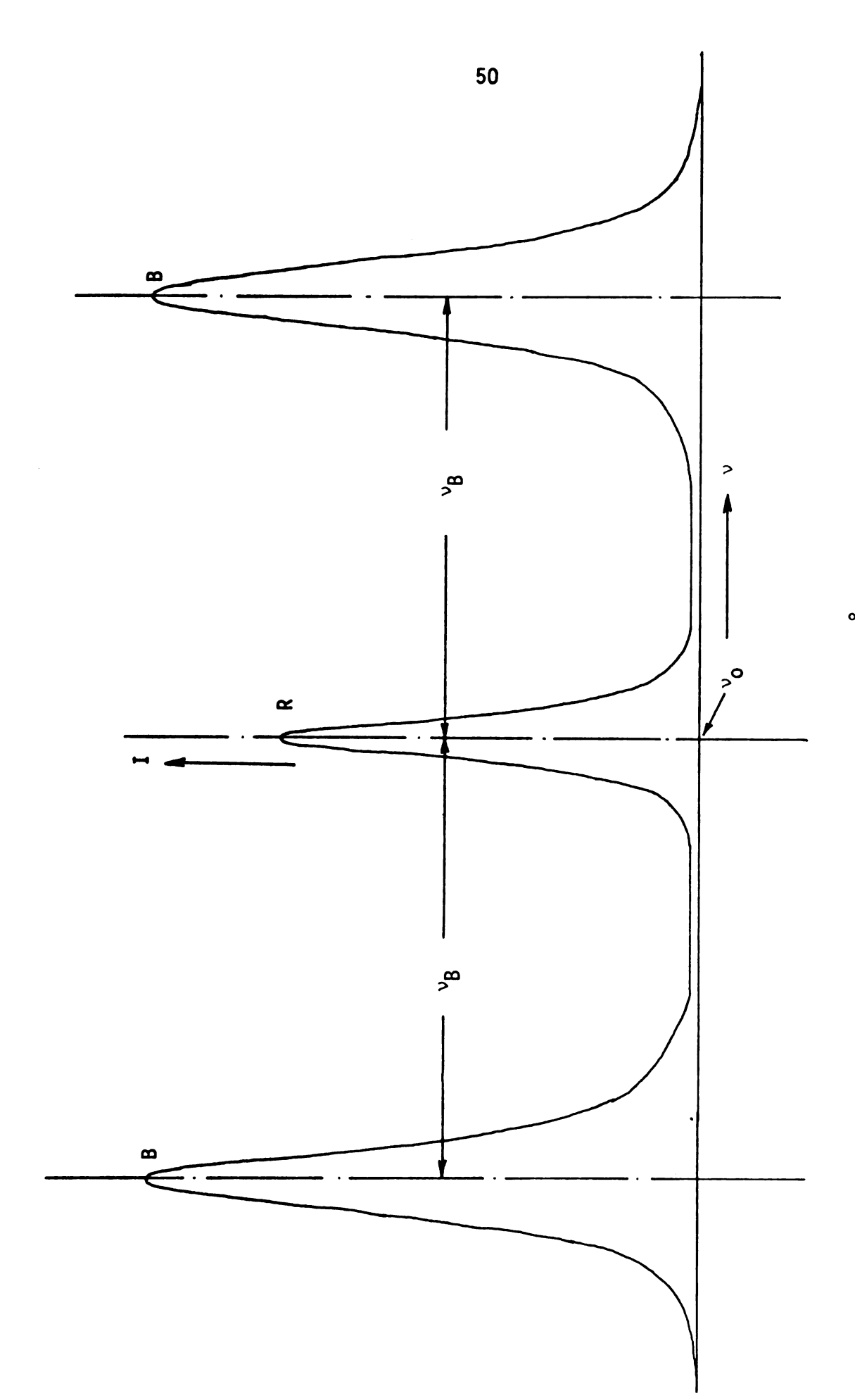
2. Variation of the Brillouin-Shift v_B with Temperature T_c and Molecular Weight.

Light waves scattered from the sonic waves in the liquid display a three-peaked intensity-frequency distribution, as illustrated in Figures 13 - 16. The two symmetrical Doppler-shifted side peaks are known as the Brillouin peaks and their shift, ν_B , from the central Rayleigh peak is given by the Eq. 22.

The Brillouin-shift can be measured directly from the spectrum as indicated in Figure 2 of Chapter II, and is in the gigahertz (GHz) range. From Figures 17, 18 and 19 it is clear that ν_B varies with the temperature, molecular weight and molecular structure of the silicones. Figures 17 and 18 show that ν_B varies linearly with temperature for the silicones investigated. Figure 19 provides a good comparison of how ν_B changes with temperature for linear and cyclic silicones having about the same molecular weights. The values in Tables 5-13 establish that ν_B increases with increasing molecular weight for all silicones.

These tables contain measurements of v_B and Γ_B as well as calculated values of V_S and α . Tables 14-21 contain calculations of various slopes $(dv_B/dT_C, dV_S/dT_C, \frac{d\Gamma_B}{\alpha T})$. All of these results will be utilized as required in the subsequent discussion.

Tables 16 and 18 contain values for the slope and intercept of the Brillouin-shift-temperature curves. As can be seen from Figure 20, the relation between $\frac{d\nu_B}{dT_C}$ and molecular weight for linear silicones is nonlinear, whereas the relation between $\frac{d\nu_B}{dT_C}$ and molecular weight for cyclic silicones is linear.



 $\theta = 90^{\circ}$ and $\lambda_0 = 5145 \text{ Å}$. Fig. 13. Spectrum for MM at 70°C,

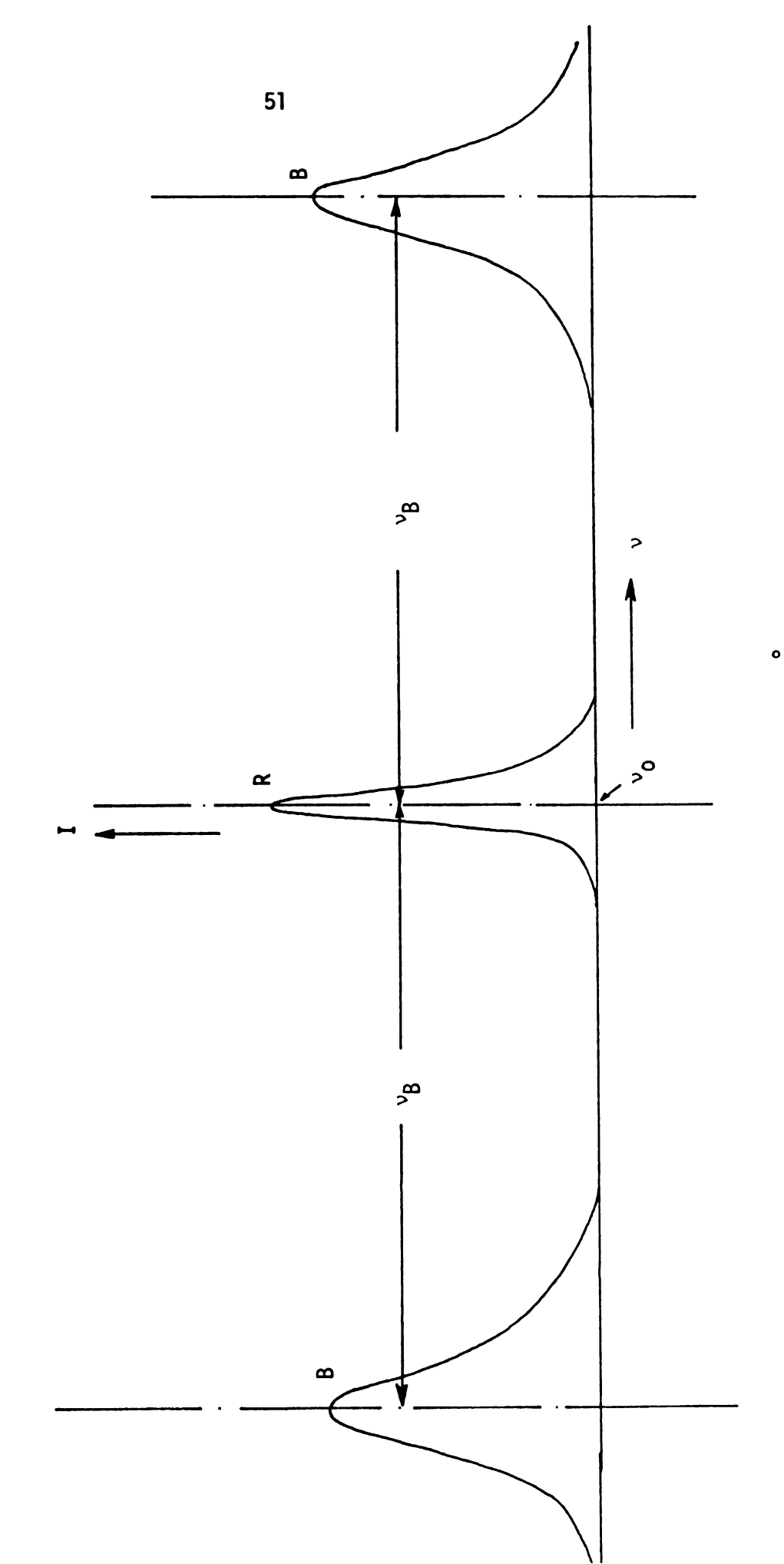


Fig. 14. Spectrum for MD₇M at 40.0°C, $\theta = 90^{\circ}$ and $\lambda_0 = 5145$ Å.

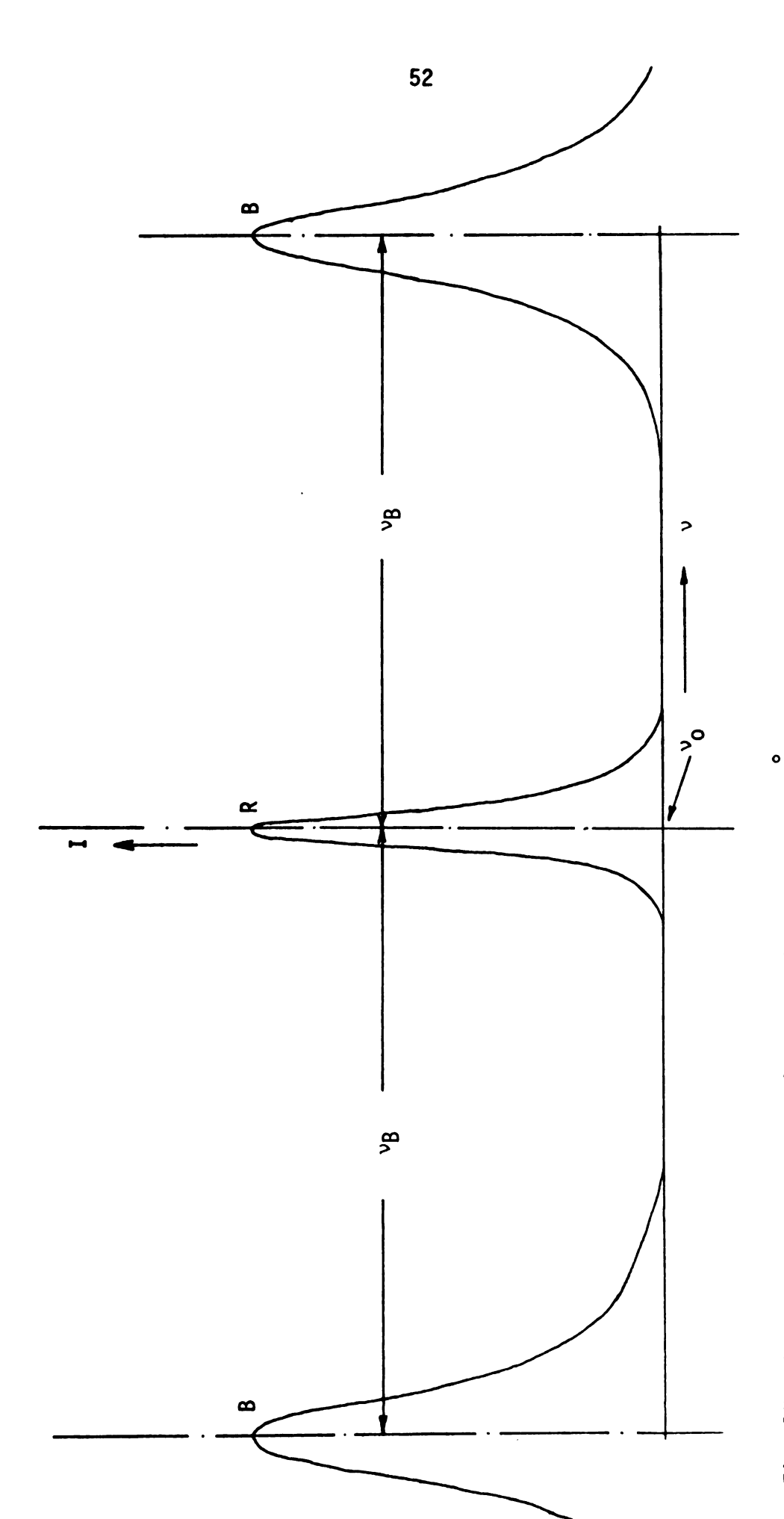


Fig. 15. Spectrum for MD₇M at 50°C, $\theta = 90^{\circ}$ and $\lambda_0 = 5145$ Å.

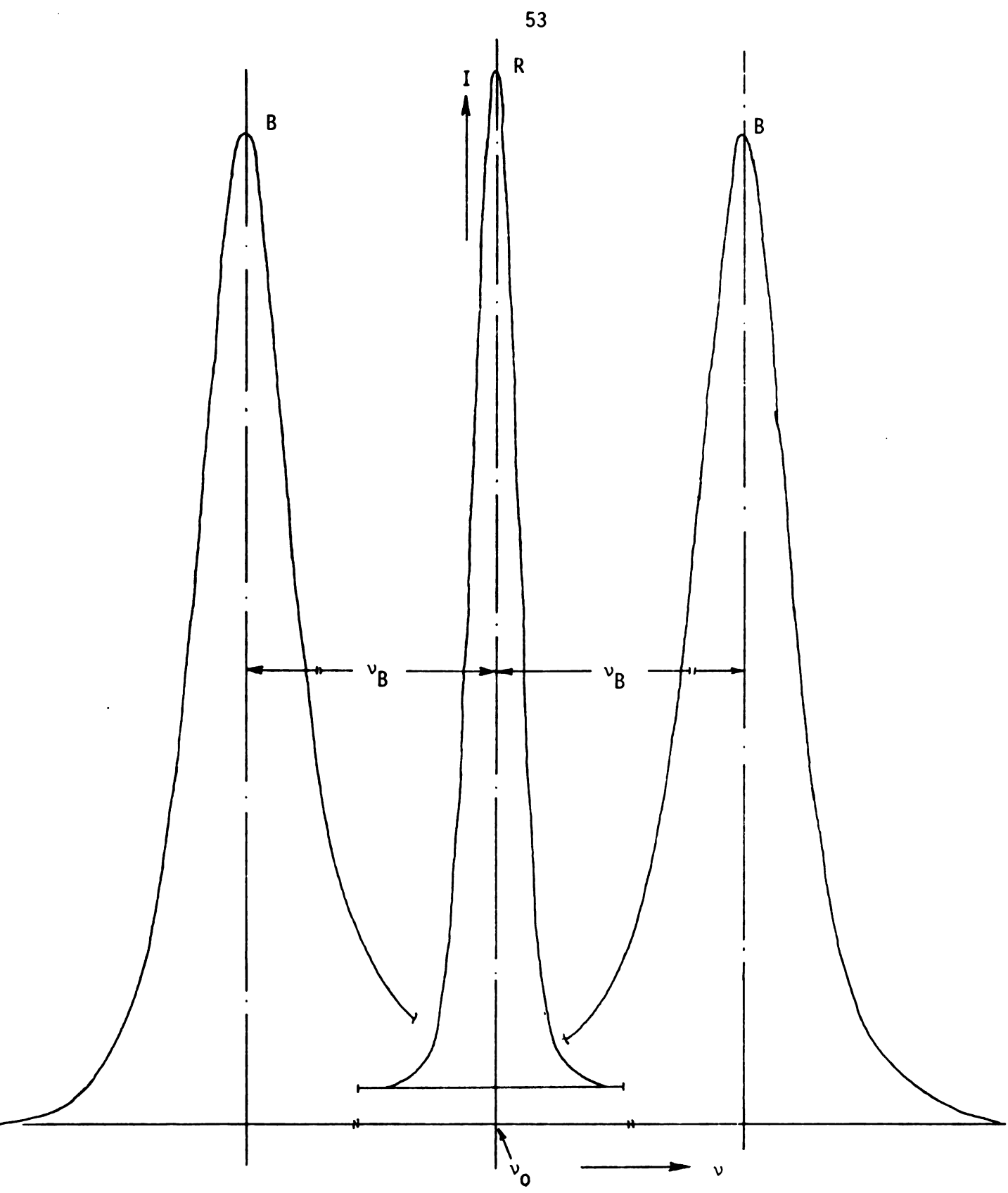


Fig. 16. Spectrum for D₅ at 45°C, θ = 90° and λ ₀ = 5145 Å.

Te

Tc

24 29

34.

38

43

48

53

58 67.

77.

TABLE 5
Observed Brillouin Frequency Shifts (ν_B), Velocities (ν_S), Temporal Attenuation Coefficients (ν_B), Life Times (ν_B) and Spatial Attenuation Coefficients (ν_B) of MM

as a Function of Temperature.

 $r_{\rm B} \times 10^6 \quad \frac{1}{r_{\rm R}} \times 10^{-9} \quad \alpha = \frac{r_{\rm B}}{V_{\rm S}}$ ν_B x 10⁹ V_S Temp T_c (°C) Hz m sec Hz Hz 24.75 3.3438 882.37 95.403 10.482 1081.22 29.32 3.3507 885.92 96.013 10.415 1083.76 34.21 3.3193 879.40 87.785 11.392 998.22 38.88 3.1485 835.70 97.978 10.206 1172.27 92.919 43.84 3.0456 810.19 10.762 1146.88 48.60 2.9640 790.06 88.668 11.278 1122.29 2.9071 53.30 776.46 102.970 9.712 1326.15 58.25 89.762 2.7766 743.14 11.141 1207.88 67.80 2.6210 704.40 82.404 12.135 1169.85 77.60 2.5600 690.92 80.628 12.403 1166.96

TABLE 6 Observed Brillouin Frequency Shifts (ν_B), Velocities (ν_S), Temporal Attenuation Coefficients (ν_B), Life Times (ν_B)

and Spatial Attenuation Coefficients of $\ensuremath{\mathsf{MD}_3}\xspace^{\ensuremath{\mathsf{M}}\xspace}$ as Function of Temperature.

Temp	ν _B x 10 ⁹	٧s	ΓВ	$\frac{1}{\Gamma_{\rm B}} \times 10^{-9}$	$\alpha = \frac{\Gamma_B}{V_S}$
T _c (°C)	Hz	m sec	x 10 ⁶ Hz	Hz	Cm ⁻¹
24.75	3.6342	948.40	163.195	6.128	1720.74
29.32	3.5738	934.04	155.747	6.420	1667.46
34.21	3.4704	908.46	156.480	6.391	1722.46
38.88	3.4326	899.99	161.726	6.183	1796.98
43.84	3.4224	898.81	143.424	6.972	1595.71
48.60	3.2903	865.48	139.262	7.181	1609.08
53.30	3.2445	8 54 .73	140.909	7.097	1648.58
58.25	3.1803	839.23	115.959	8.624	1381.74
67.80	3.0770	814.55	119.022	8.402	1461.19
77.60	2.9343	779.84	95.356	10.487	1222.76

TABLE 7

Observed Brillouin Frequency Shifts (ν_B), Velocities (V_S), Temporal Attenuation Co-efficients (Γ_B), Life Times ($\frac{1}{\Gamma_B}$) and Spatial Attenuation Co-efficient (α) of IID₇M as a Function of Temperature.

Temp.	ν _B x 10 ⁻⁹	v _s	$r_{\rm B} \times 10^{-6}$	$\frac{1}{\Gamma_{\rm B}} \times 10^{-9}$	$\alpha = \frac{\Gamma_n}{V_S}$
(°C)	Hz	m sec	Hz	sec	Cm ⁻¹
22.35	3.8265	9 9 8.6	195.082	5.1260	1953.45
29.60	3.8026	992.4	208.338	4.800	2099.30
40.31	3.6327	948.1	196.455	5.090	2072.18
49.97	3.5867	936.1	174.090	5.744	1854.80
57.35	3.5035	914.43	140.945	7.095	1541.48

.

Obser

Ten

and S

Temp

T_c(°C)

24.75

29.32

34.21

38.88

43.84

48.60

53.30

58.25

67.80

77.60

and Spatial Attenuation Coefficients (α) of D.C. 200 fluid,100 cts. as a Function of Temperature.

Temp	ν _B x 10 ⁹	v _s	г _в х 10 ⁶	$\frac{1}{10^{-9}} \times 10^{-9}$	$\alpha = \frac{\Gamma_B}{V_S}$
T _c (°C)	Hz	m sec	Hz	Hz	Cm ⁻¹
24.75	3.9334	1017.6	260.96	3.8321	2564.3
29.32	3.6476	944.9	216.96	4.609	2296.2
34.21	3.6812	954. 9	220.26	4.540	2306.7
38.88	3.6992	960.7	192.25	5.201	
43.84	3.5638	926.8	196.73	5.083	2122.7
48.60	3.5799	932.1	213.16	4.691	2286.7
53.30	3.6466	950.7	209.63	4.770	2204.9
58.25	3.4067	889.4	197.49	5.064	2220.4
67.80	3.3670	881.3	195.79	5.103	2221.4
77.60	3.2554	854.4	198.58	5.035	2324.3

ě

		•	
			. •
			ž.
			4 ¹ .
			Ş
			2.4
			¥ .

TABLE 9 Observed Brillouin Frequency Shifts (ν_B), Velocities (V_S), Temporal Attenuation Coefficients (Γ_B), Life Times ($1/\Gamma_B$)

and Spatial Attenuation Coefficients (α) of D.C. 200 Fluid, $10^5 \text{ Cts as a Function of Temperature}.$

Temp	ν _B x 10 ⁻⁹	v_{s}	г _в х 10 ⁶	$\frac{1}{\Gamma_{\rm B}} \times 10^{-9}$	$\alpha = \frac{\Gamma_B}{V_S}$
T _c (°C)	Hz	m sec.	Hz	Hz	Cm ⁻¹
24.75	4.2614	1102.2	144.32	6.929	1309.35
29.32	4.0813	1056.8	137.68	7.263	1302.75
34.21	4.1456	1074.8	140.69	7.108	1308.99
38.80	3.9852	1034.5	186.07	5.374	1798.65
43.84	3.8796	1008.4	142.87	6.999	1416.89
48.60	3.8311	997.1	161.93	6.176	1624.02
53.30	3.9480	1028.7	154.92	6.455	1505.91
5 8.25	3.7388	975.5	136.46	7.328	1398.88
62.90	3.6730	959.5	119.39	8.376	1244.26
67.80	3.538	925.3	140.28	7.128	1516.03
77.60	3.489	915.0	133.11	7.513	1454.68

TABLE 10

Observed Brillouin Frequency Shifts (ν_B), Velocities (ν_S), Temporal Attenuation Co-efficients (ν_B), Life Times (ν_B) and Spatial Attenuation Co-efficients (ν_B) of D₅ as a Function of Temperature.

T _c	ν _B x 10 ⁹	V _S	г _в х 10 ⁶	$\frac{1}{\Gamma_{\rm B}}$ x 10^{-9}	$\alpha = \frac{\Gamma_B}{V_S}$
(°C)	Hz	m sec.	Hz	Sec.	Cm ⁻¹
24.75	3.6416	947. 8	245.91	4.067	2594.5
29.32	3.4905	908.5	222.39	4.497	2447.9
34.21	3.3999	884.9	202.55	4.937	2289.0
38.88	3.3748	878.4	211.47	4.729	2407.5
43.84	3.3036	859.8	174.85	5.719	2033.5
52.58	3.1891	830.0	162.01	6.173	1951.8

TABLE 11

Observed Brillouin Frequency Shifts (ν_B), Velocities (V_S), Temporal Attenuation Co-efficients (Γ_B), Life Times ($\frac{1}{\Gamma_B}$) and Spatial Attenuation Co-efficients (α) of D $_3$ as a Function of Temperature.

Temp.	ν _B x 10 ⁹	V _S	$r_B \times 10^6$	$\frac{1}{\Gamma_{\rm B}}$ x 10^{-9}	$\alpha = \frac{\Gamma_B}{V_S}$
T _c (°C)	Hz	m sec	Hz	Hz	Cm ⁻¹
62.90	2.8279	752.50	118.438	8.4 43	1573.9
67.80	2.8162	750.86	119.278	8.384	1588.5
72.64	2.7336	730.29	102.283	9.777	1400.6
77.60	2.6346	705.25	120.842	8.275	1713.5
82.28	2.5949	695.89			

TABLE 12 Observed Brillouin Frequency Shifts (v_B), Velocities (V_S), Temporal Attenuation Co-efficients (V_B), Life Times (V_B) and Spatial Attenuation Coefficients (V_B) of V_B 0 as a Funtion of Temperature.

Temp.	ν _B x 10 ⁹	V _S	г _В х 10 ⁶	$\frac{1}{\Gamma_{\rm B}} \times 10^{-9}$	$\alpha = \frac{\Gamma_{B}}{V_{S}}$
T _c (°C)	Hz	m sec.	Hz	Hz	Cm ⁻¹
24.75	3.9828	1027.06	266.25	3.756	2592. 3
29.32	3.9211	1013.01	239.30	4.179	2362.2
34.21	3.7909	981.34	271.65	3.681	2768.1
38.88	3.5829	9 29. 21	269 .6 8	3.708	2902.2
43.84	3.7233	967.62	275.48	3.630	28 47. 0
48.60	3.6591	952.76	256.60	3.897	2693.2
53.30	3.5547	927.37	241.67	4.138	2605.9
58.25	3.5222	920 76	233.05	4.291	2531.1
67.80	3.4099	894.94	215.91	4.6316	2412.5

and the second of the second o

33. The second of the second o

TABLE 13 Observed Brillouin Frequency Shifts (v_B), Velocities (V_S), Temporal Attenuation Co-efficients (V_B), Life Times (V_B) and Spatial Attenuation (V_B) of D₁₅ as a Function of Temperature.

Temp.	ν _B x 10 ⁹	v _s	$r_B \times 10^6$	$\frac{1}{\Gamma_{\rm B}} \times 10^{-9}$	$\alpha = \frac{\Gamma_{B}}{V_{S}}$
T _c (°C)	Hz	m sec.	Hz	Hz	Cm ⁻¹
24.75	4.0290	1040.6	246.72	4.053	2370.9
34.21	3.8941	1008.4	189.78	5.269	1882.0
38.80	3.951	1024.5	227.81	4.390	2223.6
53.30	3.6591	952.5	192.79	5.187	2024.0
58.25	3.6026	939.1	192.25	5.202	2047.1
62.90	3.6111	942.5	197.31	5.068	2093.5
77.60	3.3734	884.1	187.87	5.323	2125.0

Liquid	Α	$B = (\frac{9L}{9LB})$	Standard error
	Hz	Hz/°C	of estimate for A
MM	104	-0.284	3
MD ₃ M	199	-1.261	7
MD ₇ M	246	-1.574	12
D.C. 200 fluid, 100 cts.	247	-7.698	15
D.C. 200 fluid, 10 ⁵ cts.	163	-3.612	16

TABLE 15 Intercept and Slope for the Absorption Co-efficient-Temperature Relationship; α = A + BT_C.

Liquid	Α	$B = (\frac{\partial I}{\partial \alpha})$	Standard error
	cm^{-1}	cm ⁻¹ /°C	of estimate for A
MM	1017	2.365	46
MD ₃ M	2016	-0.100	82
MD ₇ M	2372	-11.682	134
D.C. 200 fluid 100 cts	1, 2429	-3.005	105
D.C. 200 fluid 105 cts	1, 1386	1.165	154

TABLE 16 Intercept and Slope for the Brillouin-shift- Temperature Relationship; $v_{\rm B}$ = A + BT $_{\rm C}$

Liquid	Α	$B = (\frac{\partial I^{c}}{\partial A^{B}})$	Standard error
	Hz	Hz/°C	of estimate for B
MM	3.812	-0.0170	0.045
MD ₃ M	3.947	-0.0130	0.021
MD ₇ M	4.053	-0.0096	0.022
D.C. 200 flu 100 cts.	id,4.079	-0.0105	0.062
D.C. 200 fluid 105 cts.	d, 4.567	-0.0142	0.062

TABLE 17 Intercept and Slope for the Sound Velocity-Temperature Relationship; $V_S = A + BT_C$.

Liquid	Α	$B = \left(\frac{\partial L^{c}}{\partial A^{c}}\right)$	Standard error
	m/sec.	m/sec/°C	of estimate for B
ММ	1010	-4.36	11
$MD_{3}M$	1021	-3.10	6
MD ₇ M	1058	-2. 50	6
D.C. 200 fluid 100 cts.	1050	-2.49	19
D.C. 200 fluid, 10 ⁵ cts.	1176	-3.44	16

Liquid	А	$B = (\frac{91}{9})$	Standard error	
	Hz	Hz/°C	of estimate for B	
D3	3.691	-0.0133	0.020	
^D 3 D ₅	3.940	-0.0140	0.022	
D ₉	4.240	-0.0126	0.064	
D ₁₅	4.357	-0.0125	0.041	

Liquid	Α	$B = \left(\frac{\partial V}{\partial T_{c}}\right)$	Standard error
	m/sec.	m/sec/°C	of estimate for A
D3	965	-3.272	5
D ₃ D ₅	1018	-3.375	6
D ₉	1045	-2.877	17
D ₁₅	1118	-2.990	11

TABLE 20 Intercept and Slope for the Brillouin Half-width ($\Gamma_{\rm B}$)-Temperature Relationship; $\Gamma_{\rm B}$ = A + BT $_{\rm C}$.

Liquid	Α	В	Standard error
	Hz	Hz/°C	of estimate for A
D ₃	129	-0.194	7
D ₅	230	-0.677	11
D ₉	293	-0.9 49	14
D ₁₅	249	-0.884	15

TABLE 21 $\label{eq:TABLE} \mbox{Intercept and Slope for the Absorption Co-efficient (α) - } \\ \mbox{Temperature Relationship; α = A + BT_{C}. }$

Liquid	Α	В	Standard error	
	Cm ⁻¹	cm ⁻¹ /°c	of estimate for A	
D_{3}	1231	4.808	108	
^D 3 D ₅	2261	1.050	120	
D ₉	268 9	-1.947	154	
D ₁₅	2230	-2.405	138	

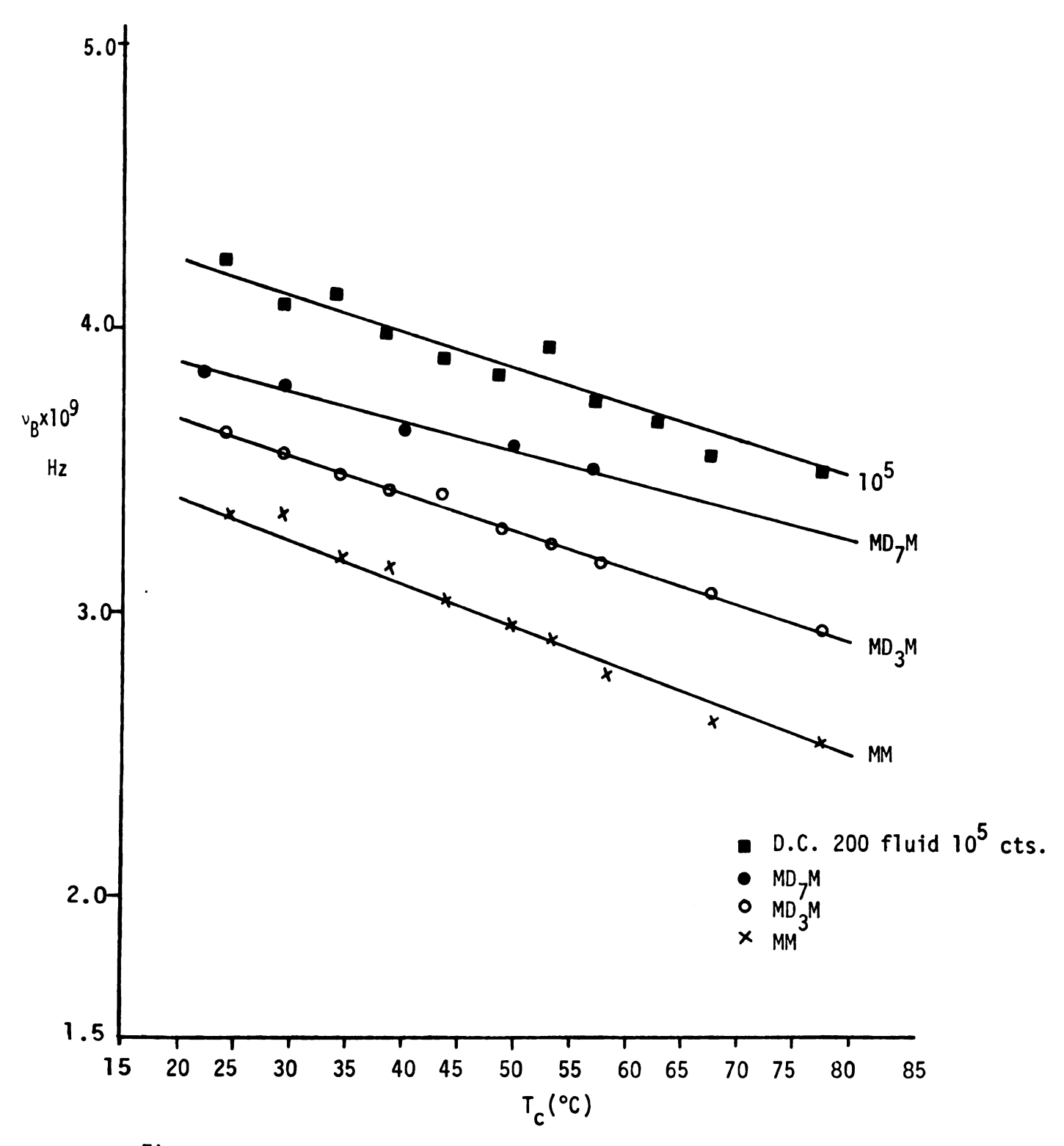


Figure 17. Brillouin Shift Versus Temperature for MM, MD $_3$ M, MD $_7$ M and D.C. 200 fluid, 10^5 cts.

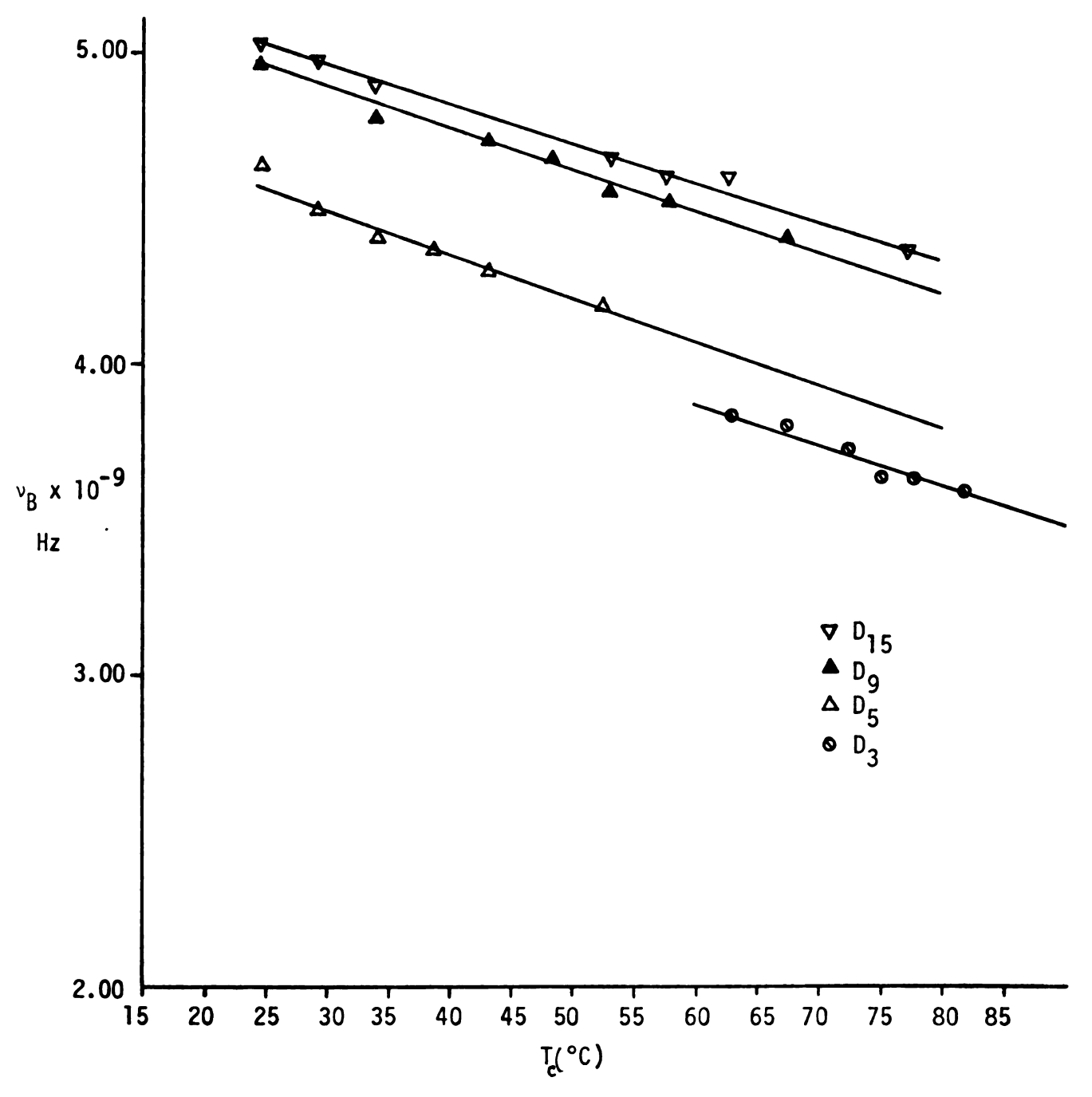


Figure 18. Brillouin Shift Versus Temperature for D_3 , D_5 , D_9 and D_{15} .

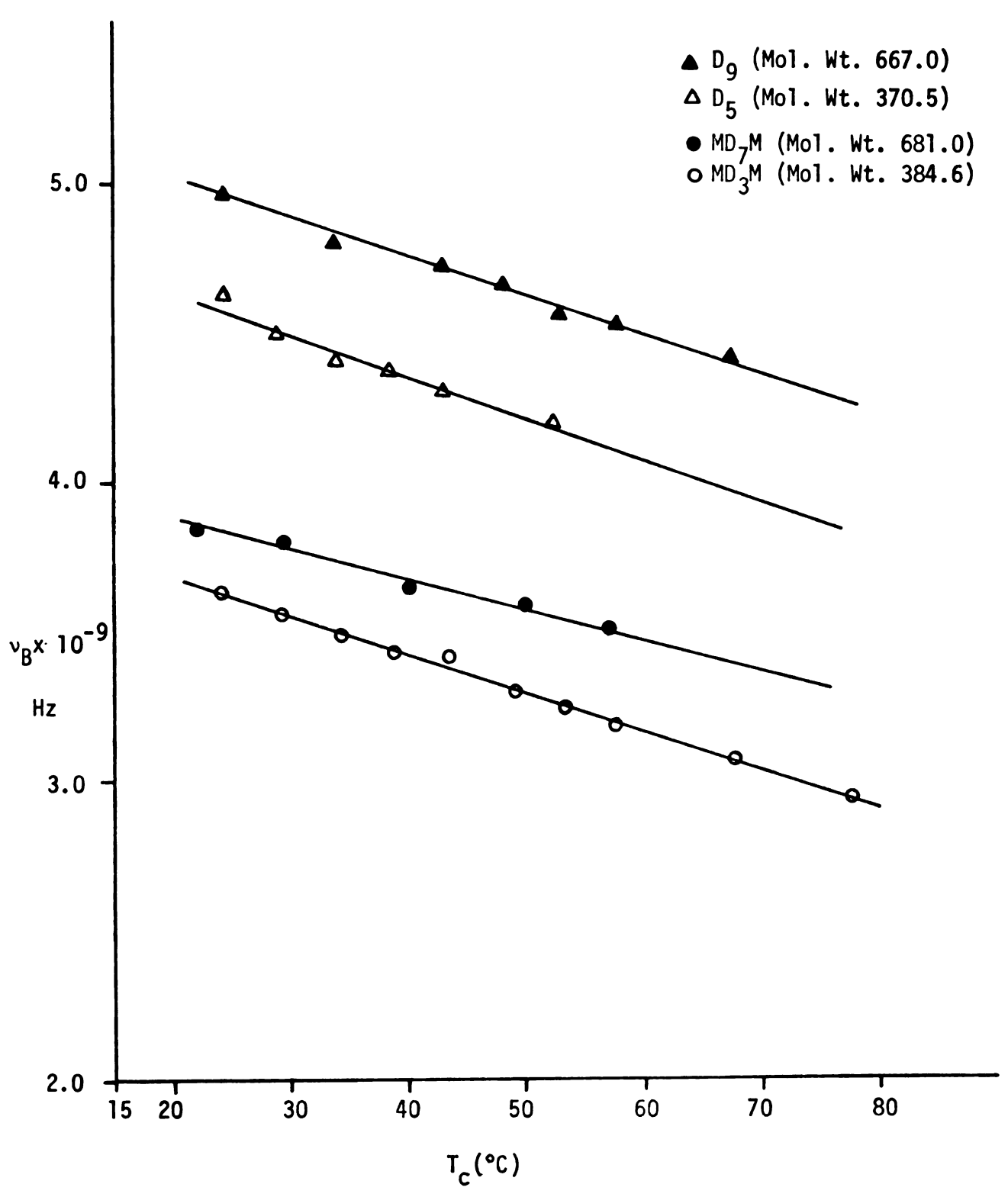
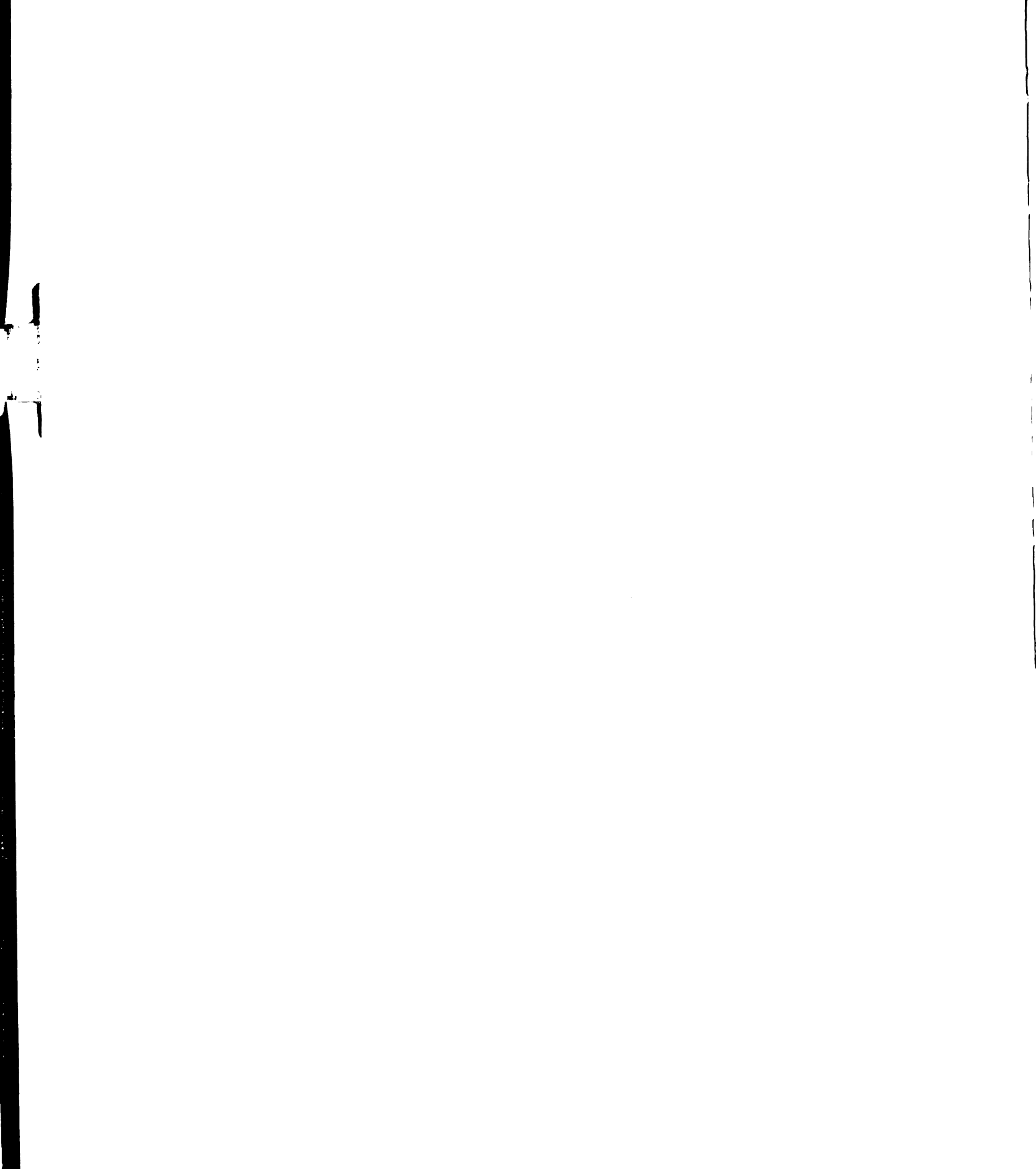


Figure 19. Brillouin Shift Versus Temperature for D_9 , D_5 , MD_7M and MD_3M .



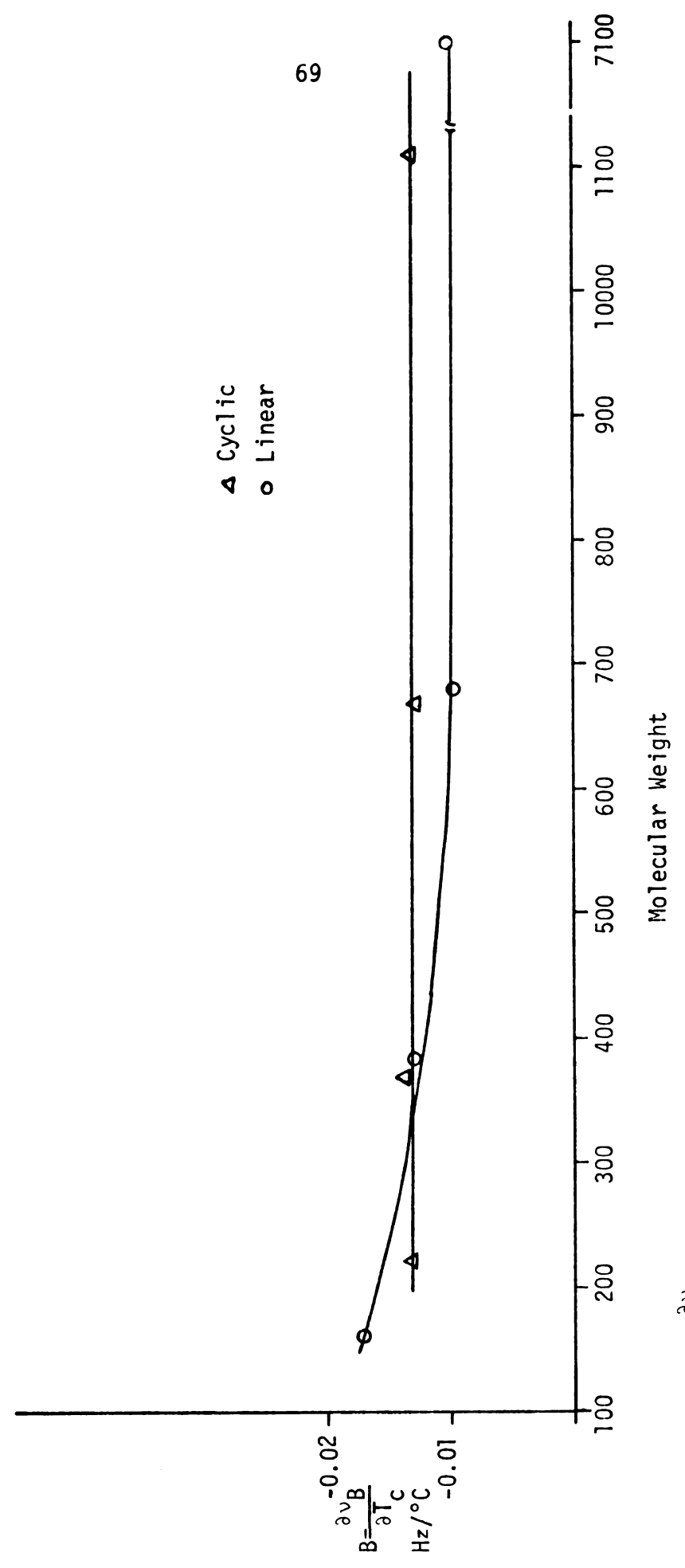


Figure 20. $\frac{3v_{B}}{3T_{c}}$ Versus Molecular Weight for Linear and Cyclic Silicones.

3. Dispersion Measurements.

The frequency shift of the Brillouin peaks v_B increases with an increasing scattering angle θ and is given by Eq. 22 (See Tables 22 and 23). Thus by increasing the angle θ we select pressure fluctuations of higher frequencies; the velocity of sound can then be calculated at the same frequencies. A plot of the Brillouin-shift against $\sin(\frac{\theta}{2})$, where θ is the scattering angle, shows a linear relationship (Figure 21). If dispersion were present in the sound velocity the relation between v_B and $\sin\frac{\theta}{2}$ would be nonlinear; so in the frequency range of interest, there is no dispersion in the velocity of sound for linear and cyclic silicones.

TABLE 22

Variations in Brillouin Frequency-Shifts (ν_B), Velocities (V_S), Temporal Attenuation Co-efficients (Γ_B), Life-Times ($\frac{1}{\Gamma_B}$), Spatial Attenuation Co-efficient (α) and Landau-Placzek Ratio (J_V) of MD₇M with Scattering Angle (θ).

0°	Sin $\frac{\theta}{2}$	ν _B x 10 ⁹	v _s	$r_{B} \times 10^{-6}$	$\frac{1}{10} \times 10^{-9}$	$\alpha = \frac{\Gamma_B}{V_S}$
		Hz	m/sec	Hz	Sec.	Cm ⁻¹
45°	0.3827	2.3665	1141.16	85.085	11.753	745.611
60°	0.50	2.7251	1005.79	97.144	10.294	965.850
75°	0.6088	3.2960	999.08	149.050	6.709	1491.880
90°	0.707	3.9068	1033.70	200.203	4.995	1936.750
105°	0.7934	4.3230	1005.50	262.403	3.810	2609.600
120°	0.8660	4.5978	979 .7 8	301.180	3.320	3073.950
135°	0.9239	5.0720	1013.08	356.732	2.803	3521.200

Temp.	Ic	IB	JV	Fineness
(°C)				
20.44	1.80	3.866	0.2332	41.0
20.40	2.00	4.165	0.2401	39.4
20.28	1.24	2.430	0.2551	31.3
20.40	2.65	4.840	0.2732	44.7
20.40				41.2
20.36	1.31	2.295	0.2843	41.0

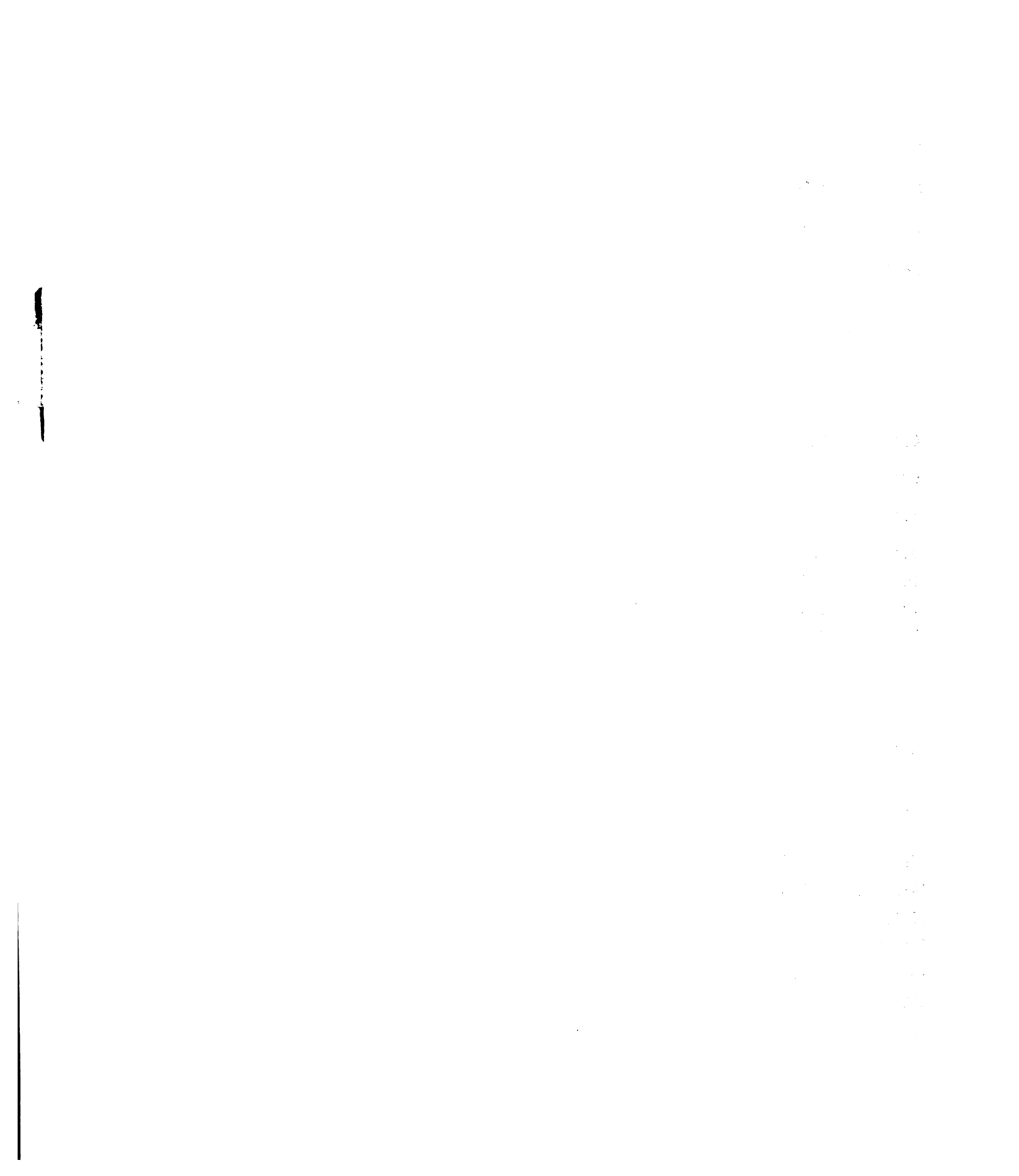


TABLE 23

Variations in Brillouin Frequency - Shifts (ν_B), Velocities, Temporal Attenuation Coefficient (Γ_B), Life Times ($\frac{1}{\Gamma_B}$), Spatial Attenuation Coefficient (α) and Landau-Placzek Ratio (J_V) of D_5 with Scattering Angle (θ).

θ•	Sin $\frac{\theta}{2}$		ν _B 9 Hz	V _S m/sec	г _в х 10 ⁶ Hz	$\frac{1}{\Gamma_{B}} \times 10^{-9}$ Cm ⁻¹
45°	0.3827	2.	1077	1013.6	80.462	12.428
60°	0.500	2.7	7861	1025.5	145.568	6.870
75°	0.6088	3.0	0829	932.0	180.968	5.526
90°	0.7071	3.	582	932.3	200.306	4.992
105°	0.7934	4.	189	971.7	261.880	3.819
▼ 20°	0.8660	4.	580	973.4	314.867	3.176
135°	0.9239	4.8	885	973.1	392.462	2.548
$\alpha = \frac{\Gamma_E}{V_\zeta}$ Cm^{-1}	<u>з</u> т _с ((°C)	I _c	I _B	J _V	Fineness
793.81	14 19.	.70°C	4.000	8.145	0.2456	30
1419.47	⁷ 5 19.	.68°C	3.235	6.717	0.2408	35
1941.80	06 19.	.65°C	3.835	7.100	0.2701	39
2148.52	24 19.	.7°C	3.900	6.792	0.2871	30
2694.95	50 19.	.7°C	2.275	3.76 0	0.3025	31
3234.73	30 19.	.65°C	2.140	3.700	0.2892	34
4033.19	90 19.	.65°C	3.020	5.757	0.2623	34

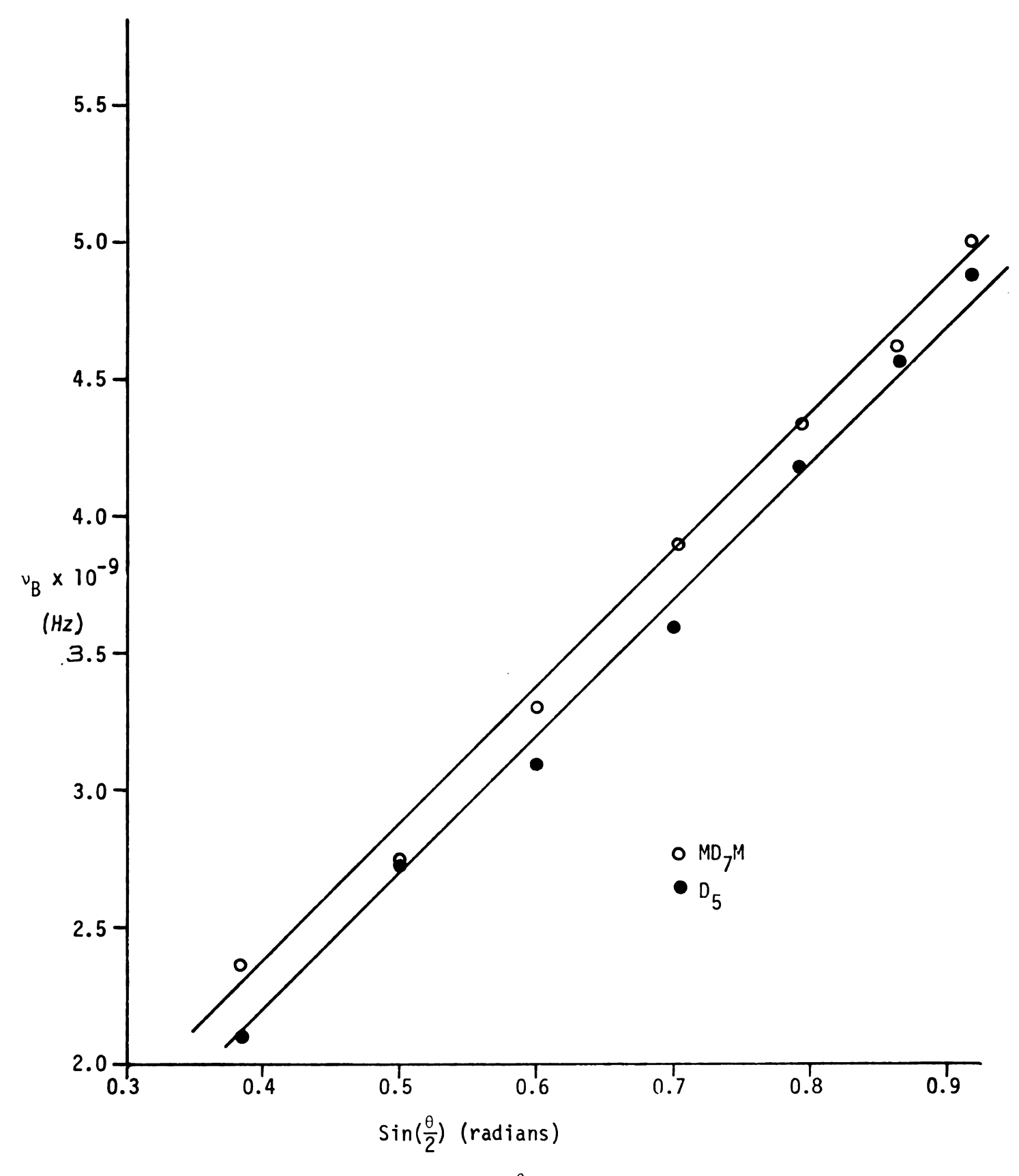


Figure 21. Brillouin-shift Versus Sin $\frac{\theta}{2}$ for MD_7M and $\text{D}_5.$

4. Velocity of Sound V_S and Adiabatic Compressibility β_S .

Ultrasonic data in the megahertz range have been used for monitoring structural changes in liquid silicones [36,37,54]; hypersonic data in the gigahertz range obtained from Brillouin scattering can be used to give analogous information at different frequency intervals. The velocity of sound in a liquid varies with the compressibility, which in turn is related to intermolecular forces.

Velocity of sound results calculated by means of the Brillouin scattering technique and from ultrasonic data are in very good agreement, as can be seen from Table 24 and Figure 22.

Table 24

Molecular	Velocity of Sound*
Wt.	m sec.
162.2	873.2
236.3	901.3
310.4	919.0
384.5	931.3
520.0	942.2
720.0	953.8
1,160.0	966.5

^{*} Ultrasonic measurements by Weissler $^{[36]}$.

If there is no structural change in going from one liquid to another, then the change in the velocity of sound of the different liquids (i.e., of different molecular weights) will be a smooth, continuous function and the change in $\frac{dV_S}{dT_C}$ with molecular weight will be a function with the same

properties.

Tables 5-13 display Brillouin frequency shifts and velocities of sound as functions of temperature for linear and cyclic silicones. Tables 17 and 19 contain values for $\frac{dV_S}{dT_C}$ for all of the silicones investigated. The velocity-temperature curve for each liquid satisfies the linear relationship $V_S = A + BT_C$.

From Figures 22 and 23 it is clear that there is a nonlinear dependence between the velocity of sound and molecular weight for linear and cyclic compounds. Figures 24 and 25 show that for every liquid investigated the velocity of sound and temperature were linearly related, but with different slopes. Figure 26 provides a better comparison between linear and cyclic compounds having about the same molecular weight.

It is clear from all these graphs that if the basic structure of the silicones is changed, (linear to cyclic or cyclic to linear) then a sharp change in their properties will occur. It can be seen in Figure 27 that the relationship between $\frac{dV_S}{dT_C}$ and molecular weight for the cyclic compound is linear, whereas for the linear compound the same relation is nonlinear.

The adiabatic compressibility β_S can be calculated from velocity of sound and density data by means of Eq. (49).

Table 25 contains values of β_S for silicones at 22.0°C, while Table 26 contains the corresponding values for D₉ and D₁₅.

The adiabatic compressibility of a liquid is inversely proportional to the force of attraction between its molecules, which in turn depends directly on the velocity of sound in the liquid. By examining changes of $\frac{dV_S}{dT_C}$ with molecular weight and temperature, insight into local structural changes can be gained.

It is obvious from Figure 28 that as the molecular weight is increased the adiabatic compressibility decreases. This indicates that intermolecular forces are increasing as the molecular weight increases for both linear and cyclic silicones. It can also be concluded from Figure 28 that the adiabatic compressibilities of the linear silicones are greater than those of the cyclic silicones for the same molecular weight. The implication is that in this case intermolecular forces are stronger in cyclic chains than in linear chains.

Figure 29 shows that β_S increases linearly as the temperature is increased, which suggests that intermolecular forces (attraction between Si and 0) are decreasing with increasing temperature.

TABLE 25

Adiabatic Compressibility of MM, MD $_3$ M, MD $_7$ M, D.C. 200 fluid, 100 cts., D $_5$, D $_9$ and D $_{15}$ at 22°C.

Liquid	Velocity	Density	Adiabatic
	of Sound		Compressibility
	m sec.	g/ml	β _S
			Sq. cm/dyne
MM	898	0.7636	162.4×10^{-12}
MD ₃ M	953	0.8755	125.8×10^{-12}
MD ₇ M	998	0.9180	109.4×10^{-12}
D.C. 200 fluid 100	Cts.1048	0.9579	95.1 x 10 ⁻¹²
D ₅	962	0.9593	112.6 x 10 ⁻¹²
D ₉	1048	0.9756	93.3×10^{-12}
D ₁₅	1055	0.9737	92.3 \times 10 ⁻¹²

TABLE 26

Adiabatic Compressibility of ${\bf D_9}$ as a Function of Temperature.

T _c (°C)	Velocity of Sound	Density [*] g/ml	Adiabatic Compressibility
	m/sec.	•	βs
			Sq. Cm/dyne
24.75	1027.06	0.9756	97.2×10^{-12}
38.88	970.00	0.9624	110.4×10^{-12}
58.25	920.76	0.9440	124.9×10^{-12}

Adiabatic Compressibility of D_{15} as a Function of Temperature.

T _c (°C)	Velocity of Sound	Density*	Adiabatic Compressibility
	m/sec.	g/ml	^β s
			Sq. Cm/dyne
24.75	1044.0	0.9737	94.2×10^{-12}
38.88	1001.7	0.9610	103.7 x 10 ⁻¹²
58.25	943.8	0.9435	119.0 x 10 ⁻¹²

* Density measurements for D_9 and D_{15} at different temperatures were obtained from Dr. J. F. Hampton, Dow Corning Corporation, Midland, Michigan.

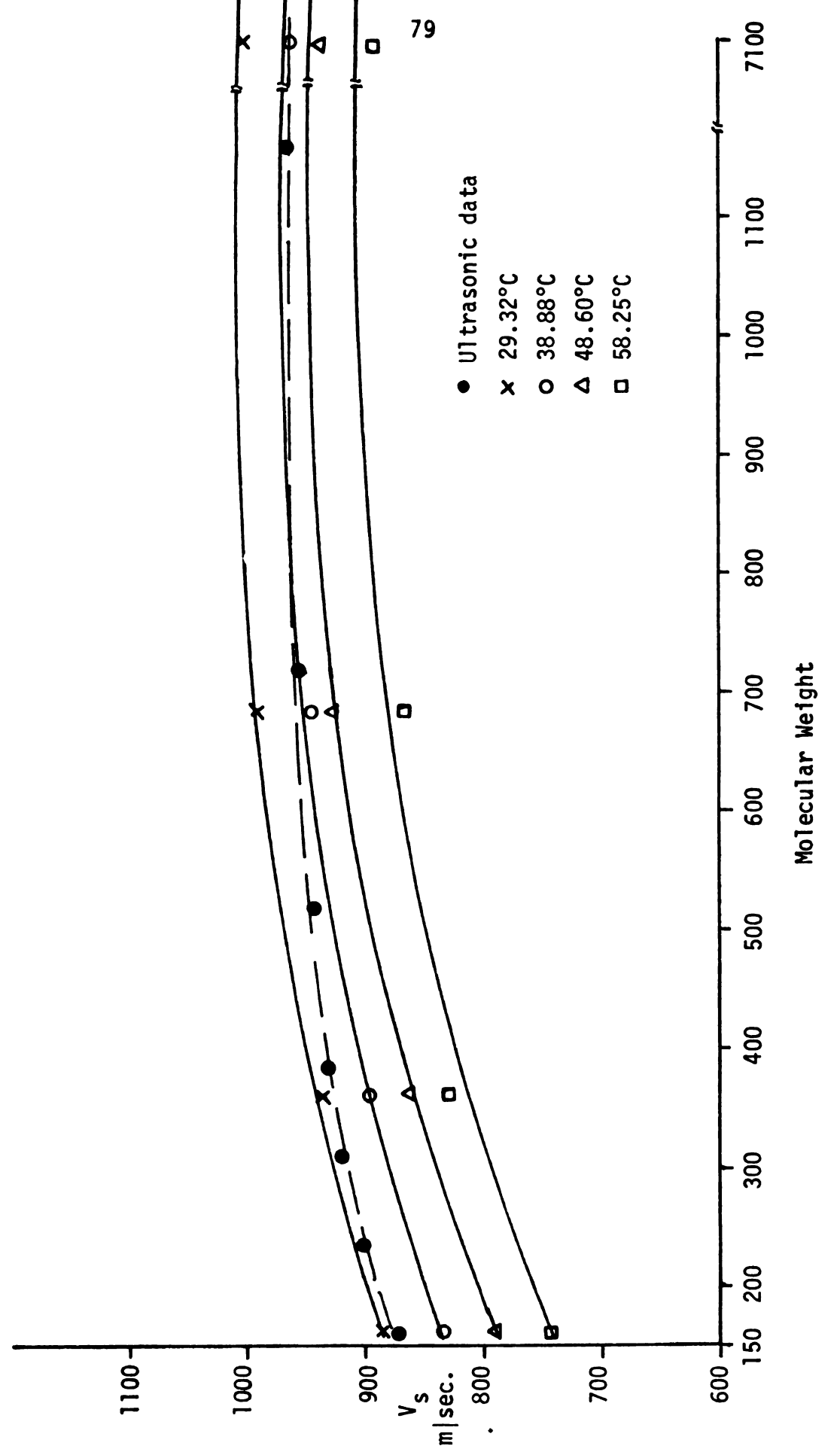


Figure 22. Velocity of Sound Versus Molecular Weight for Linear Silicones at 29.32°C, 38.88°C,

48.60°C, and 58.25°C.

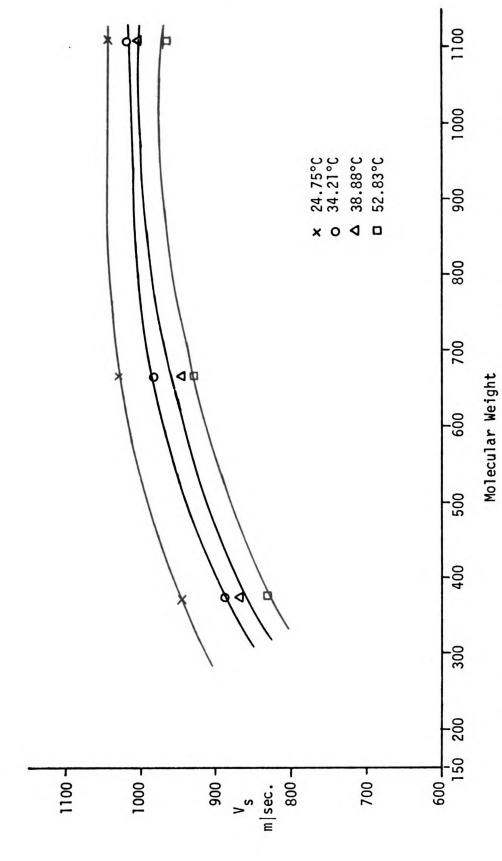


Figure 23. Velocity of Sound Versus Molecular Weight for Cyclic Silicones at 24.75°C, 34.21°C, 38.88°C, and 52.83°C.

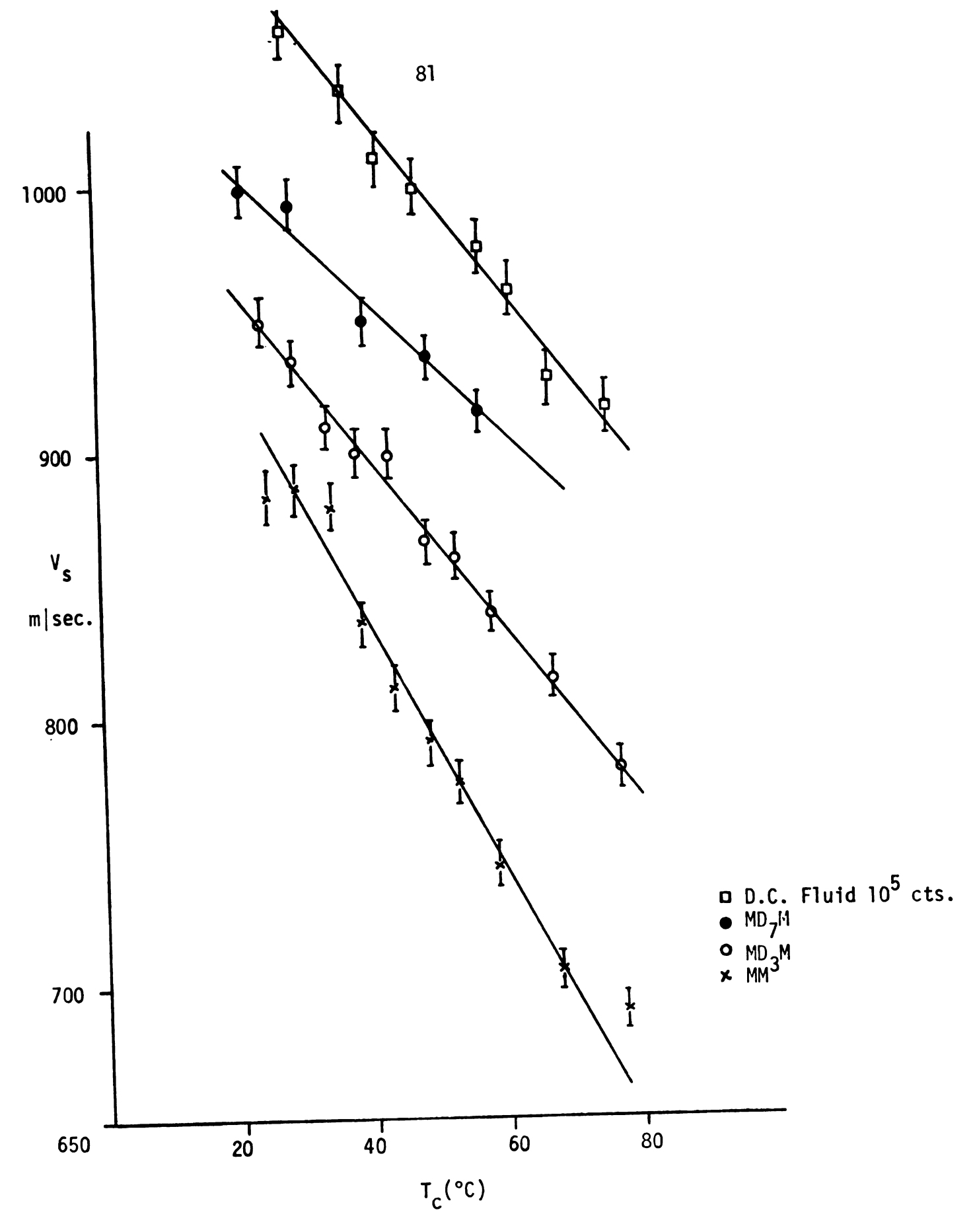


Figure 24. Variation of the Velocity of Sound with Temperature for MM, MD $_3$ M, MD $_7$ M and D.C. Fluid 10^5 cts.

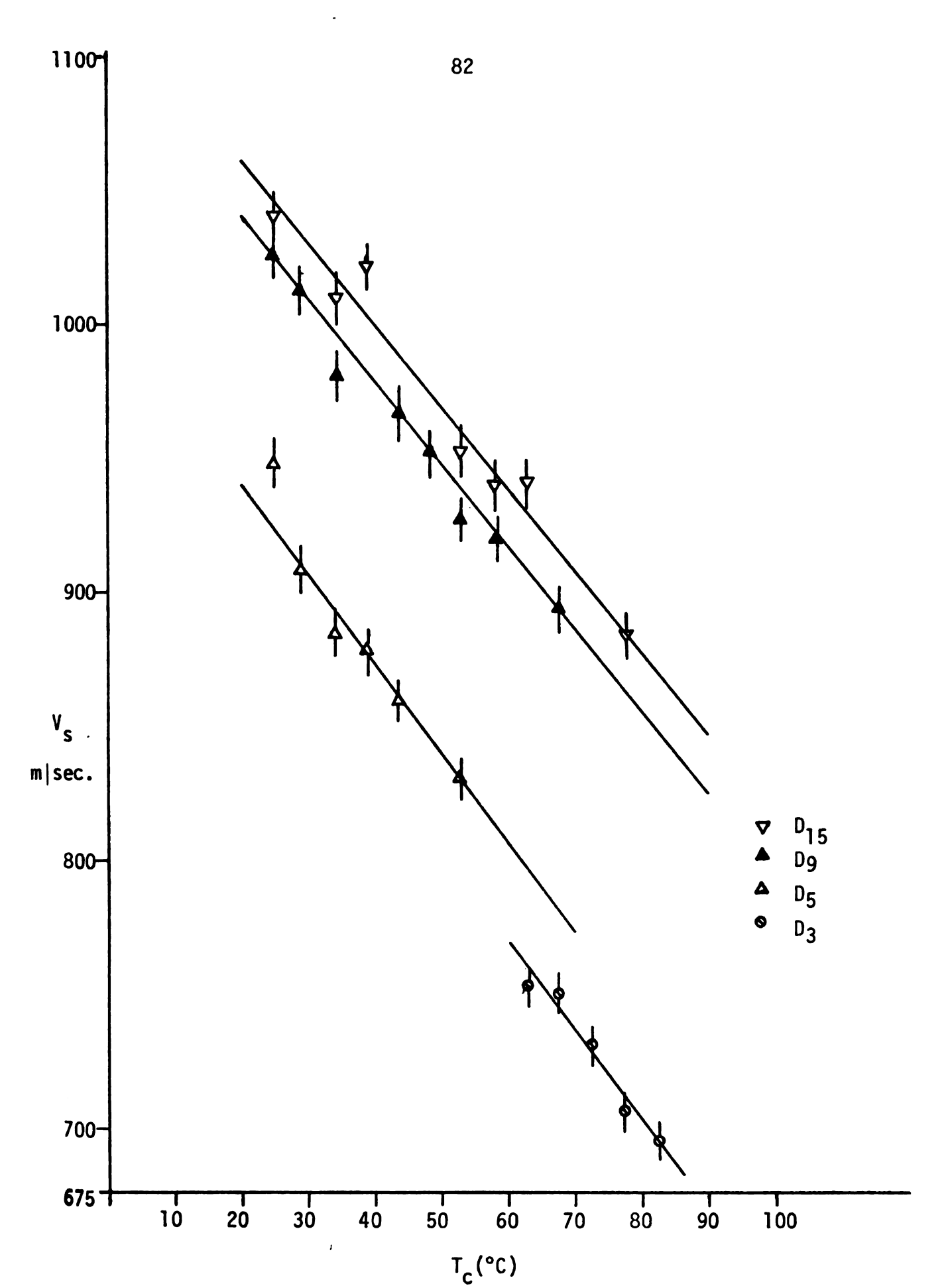


Figure 25. Variation of the Velocity of Sound with Temperature for $\rm D_3,\ D_5$ $\rm D_9$ and $\rm D_{15}$

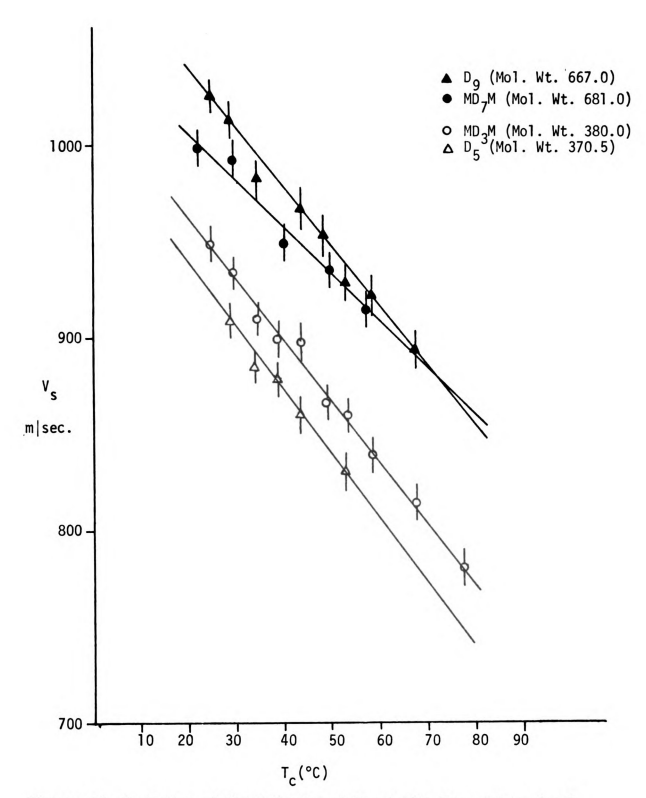


Figure 26. Variation of the Velocity of Sound with Temperature for $\rm D_{9}$, $\rm MD_{7}M$, $\rm MD_{3}M$ and $\rm D_{5}.$

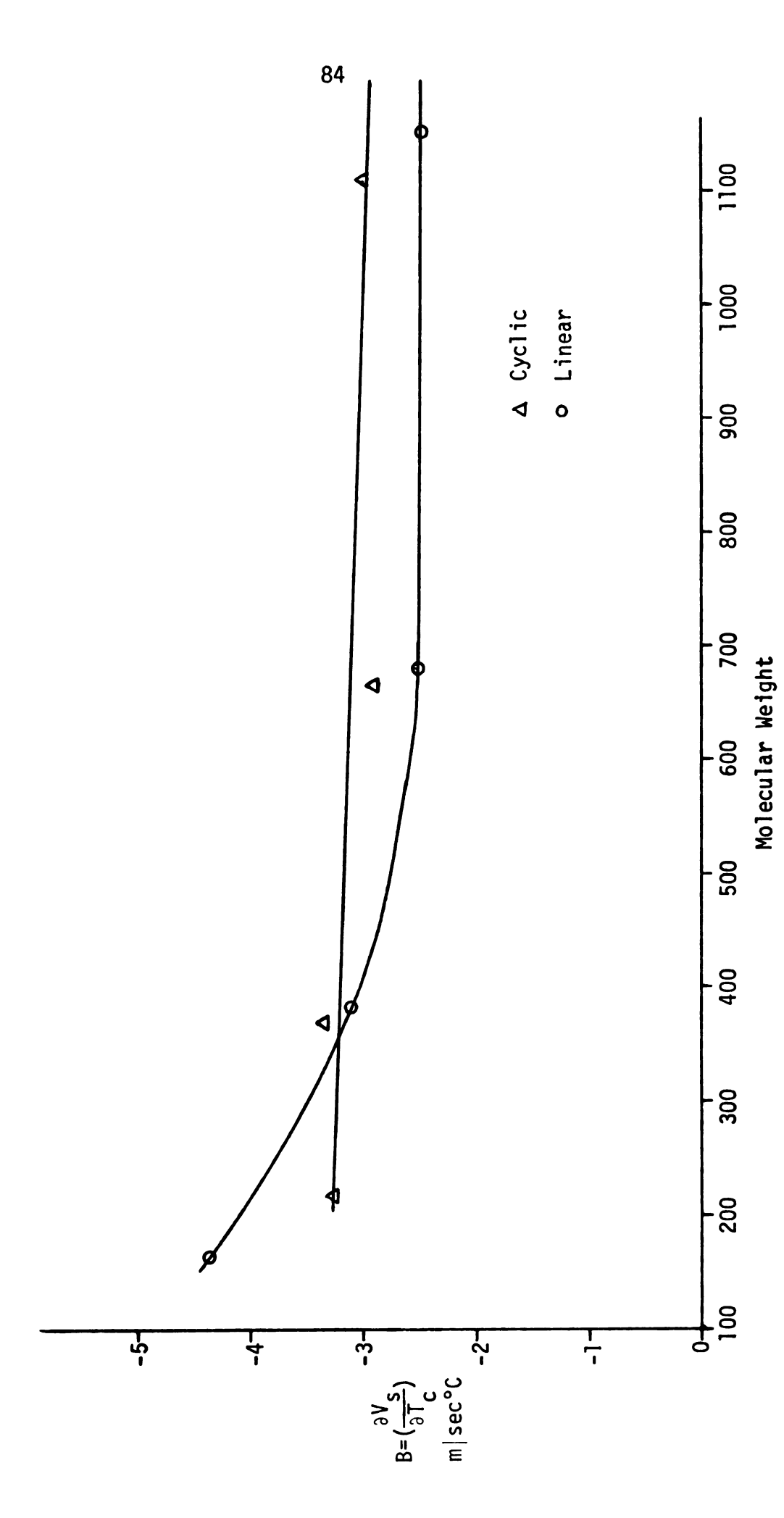


Figure 27. Temperature Co-efficient of the Velocity of Sound Versus Molecular Weight for Linear and Cyclic Silicones.

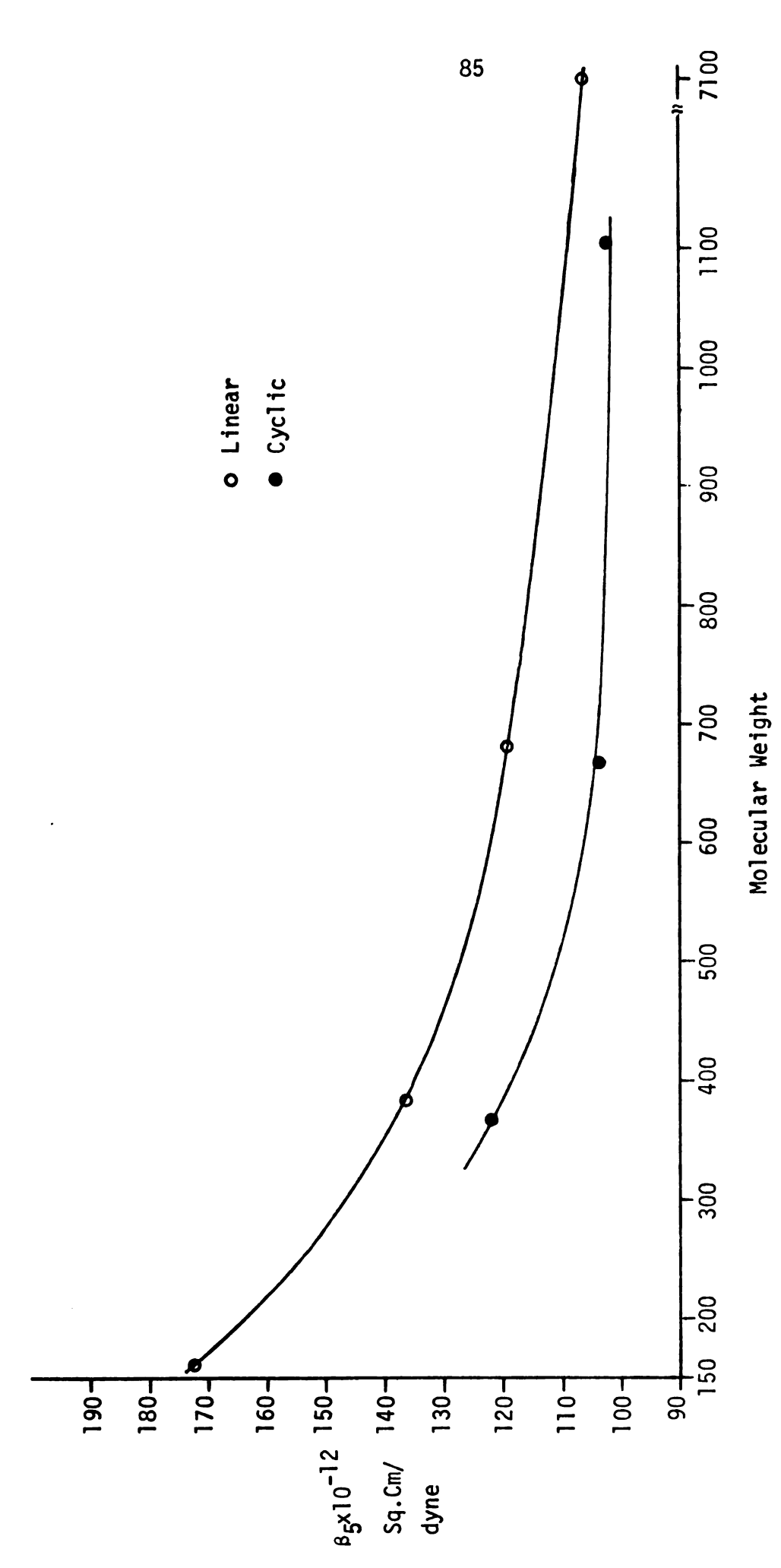


Figure 28. Adiabatic Compressibility as a Function of Molecular Weight at Constant Temperature of 22°C.

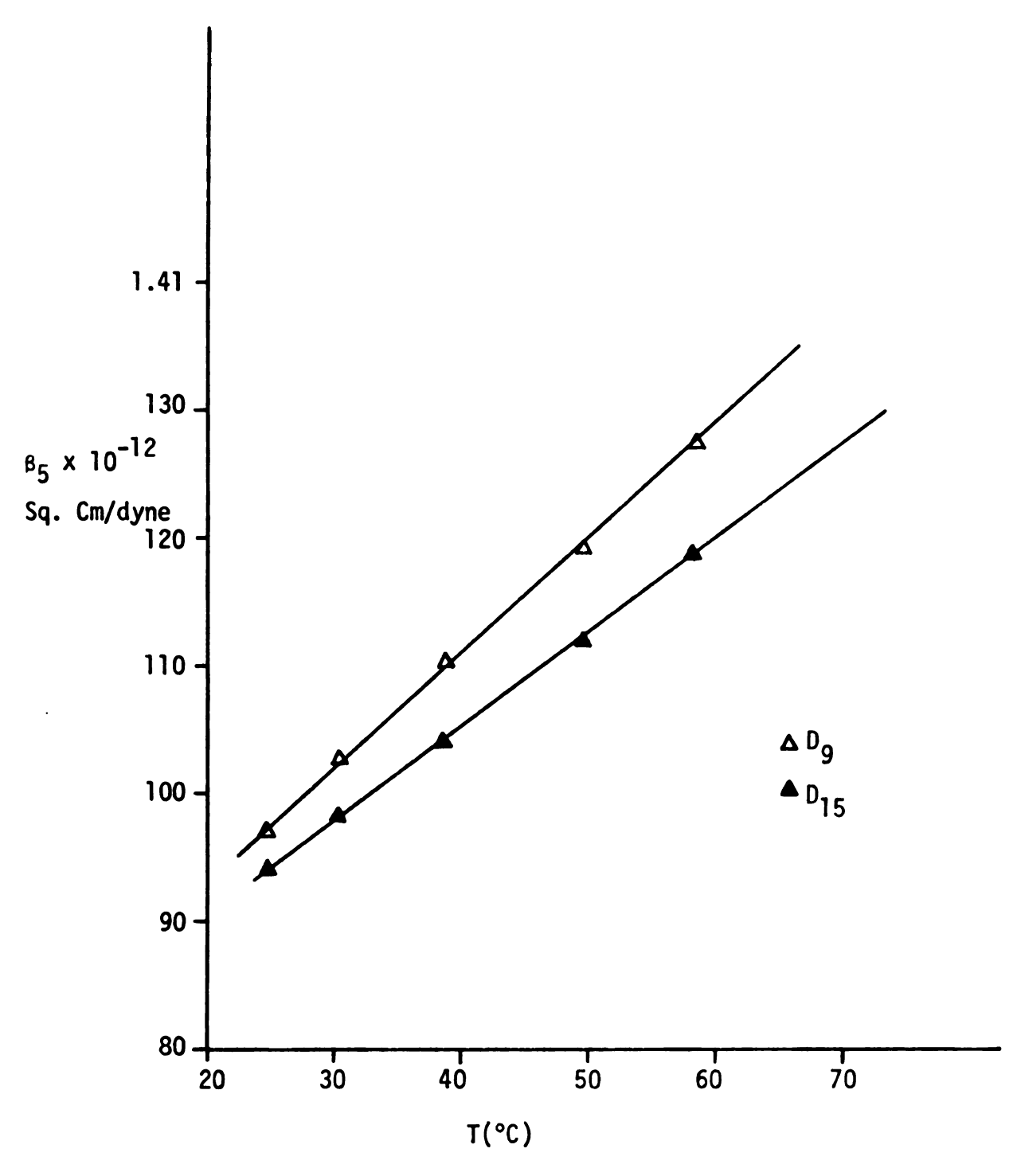


Figure 29. Adiabatic Compressibility Versus Temperature for $\mathbf{D_9}$ and $\mathbf{D_{15}}$.

5. Variation of the Brillouin Line Width r_B and the Sonic Absorption Coefficient α with Temperature and Molecular Weight.

For a nonrelaxing liquid the Brillouin spectrum contains three Lorentzian peaks [22] but for relaxing liquids each peak may represent a continuation of simple Lorentzian forms. If the peaks are simple Lorentzian shapes the true Brillouin line width $(2r_B)$ can be obtained from the following equation:

$$2\Gamma_{B} = 2\Gamma_{BO} - \Gamma_{C} \tag{51}$$

where Γ_{BO} is the observed line width of the Brillouin peak and Γ_{C} is the instrumental line width, which is the width of the central peak at its half-height. To identify the actual shapes thirty points were picked from each of the three peaks and compared with the analytical Lorentzian form. In general, the central portion of the experimental peak (approximately fifteen points) fitted the Lorentzian equation very well, while deviating slightly both at the top and at the bottom.

The calculated values of the Brillouin line widths (using Eq. 51) are tabulated in Tables 5-13 presented earlier. Values for $\frac{d\Gamma_B}{dT_C}$ are tabulated in Tables 14 and 20. Typical plots of Billouin line width versus temperature for different silicones are shown in Figures 30-31. For linear silicones the line width is found to decrease linearly with a rise in the temperature; however, for cyclic silicones the decrease is nonlinear with temperature. A plot of $\frac{d\Gamma_B}{dT_C}$ versus molecular weight for linear compounds shows an increasing nonlinear trend as molecular weight increases; for cyclic compounds the same trend occurs but terminates with an asymptotic approach to a single value (See Figure 32). The Brillouin line width also

has angular dependence, as predicted by Eq. 43. This dependence can clearly be seen in Tables 22 and 23 of Section 3.

According to hydrodynamic theory [54] the absorption co-efficient α is given by Eq. (50),

$$\alpha = \frac{\Gamma_{B}}{V_{S}} \qquad .$$

Tables 5-13 list values of the absorption co-efficient for all silicones studied as a function of the temperature T_{C} .

The absorption of sound is related to the effectiveness of the transfer of internal vibrational energy to translational energy in a liquid. It is believed that if the collisions between the molecules in a liquid are inefficient in producing a transfer of energy, the absorption will increase. On the other hand, if the efficiency of transfer of the internal vibrational energy into the translational energy is higher, then the absorption will decrease and sound propagation will be sustained longer. Due to temperature change there will be some structural change in the liquid, and this change should be reflected in the variation of the sonic absorption co-efficient with temperature because of modified molecular interactions.

Tables 15 and 21 give the experimental values for the temperature deviation of the sonic absorption co-efficient. From Figure 33 it can be seen that α decreases linearly with an increase in temperature, thereby indicating higher energy transfer. Figure 33 provides a comparative view of linear and cyclic silicones of about the same molecular weight. As the temperature is increased, intermolecular interaction increases; hence α decreases.

Values for the temperature derivative of the sonic absorption

co-efficient were also calculated for all of the silicones investigated; a typical graph of $\frac{d\alpha}{dT_C}$ versus molecular weight is shown in Figure 34. The negative values of $\frac{d\alpha}{dT_C}$ indicate that according to the classification scheme of Herzfeld and Litovitz^[54], these silicones are "associated fluids".

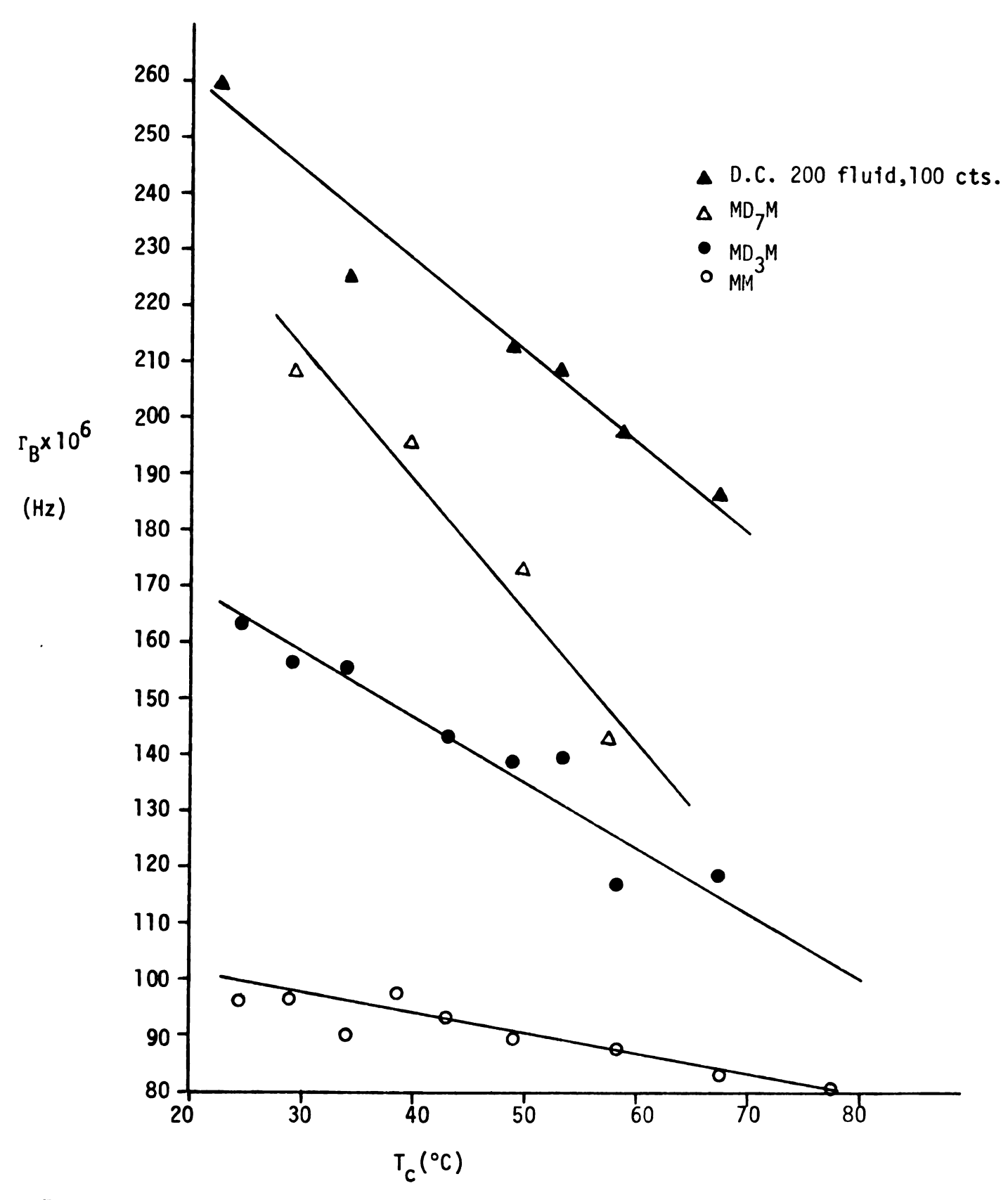


Figure 30. Half of Brillouin Line Width Versus Temperatures for MM, MD_3M , MD_7M and D.C. 200 fluid, 100 cts.

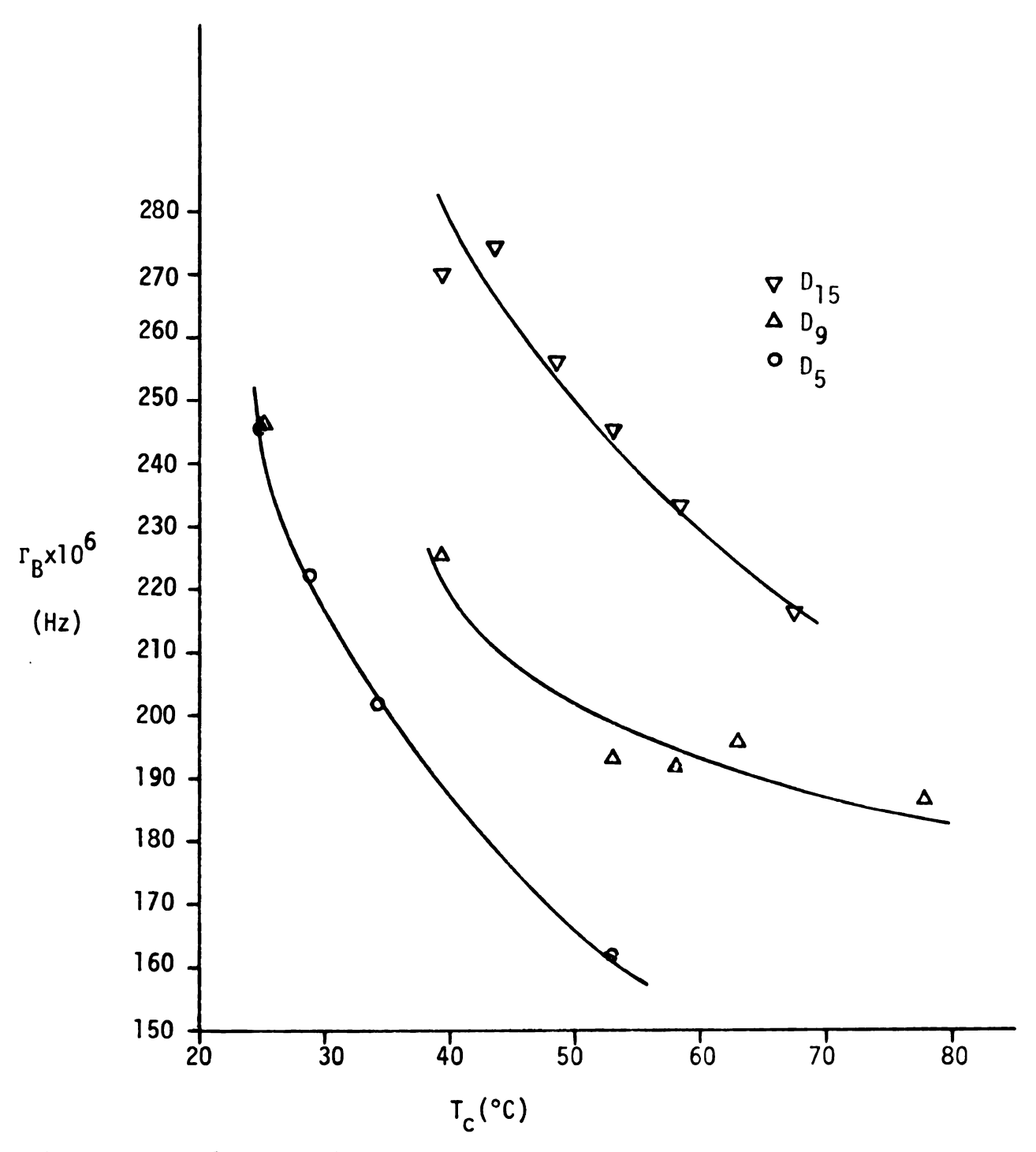


Figure 31. Half of Brillouin Line Width Versus Temperature for ${\rm D}_5$, ${\rm D}_9$ and ${\rm D}_{15}.$

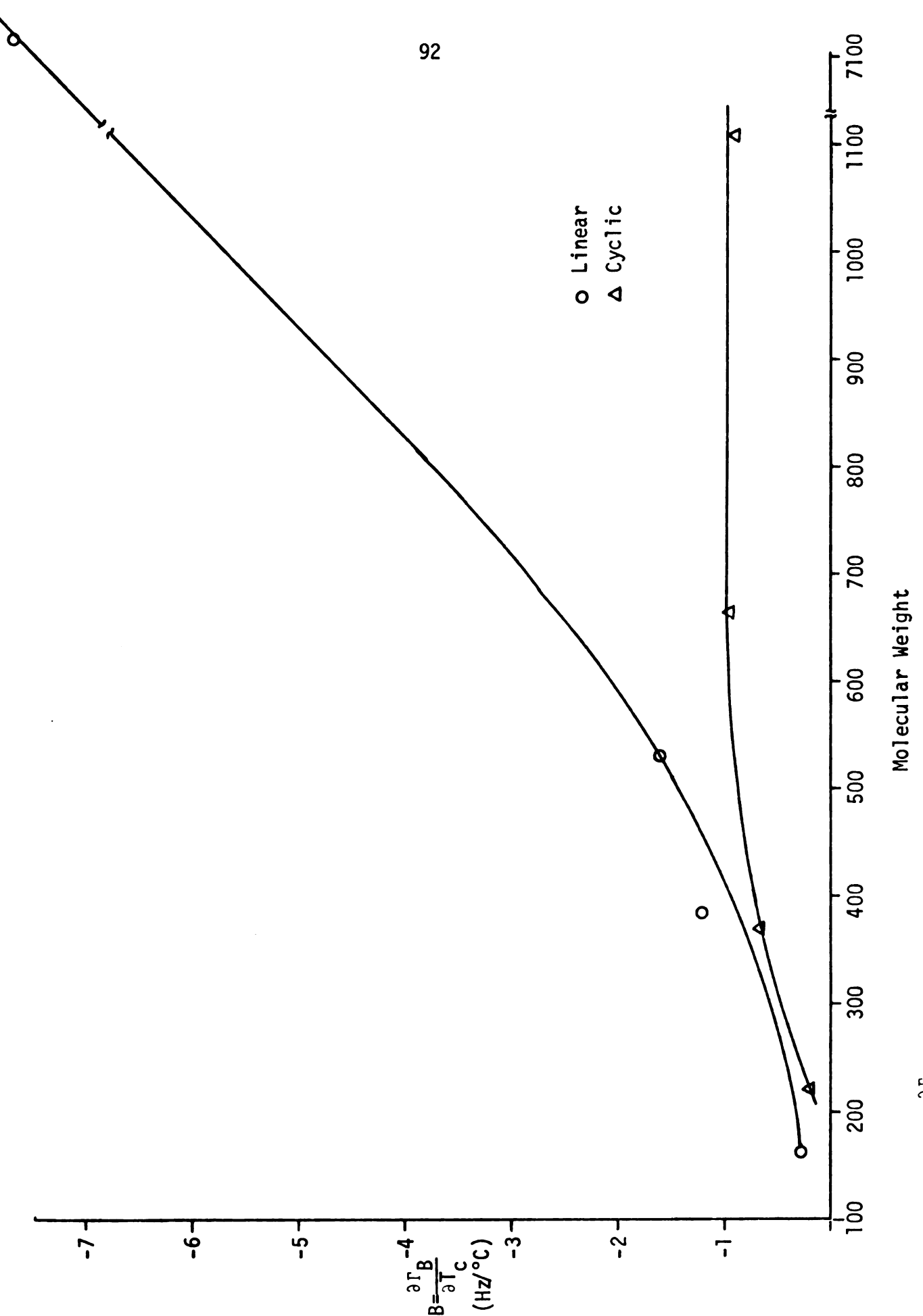


Figure 32. $(\frac{\partial \Gamma_B}{\partial T_c})$ Versus Molecular Weight for Linear and Cyclic Silicones.

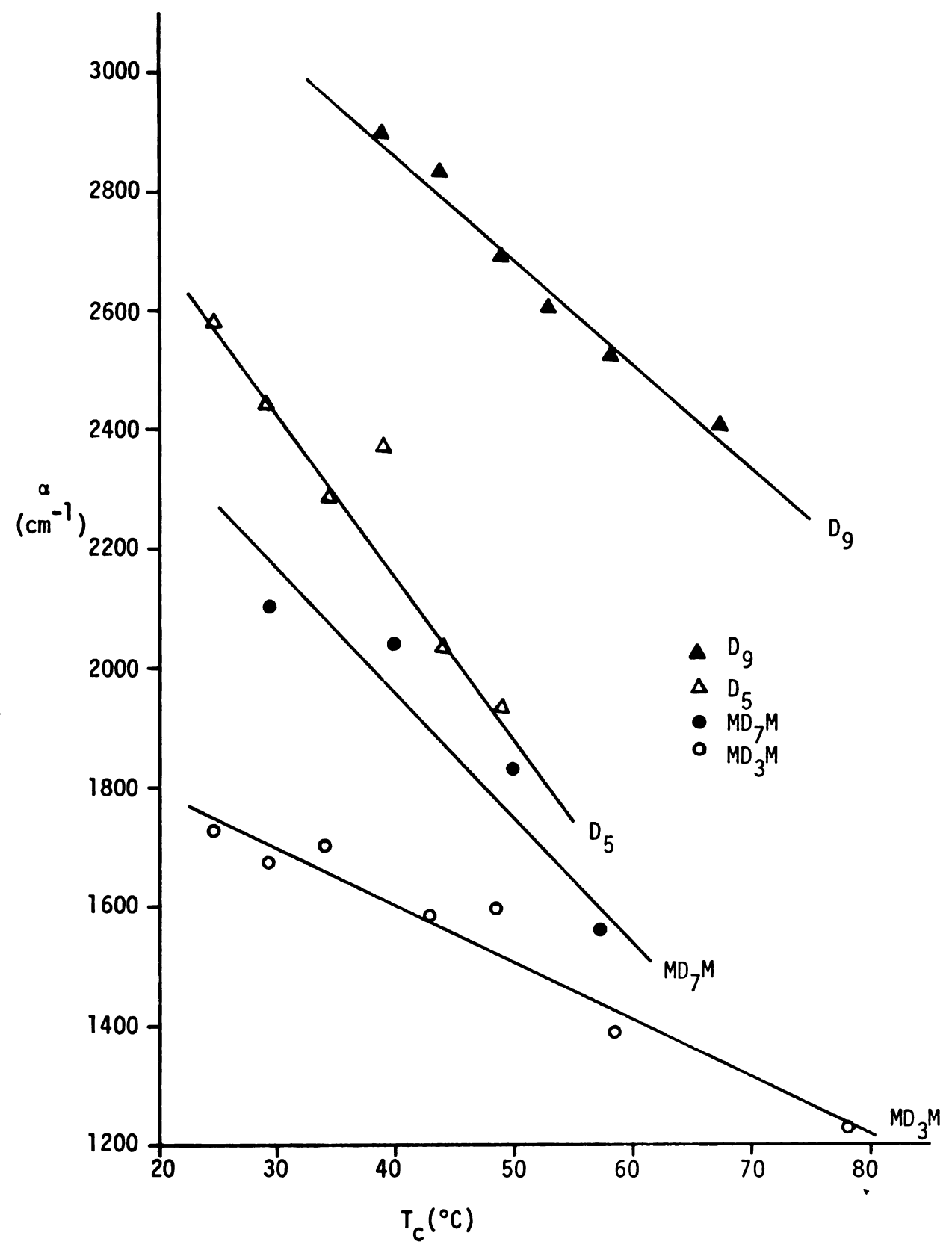
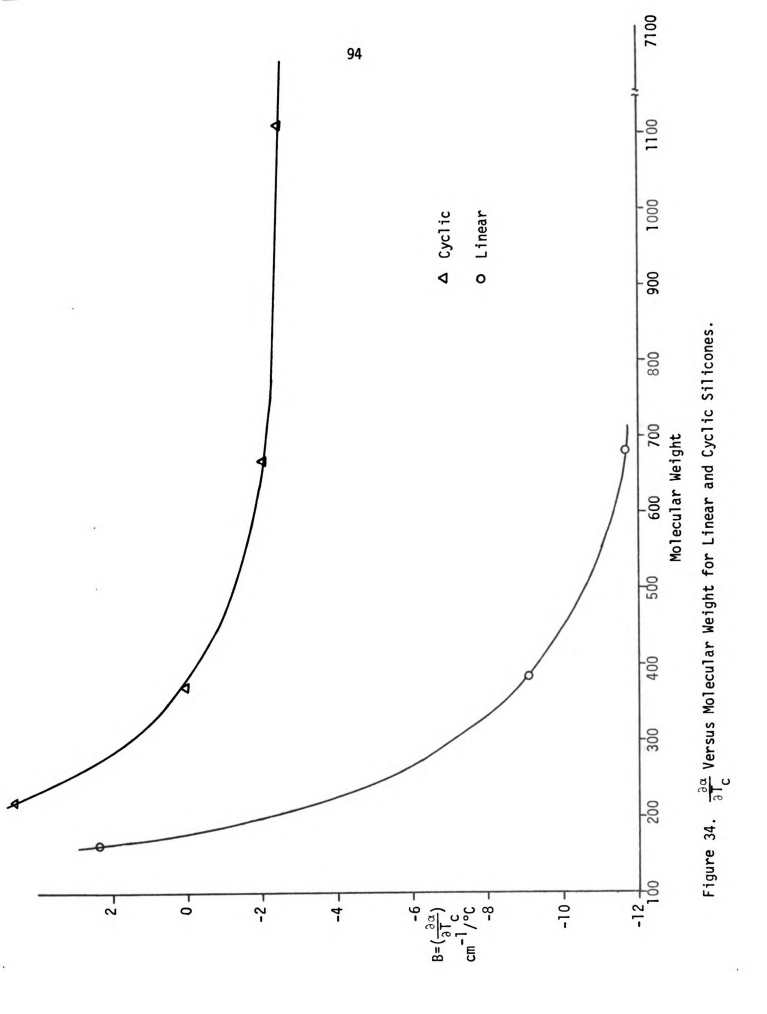


Figure 33.Sonic Absorption Co-efficient (α) Versus Temperature ($T_{\rm C}$) for D_9 , D_5 , MD_7M and MD_3M .



6. Variation of the Ratio of the Intensities of the Central and Shifted Peaks, J_V , with Temperature.

Tables 27-35 contain values of J_V expressed as a function of temperature for all of the silicones under consideration. An ideal way of comparing theoretical and experimental values would be to compare results calculated from Eq. 44 with the experimental values of J_V listed in these tables. However, no data exists for several of the quantities that appear in Eq. 44, so it is not possible to do more than present a semi-quantitative explanation for the change in J_V with temperature and molecular weight.

It is obvious from Figure 35 that J_V decreases with an increase in temperature. This decrease follows from the decrease in the damping forces in the liquid with increasing temperature. The magnitude of the pressure fluctuations is increased because of the decrease in the damping forces. This in turn is responsible for the change in the Brillouin peaks which decreases J_V .

It can be seen from Figure 36 that as the molecular weight is increased J_V also increases, but that the increase is slow compared with that for other liquids, like ethylene glycol and l-octyl alcohol [63]. Moreover, the value of J_V is higher for cyclic silicones than for linear silicones at the same temperature. It is also clear from Figure 37 that the rate of change of J_V with temperature increases with molecular weight, but tends toward a constant value of -2×10^{-3} for cyclic silicones beyond a molecular weight of 600. For the linear silicones, no such definite trend was observed (Table 36).

TABLE 27

Observed Landau-Placzek Ratio J_V of MM

as a Function of Temperature

T _c (°C)	ľc	IB	J_{V}
24.75	0.915	1.612	0.2837
29.32	0.970	1.858	0.2610
34.21	1.045	1.907	0.2739
38.88	0.915	1.807	0.2531
43.84	1.065	2.095	0.2542
48.60	1.180	2.252	0.2619
53.30	1.255	2.407	0.2606
58.25	1.190	2.227	0.2671
67.80	1.415	2.777	0.2547
77.60	1.555	3.087	0.2518

TABLE 28
Observed Landau-Placzek Ratio J_V of MD $_3$ M as a Function of Temperature.

T _c (°C)	Ic	IB	J_V
24.75	1.915	3.907	0.2450
29.32	2.015	4.332	0.2325
34.21	1.845	4.252	0.2169
38. 88	2.185	4.593	0.2378
43.84	1.935	4.562	0.2121
48.60	2.075	4.497	0.2307
53.30	1.885	4.642	0.2030
58.25	2.425	5.785	0.2096
67.80	0.790	1.935	0.2041
77.60	0.815	2.215	0.1840

T _c (°C)	Ic	IB	J_{V}
24.75	2.885	5.183	0.2783
29.32	2.340	4.275	0.2737
34.21	2.565	4.737	0.2707
38.88	2.310	4.697	0.2459
43.84	2.330	4.600	0.2533
48.60	2.425	5.222	0.2322
53.30	2.585	5.250	0.2462
58.25	3.040	6.415	0.2369
67.80	2.673	6.024	0.2219
77.60	2.523	5.946	0.2122

TABLE 30 ${\tt Observed\ Landau-Placzek\ Ratio\ of\ MD_7M\ as}$ a Function of Temperature .

Temp.	Ic	IB	JV
(0 _c)			
22.35	1.910	3.830	0.25
29.60	0.670	1.423	0.24
40.31	0.705	1.530	0.23
49.97	1.065	2.390	0.22
57.35	1.065	2.5 88	0.21

TABLE 31
Observed Landau-Placzek Ratio J_V of D.C. 200 Fluid, 10^5 Cts. as a Function of Temperature.

T _c (°C)	Ic	IB	JV
24.75	2.830	0.662	2.1358
29.32	4.045	0.660	3.0644
34.21	3.850	0.720	2.6736
38.88	2.435	0.745	1.6342
43.84	3.675	0.777	2.3633
48.60	1.915	0.845	1.1331
53.30	3.456	0.896	1.9290
58.25	2.320	0.957	1.2115
62.90	2.265	0.960	1.1797
67.80	3.685	0.985	1.8706
77.60	1.995	1.205	0.8278

TABLE 32 Observed Landau-Placzek Ratio ${\rm J_V}$ of ${\rm D_3}$ as a Function of Temperature

T _c (°C)	Ic	IB	JV
62.90	1.120	2.880	0.1944
67.80	1.536	1.815	0.4233
72.64	1.060	2.085	0.2542
77.60	2.100	2.445	0.5000
82.80	0.965	2.345	0.2058

a Function of Temperature

T _c (°C)	Ic	IB	٦
24.75	2.825	5.092	0.2770
29.32	3.050	5.800	0.2620
34.21	3.260	6.090	0.2676
38.88	3.440	6.860	0.2507
43.84	3.50	7.210	0.2427
52.58	4.235	8.995	0.2352

TABLE 34 $\mbox{Observed Landau-Placzek Ratio} \mbox{ J_V of D_9 as } \\ \mbox{ a Function of Temperature.}$

T _c (°C)	Ic	IB	JV
24.75	1.505	2.570	0.2928
29.32	1.145	1.935	0.2957
34.21	2.013	.305	0.3300
38.88	1.385	2.6625	0.2601
43.84	3.055	6.0525	0.2524
48.60	3.145	6.390	0.2461
53.30	3.255	6.6325	0.2454
58.25	3.295	7.035	0.2342
67.80	1.095	2.4475	0.2237

T _c (°C)	Ic	IB	JV
24.75	3.055	2.6975	0.4569
34.21	2.465	3.0625	0.4024
38.80	2.620	3.2825	0.3991
53.30	2.773	3.448	0.4021
58.25	2.895	3.8225	0.3787
62.90	2.975	3.8375	0.3876
77.60	2.905	4.59	0.3164

TABLE 36

Intercept and Slope for the Intensity Ratio of the Scattered Light (J_V) — Temperature (T_C) Relationship $J_V = A + BT$.

Liquid	Α	$B = \frac{dJ_V}{dT_C}$
ММ	0.279	-3.632×10^{-4}
MD ₃ M	0.263	-9.612×10^{-4}
MD ₇ M	0.274	-1.102×10^{-3}
D.C. 200 fluid, 100 Ct.S.	0.307	-1.245×10^{-3}
D.C. 200 fluid, 10 ⁵ Ct.S.	3.347	-3.113 x 10 ⁻²
D ₃	1.163	-1.102×10^{-2}
^D 5	0.313	-1.515 x 10 ⁻³
D ₉	0.356	-2.073×10^{-3}
D ₁₅	0.493	-2.031×10^{-3}

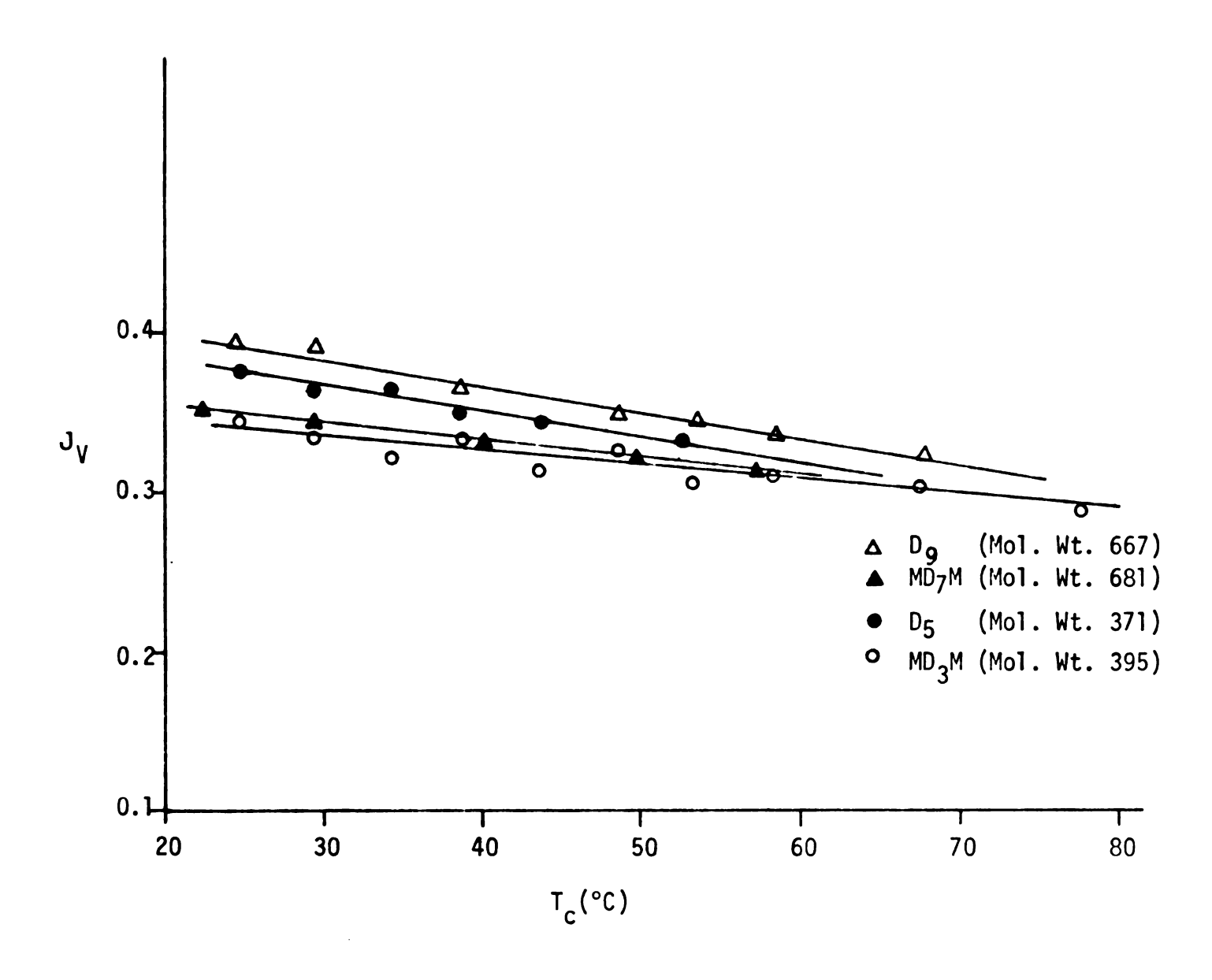


Fig.35. J_V Versus Temperature for D_9 , MD_7M , D_5 and MD_3M .



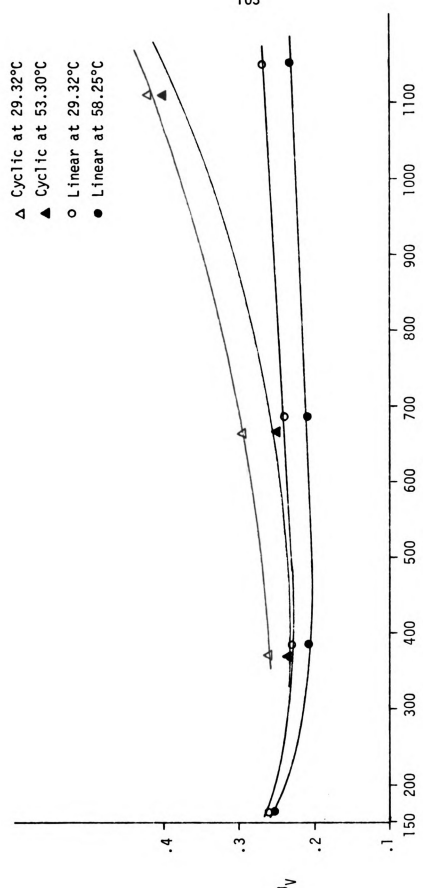


Fig. 36. $\ensuremath{\mathrm{J}}_{\gamma}$ Versus Molecular Weight for Linear and Cyclic Silicones.

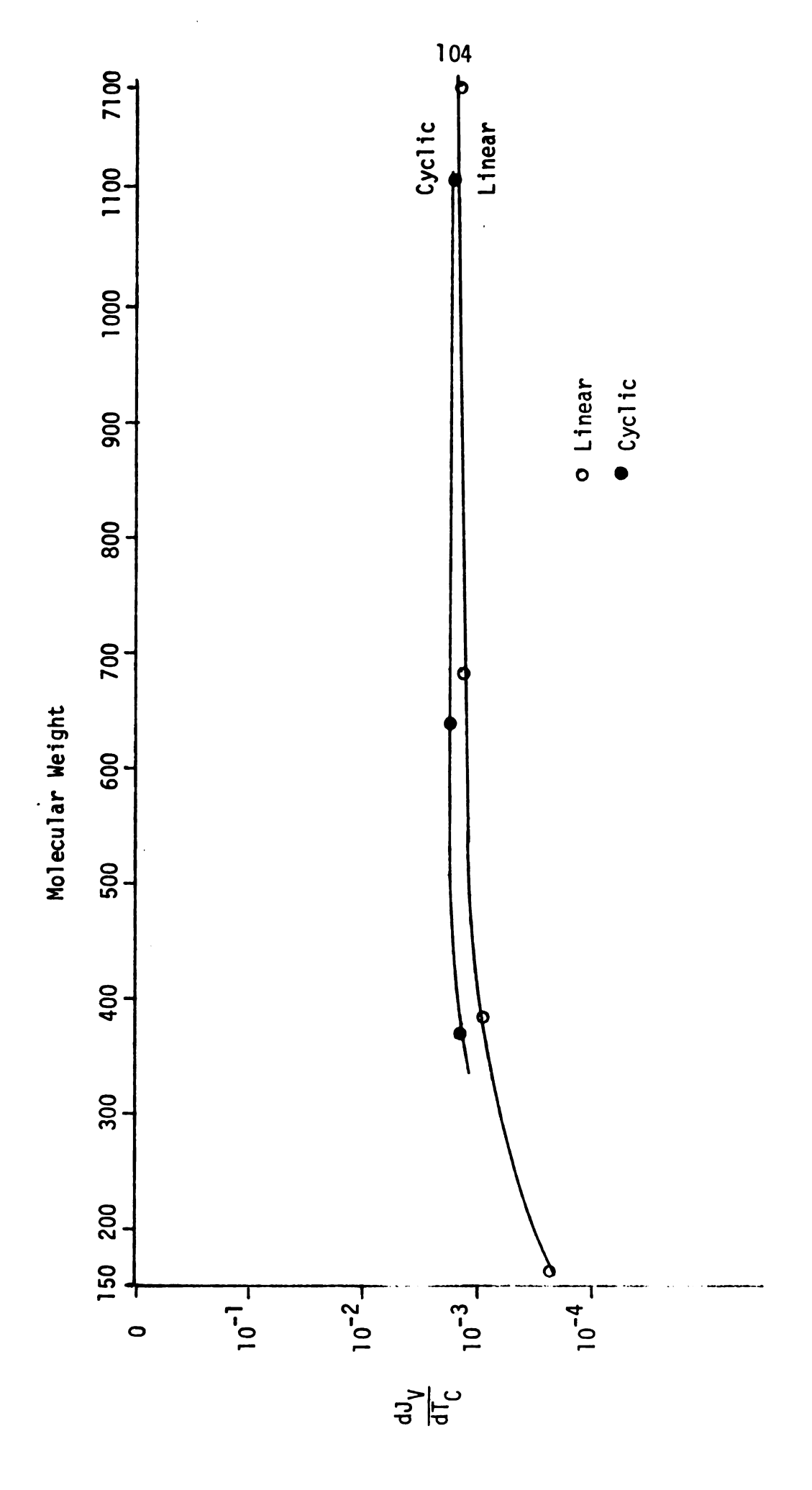


Fig. 37. $\frac{dJ_V}{dT_C}$ Versus Molecular Weight for Linear and Cyclic Silicones.

7. Depolarization Measurements.

Identical intensity ratios were obtained using vertically-polarized incident light with or without a vertical polarizer immediately in front of the detector, thus confirming the idea that Brillouin spectra result from vertically-polarized light alone. There was no indication of resolvable peaks for a horizontally-oriented polarizer.

The depolarization ratios ρ_V and ρ_h are defined as

$$\rho_{V} = \frac{H_{V}}{V_{V}} \quad \text{and} \quad \rho_{h} = \frac{V_{h}}{H_{h}} \quad , \tag{52}$$

where V_V is the intensity of the scattered light whose polarization vector is perpendicular to the scattering plane before and after scattering, H_V is the intensity of the scattered light whose polarization vector is vertical before scattering and horizontal after scattering, V_h defines the case where the polarization vector is horizontal before and vertical afterward, and H_h the case where the polarization vector is horizontal both before and after scattering. Calculated values of ρ_V and ρ_h are tabulated in Tables 37 and 38 for a number of different silicones as a function of temperature. Evidently for all silicones ρ_h has a constant value of about 1.0 regardless of temperature while the values of ρ_V decrease with increasing temperature.

TABLE 37
Observed Depolarization Ratios for MM.

•							
T _C (°C)	ρ v		ρh				
24.75	0.0618		1.17	l			
48.60	0.0279		0.9 82	2			
77.60	0.0084		1.27	5			
Observed Depolarization	Ratios	for	MD ₃ M	•			
т _с	٥		ρh				
(°C)							
24.75	0.0183		1.09	5			
48.60	0.0156		1.120	5			
77.60	0.0111		1.169	9			
Observed Depolarization	Ratios	for	MD ₇ M				
^Т с	۰		ρ h				
(°C)							
24.75	0.0369		1.03	5			
77.60	0.0227		1.000)			
Observed Depolarization	Ratios	for	D.C.	200	fluid,	100	cts.
^т с	۰ ۷		ρh				
(°C)							
48.60	0.0154		0.94	7			
77.60	0.0111		1.22	5			

Observed Depolarization Ratios for D.C. 200 fluid, 10^5 cts.

T _c	٥	ρþ
(°C)		
24.75	0.0277	0.334
48.60	0.0336	0.343

TABLE 38

	17.022	•	
Observed	Depolarizaito	n Ratios	for D ₃ .
	T _C	٩	ρh
((°C)		
•	77.60	0.0415	0.442
0bserved	Depolarizatio	n Ratios	for D ₅ .
	T _c	ρ v	٩h
((°C)	·	
4	18.60	0.0134	1.260
7	77.60	0.0101	1.108
Observed	Depolarizatio	n Ratios	for D ₉ .
	T _c	ρ _V	ρh
((°C)	•	
2	24.75	0.0131	1.105
4	18.60	0.0145	1.104
	77.60	0.0171	1.300
Observed	Depolarizatio	n Ratios	for D ₁₅ .
	T _c	٥ ٧	٩h
((°C)	·	••

0.1704

0.1475

0.1293

1.000

0.900

0.956

24.75

48.60

77.60

CHAPTER V

CONCLUSIONS

In linear and cyclic silicones the velocity of sound increases rapidly with molecular weight initially, but has a tendency to level off in the region of higher molecular weights (≥7,000 molecular weight). Present measurements are in good agreement with the only data that exists for such liquids, results derived from a limited number of ultrasonic measurements [36]. The rate at which the velocity of sound changes with temperature decreases from -4.4 to -2.5 meters/sec for linear silicones, and from -3.3 to -2.9 meters/sec for cyclic silicones, as one goes from lower to higher molecular weights. Such slopes are normal for liquids having a low molecular weight and considerable dependence of viscosity on temperature. However, silicones exhibit about the same slopes, even though their molecular weight is high and the dependence of their viscosity on temperature is negligible.

It was found that as molecular chains lengthened, the sound velocity increased, while the adiabatic compressibility decreased. The latter is inversely proportional to the magnitude of the intermolecular forces. Thus an increase in molecular weight increases the strength of intermolecular forces. Compared to other liquids having similar molecular weights, values of the adiabatic compressibility were unusually high for all of the silicones studied.

Increasing the temperature increases the number of molecular interactions, which in turn increases the efficiency of transferring internal vibrational energy to translational energy. This causes a decrease in the sonic absorption co-efficient α , as appears in Figure 33. Figure 34 establishes that $\frac{d\alpha}{dT_C}$ becomes negative at higher molecular weights, which indicates that most of the silicones studied may be classified as "associated fluids" [54]. Values of α ranged from $1000~\text{cm}^{-1}$ to $2500~\text{cm}^{-1}$. These high values may be caused by structural absorption - related to the fact that molecules in an associated liquid can undergo a transition from one type of structure to another under the influence of a propagating hypersonic wave.

The Mountain theory outlined in Chapter II predicts an extra relaxation peak centered at the incident frequency for a thermally-relaxing liquid. This "Mountain line" arises from the exchange of energy between internal vibrational and transitional modes, which decays with a lifetime of the order of the relaxation time τ . Though observed in carbon tetrachloride (CCl₄) by Cornall [30], et. al., no trace of such a line was found during the present investigation.

The temporal attenuation co-efficient Γ_B , is strongly dependent upon the wave number squared (K^2) as can be seen from Eq. (43). Tables 22 and 23 confirm that Γ_R decreases rapidly with K in the present case.

The ratio J_V of the scattered light intensities decreases monotonically with temperature for all silicones (Figure 35). Moreover, J_V consistently increased with molecular weight. Consequently it is concluded that the anisotropy of liquid silicones increases with an increase in their molecular weight. As the chains lengthen more light is scattered at the incident frequency, increasing the magnitude of the peak. Values of J_V ranged from 0.2 to 2.0 for the silicones studied. Low values like these

are commonly observed for water, ethyl alcohol and other low molecular weight liquids [64], but are scarcely what one would expect for high molecular weight substances.

Heat capacity depends upon temperature changes, but also upon the manner of heating. The specific heat at constant pressure (C_p) is expected to be larger than the specific heat at constant volume (C_v) , because when the substance is heated at constant pressure it may expand and do work against the external pressure, whereas when it is heated at constant volume, it will do no external work. However the values of J_v obtained for silicones establish that the ratio C_p/C_v remains fairly close to unity (1.2 to 3.07), contrary to what might be expected for polymers (\simeq 1000 - 2000).

Brillouin spectra were recorded over a range of scattering angles from 45° to 135° for D_5 and MD_7M with a single interferometer mirror separation (Tables 22 and 23); but no dispersion in the velocity was detected in this range (2 x 10^9 Hz to 5 x 10^9 Hz). It should also be noted that refractive indices were measured for 5890 Å wavelength and calculated for 5145 Å wavelength. Figures 10 and 11 support the contention that refractive index and temperature are linearly related in the range from 20°C to 80°C.

₫			
: :			
•			
			·



BIBLIOGRAPHY

- Rayleigh, J. W., Phil. Mag., 41, 447 (1871).
- 2. J. W. Rayleigh, Phil Mag. 12, 81 (1881).
- 3. M. S. Smoluchowski, Ann. Physik 25 205 (1908).
- 4. A. Einstein, Ann d. Physik 38 1275 (1910).
- 5. Mie, P., Ann. Phys. Lpz., 25, 3, 771 (1908).
- 6. Rolfe, E., J. K. Silk, S. Booth, K. Meister and R. M. Young NASA Contractor Report, NASA CR-1199 (1968).
- Investigation and Calculation of Basic Parameter for the Application of the L. D. V. - Meyers, J. F., NASA Technical Note NASA - TN D-6125.
- 8. Goldstein, R. J., R. J. Adrian and D. K. Kreid IAEC Fundamentals Vol 8 No. 3. 498 (1969).
- 9. Brillouin, L., Ann. de Phisique. <u>17</u>, 88 (1922).
- 10. Gross, B., Nature, <u>126</u> 201 (1930).
- 11. Raman, C. V., Indian J. Phys., 2, 1 (1928).
- 12. Debye, P., J. App. Phys. <u>15</u> 338 (1944).
- 13. Debye, P., J. Phys. Chem. <u>51</u> 18 (1947).
- 14. Landau, L., and G. Placzek, Physik. Zeits. Sowjetunion, 5, 172 (1934).
- 15. Miller, G. A., F. I. San Fillipo, D. K. Carpenter, Macromolecules $\underline{3}$ 125 (1970).
- 16. Miller, G. A., C. S. Lee, J. Phy. Chem. 72, 4644 (1968).
- 17. Miller, G. A., J. Phys. Chem. 71 2305 (1967).
- 18. Maiman, T. H., Phys. Rev., <u>123</u>, 1145 (1961).
- 19. Javan, A., W. R. Bennett, Jr. and D. R. Herriott, Phys, Rev. Letters, 6 106 (1961).
- 20. Cummins, H. Z., N. Kable and Y. Yeh, Phys. Rev. Letters 12, 150 (1964).

- 21. Herriott, D. R., Appl. Opt. 2, 865 (1963).
- 22. Mountain, R. D., J. Research NBS, <u>70A</u>, 207 (1966).
- 23. Mountain, R. D., Rev. Mod. Phys., 38, 205 (1966).
- 24. Mountain, R. D., J. Research, NBS, 69A 523 (1965).
- 25. Mountain, R. D., J. Acoust. Soc. Am., 42 516 (1967).
- 26. Mountain, R. D., J. Chem. Phys., 44 832 (1966).
- 27. Mountain, R. D., J. Research NBS, 72A, 95 (1968).
- 28. Bhatia, A. B., and E. Tong., Phys. Rev., 173 231 (1968).
- 29. Volterra, V., Phy. Rev., 180 No. 1, 156 (1969).
- 30. Gornall, W. S., G. I. A. Stegeman, B. P. Stoicheff, R. H. Stolen and V. Volterra, Phys. Rev. Letters, 17, 297 (1966).
- 31. Stegeman, G. I. A., W. S. Gornall, V. Volterra, and B. P. Stoicheff, J. Aco. Sc. of Am. 49 No. 3 (out 3) 979 (1971).
- 32. Stegeman, G. I. A. and B. P. Stoicheff, Phy. Rev. A <u>7</u> No. 3, 1160 (1973).
- 33. Cummins, H. Z., and R. W. Gamon, Appl. Phys. Letters, <u>6</u>, 171 (1965); J. Chem. Phys., <u>44</u> 2785 (1966).
- 34. Encyclopedia of Polymer Science and Technology, Vol 12 464 (1970).
- 35. Encyclopedia of Polymer Science and Technology, Vol 18, 221 (1970).
- 36. Weissler, A., J. Am. Chem. Soc. <u>71</u>, 93 (1949).
- 37. Weissler, A., J. Am. Chem. Soc. <u>71</u>, 419 (1949).
- 38. Bhagavantam, S., Crystal Symmetry and Physical Properties, Academic Press, N. Y. (1966).
- 39. Fishman, L., Mountain, R. D., J. Phys. Chem. 74 2178 (1970).
- 40. Cummins, H. Z., Gammon, R. W., J. Chem. Phys. 44 No. 7 2785 (1966).
- 41. Landau, I. D. and Lifshitz, E. M., Statistical Physics, Pergamon Press, Inc., New York, 1958, Sec 20 and 111.
- 42. Landau, I. D. and Lifshitz, E. M., Electrodymanics of Continuum Media, Pergamon Press, Inc., New York, 1960, Sec. 94.
- 43. Fabelinskii, I. L., "Molecular Scattering of Light", Plenium Press, New York (1968).

- 44. Volterra, V., Bucaro, J. A., Litovitz, T. A., "Molecular Motion and Light Scattering in Liquids". Verlag Chemie Gmbtt, Weinheim/Bergstr, Band 75, Heft 3/4 (1971).
- 45. J. Frenkel, "Kinetic Theory of Liquids", Dover, New York 1946, p. 235.
- **46. Gornall, W. S., Wang, C. S., Yang, C. C.,** Bloembergen, N. Phys. Rev. Lett. **26** 1094 (1971).
- 47. Van Hove, L., Phys. Rev. <u>95</u> 249 (1954).
- 48. Komarov, L. I., and Fisher, 1-2, Soviet Physics JETP <u>16</u> 1358 (1963).
- 49. Montrose, C. J., Solovyev, V. A. and Litovitz, T. A., J. Acous. Soc. of Am. 43, 117 (1968).
- 50. Gaumer, S. J., Ph.D. Thesis, Michigan State University, East Lansing, Michigan, 1972.
- 51. Met, Viktor., Laser Technology Section, p. 45, Sept. 1967.
- 52. Tannahill, M. M., Ph.D. Thesis, Michigan State University, East Lansing, Michigan, 1973.
- 53. Yuen, Henry Kwai-To, Ph.D. Thesis, Michigan State University, East Lansing, Michigan 1973.
- 54. Herzfeld, K. F. and Litovitz, T. A., Absorption and Dispersion of Ultrasonic Waves (Academic Press, New York, 1959).
- 55. Boundary layer theory Schlichting, New York, McGraw-Hill (1968).
- 56. Born, M., and Wolf, E., Principles of Optics, Pergamon Press (1964).
- 57. Goldstein, R. J., Kreid, D. K., J. of App. Mech. Transaction of the ASME, 813 (1967).
- 58. Chu, B., J. of Chem. Edu. 45 No. 4, 224 (1968).
- 59. Huffann, R. M. Fuller, G. E., Lawrence, T. R., SAE Transactions (690266) 1174, 1969.
- 60. Yeh, Y., Cummins, H. A., App. Phys. Letters <u>4</u>, No. 10, 176 (1964).
- 61. Foreman, Jr., J. W., George, E. W., and Lewis, R. D., App. Phys. Letters 7, No. 4, 77 (1965).
- 62. Nordhaus, D., Ph.D. Thesis, Michigan State University, East Lansing, Michigan 1973.
- 63. Rank, D. H., Kiess, E. M., and Fink, U., J. of the Optical Society of America <u>56</u> No. 2. 163 (1966).

64. Rank, D. H., Kiess, E. M., Fink, U., Wiggins, T. A., J. of the Optical Soc. of America <u>55</u> No. 8, 925 (1965).

•			

APPENDIX A

CALCULATION OF THE REFRACTIVE INDEX AT 5145 Å.

The refractive index for λ = 5145 Å was calculated using the equations given in the Bausch and Lomb Abbe 3-L Refractometer instrument manual. The refractive index at λ = 5145 Å (n_{5145} Å) was calculated for all silicones studied (MM, MD₃M, MD₁M, D.C. 200 fluid 100 cts., D₃, D₅, D₉, and D₁₅) at five different temperatures. The equations used were

$$n_{5145} \stackrel{\circ}{A} = A' + \frac{B'}{(514.5 \text{ nm})^2}$$
 (A-1)

$$A^{-} = 0.52364 \times 10^{6} (n_{F} - n_{C})$$
 (A-2)

$$B' = 0.52364 \times 10^{-6} B'$$
 (A-3)

$$(n_F - n_C) = A + BC \qquad (A-4)$$

where A, B and C are constants given in the Dispersion Table of the Bausch and Lomb Abbe 3-L Refractometer. A, B and C depend on the refractive index of the sample and on the drum readings of the refractometer obtained during the measurement of $n_{\rm D}$.

The dispersion, $(n_F - n_C)$ of the sample is the difference in the refractive index at wave-lengths of 656 and 486 nm. Tables 2-4 presents the values of n_{5145} \mathring{A} for the five temperatures at which the refractive-indices were measured. Tables A-1 to A-5 give the values of n_{5145} \mathring{A} for the temperatures at which all the scattering measurements were taken. Figures A-1 to A-9 display curves of the refractive index versus temperature for MM, MD₃M, MD₇M, D.C. 200 fluids, 100 cts. and 10^5 cts., D_3 , D_5 , D_9 and D_{15} . For each silicone the slope and intercept with the n_{5145} \mathring{A} axis was calculated,

$$n_{5145} \stackrel{\circ}{A} = A + BT_C$$
 (A-5)

Values of A and B are presented in the table for all silicones.

The temperature co-efficient of the refractive index $(\frac{dn}{dT_C})$ decreases with increasing molecular weight for linear silicones. For cyclic silicones there is also a decreasing trend of $\frac{dn}{dT_C}$ with increasing molecular weight which can be seen quite clearly in Figure A-10.

TABLE A-1

Temperature Dependence of the Refractive Index for λ = 5145Å.

Liquid: MD_3M ; $n_{5145\text{Å}} = -4.60947 \times 10^{-4}T_c + 1.4055$

T _c (°C)	ⁿ 5145Å
24.75	1.3941
29.32	1.3920
34.21	1.3898
38.88	1.3876
43.84	1.3853
48.60	1.3831
53.30	1.3810
58.25	1.3787
62.90	1.3765
67. 80	1.3743
77.60	1.3698

TABLE A-2

Liquid: MM; $n_{5145\text{Å}} = -5.80064 \times 10^{-4} T_c + 1.3930$

24.75	1.3787
29.32	1.3760
34.20	1.3732
38.88	1.3705
43.84	1.3676
48.60	1.3649
53.30	1.3621
58.25	1.3593
62.90	1.3566
67.80	1.3537
77.60	1.3480

TABLE A-3

Liquid: MD_7M ; $n_{5145A}^{\circ} = -4.1780 \times 10^{-4}T_c + 1.4100$

T _c (°C)	ⁿ 5145Å
24.75	1.3977
29.32	1.3978
34.21	1.3957
38.88	1.3938
43.84	1.3917
48.60	1.3397
53.30	1.3878
58.25	1.3857
62.90	1.3837
67.80	1.3817
77.60	1.3776

Liquid: D.C.200 fluid, 100 cts.; $n_{5145\text{Å}}^{\circ} = -3.79733 \times 10^{-4} \text{T}_{\text{C}} + 1.4156$

24.75	1.4062
29.32	1.4045
34.21	1.4026
3 8.88	1.4009
43.84	1.3990
48.60	1.3972
53.30	1.3954
58.25	1.3935
62.90	1.3917
67.80	1.3899
77.60	1.3862

TABLE A-4

Liquid: D.C. 200 fluid, 10^5 cts. $n_{5145\text{Å}}^{\circ} = -3.64373 \times 10^{-4} T_{\text{C}}$

T _C (°C)	ⁿ 5145Å
24.75	1.4066
29.32	1.4050
34.21	1.4032
38.88	1.4015
43.84	1.3997
48.60	1.3979
53.30	1.3962
58.25	1.3944
62.90	1.3927
67.80	1.3909
77.60	1.3874

TABLE A-5 $\begin{tabular}{ll} \textbf{Intercept and Slope for the Index of Refraction-} \\ \textbf{Temperature Relationship n}_{5145} \begin{tabular}{ll} \rat{A} &= A + BT_{c}. \\ \end{tabular}$

Liquid	Α	$B = \left(\frac{\partial^n 5145 \stackrel{\circ}{A}}{\partial T_c}\right)$ $\left(\frac{1}{o_c}\right)$
Mi4	1.3921	-5.8006
MD ₃ M	1.4055	-4.6095
MD ₇ M	1.4100	-4.1780
100 cts.	1.4156	-3.7973
10 ⁵ cts.	1.4156	-3.6437

Liquid A
$$B = (\frac{3n_{5145} \text{ Å}}{3T_c})$$

$$(\frac{1}{o_c})$$

$$D_3 \qquad 1.4015 \qquad -5.4610$$

$$D_5 \qquad 1.4110 \qquad -4.6326$$

$$D_9 \qquad 1.4250 \qquad -5.7219$$

$$D_{15} \qquad 1.4181 \qquad -3.8623$$

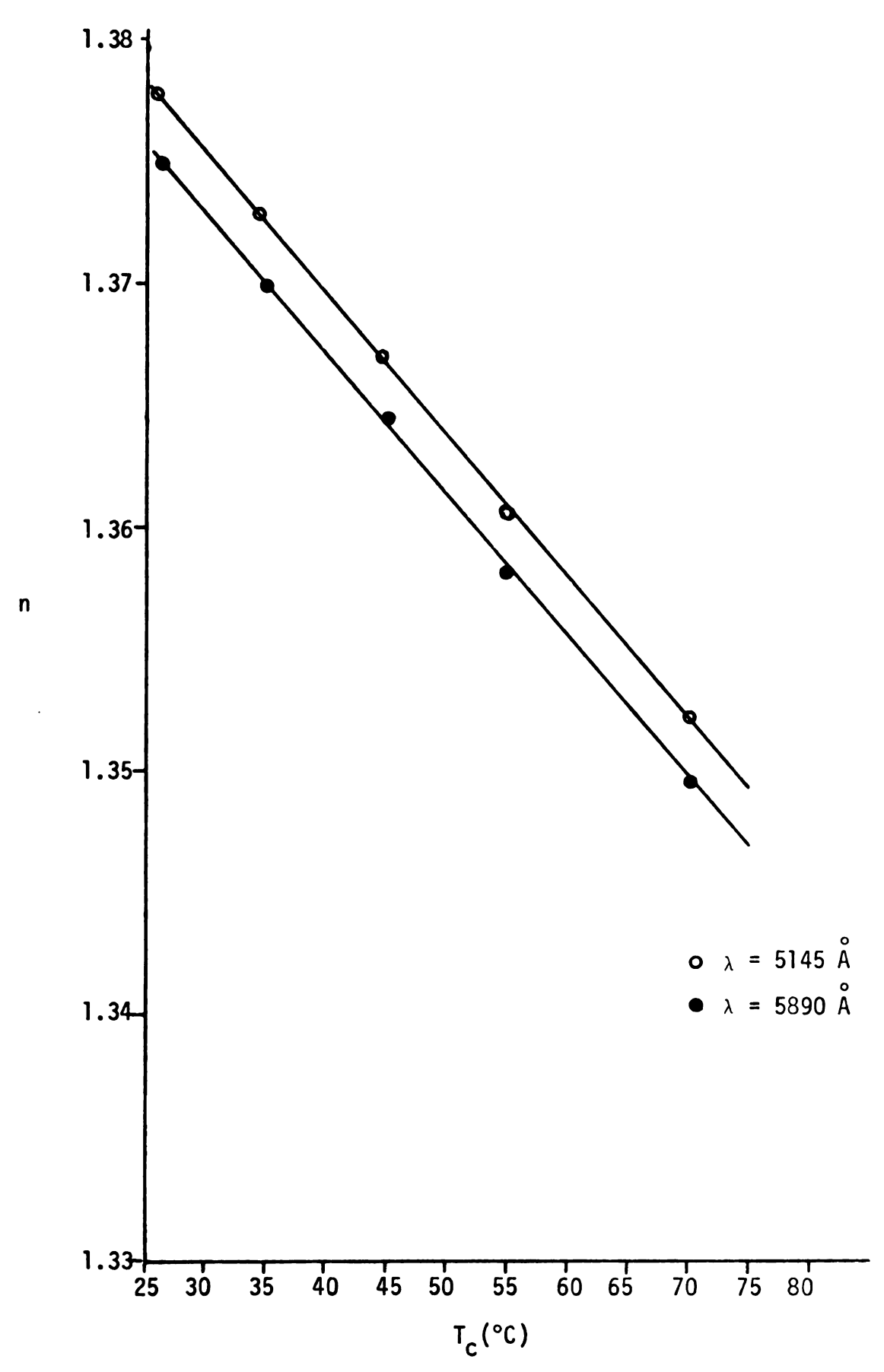


Figure A-1. Refractive Index Versus Temperature for MM.

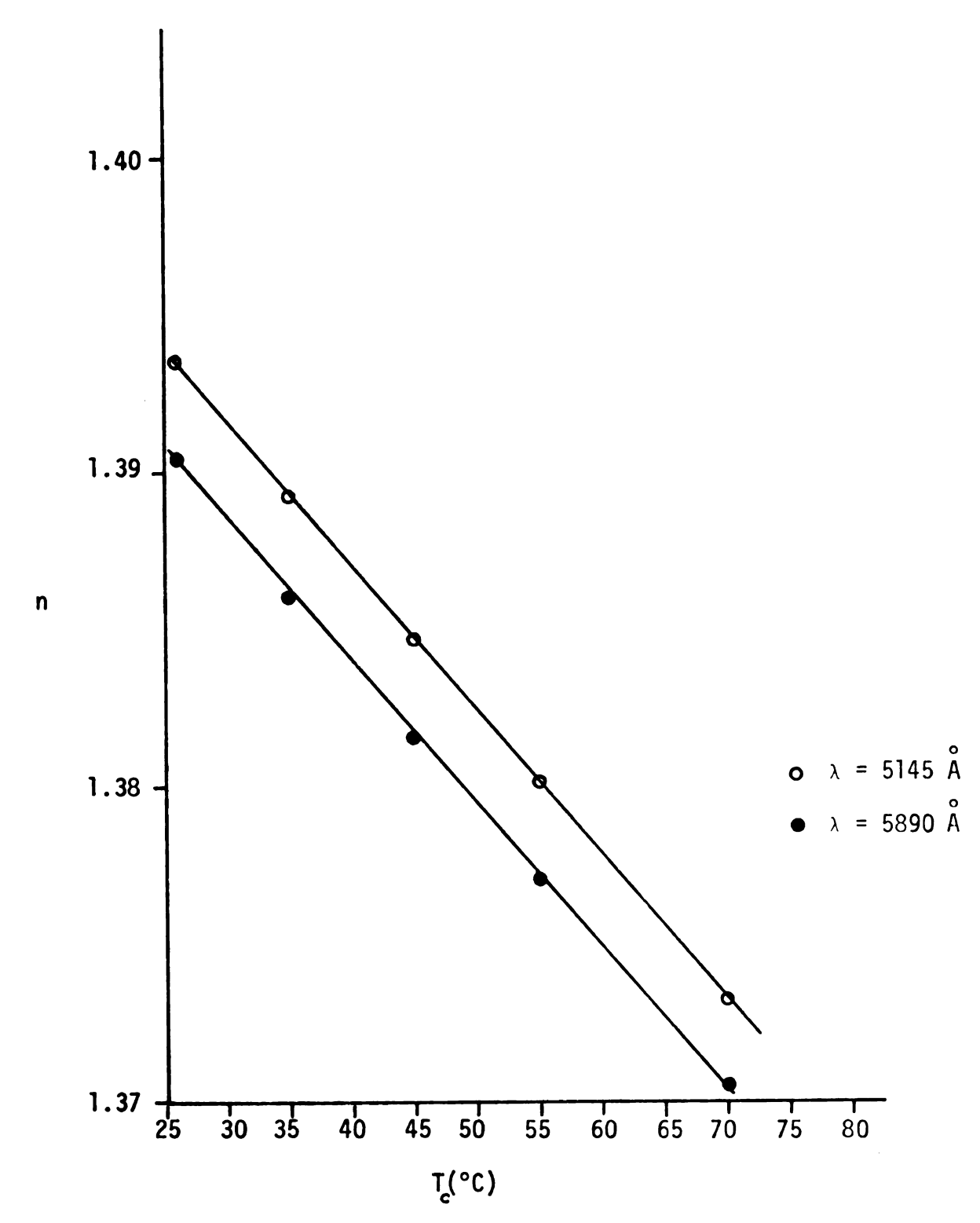
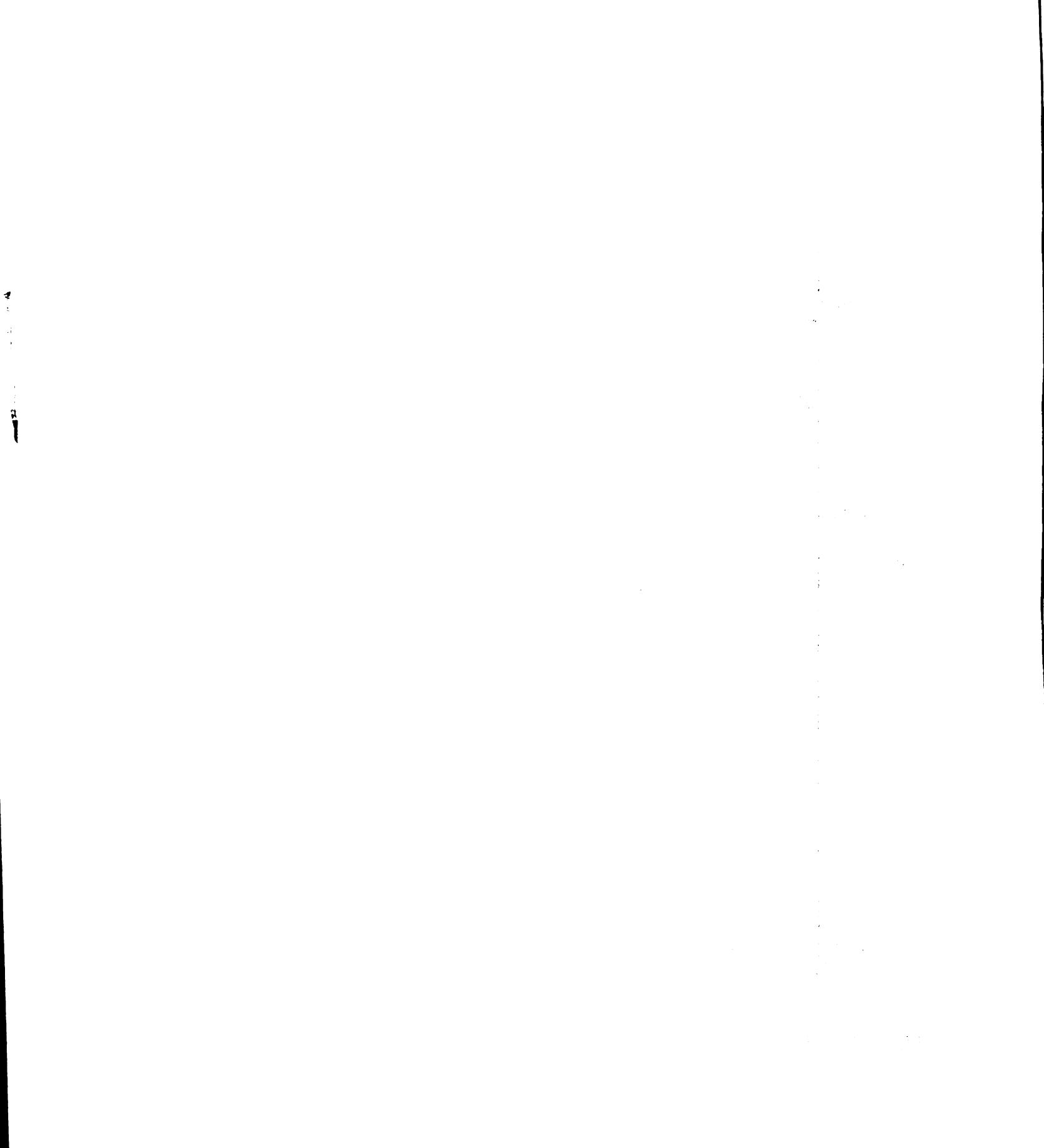


Figure A-2. Refractive Index Versus Temperature for $\mbox{MD}_{3}\mbox{M}.$



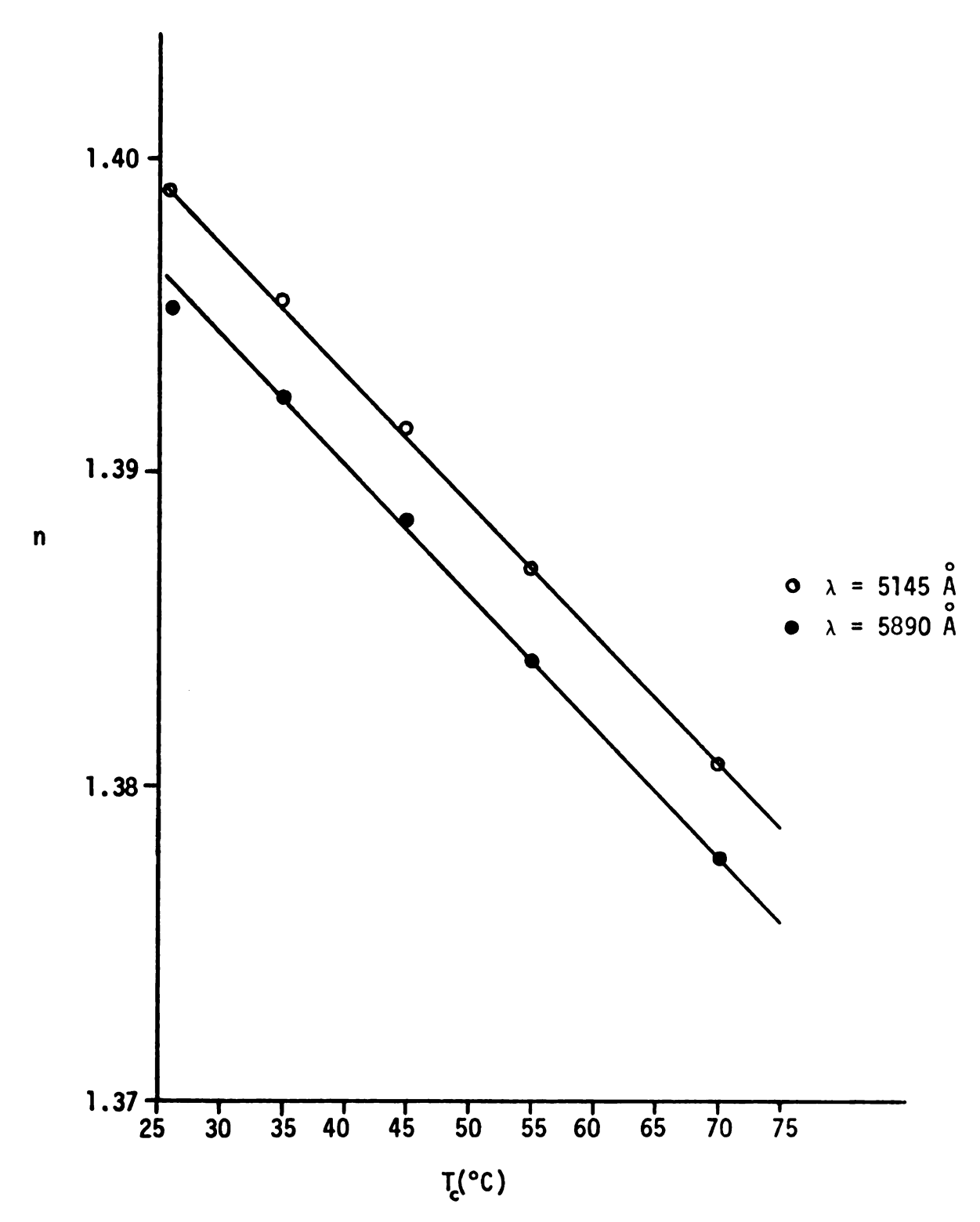


Figure A-3. Refractive Index Versus Temperature for $\mbox{MD}_{7}\mbox{M}.$

•	
·	

	•
	e e e e e e e e e e e e e e e e e e e
	:
	• • • • • • • • • • • • • • • • • • •

ŧ

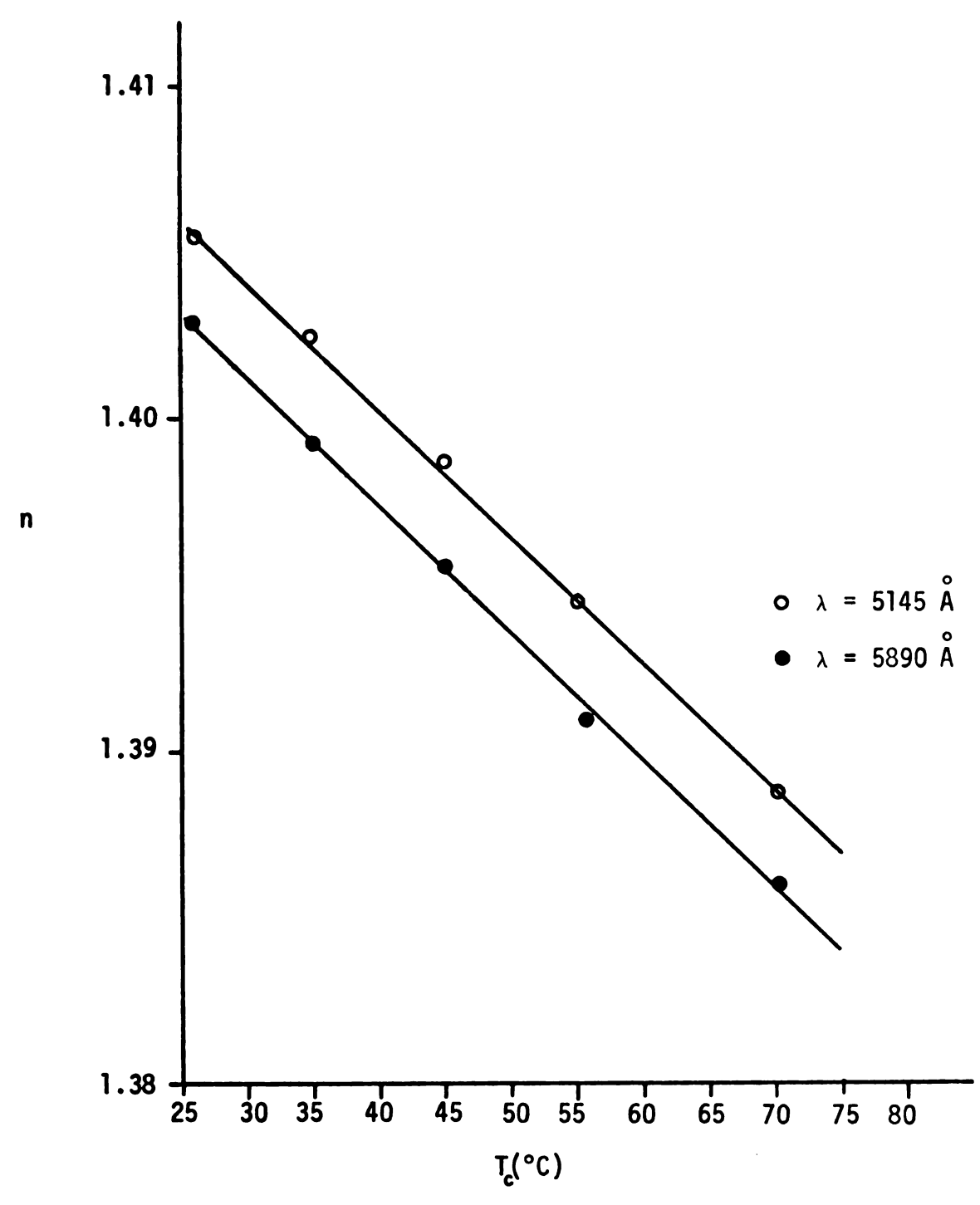


Figure A-4. Refractive Index Versus Temperature for D. C.200 Fluid, 100 cts.

Carriery Control

nwining spiranger De

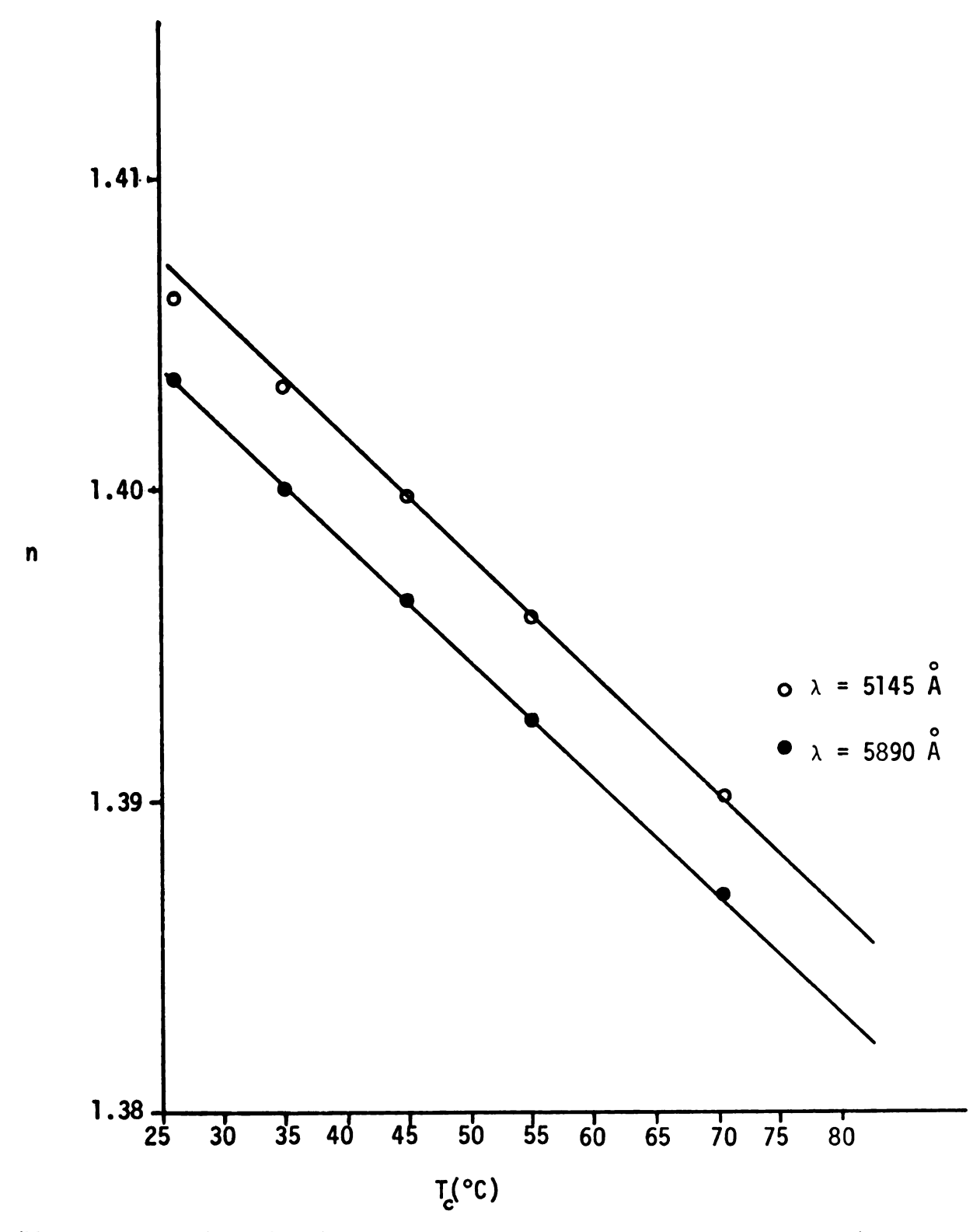


Figure A-5. Refractive Index Versus Temperature for D.C. 200 Fluid $10^5 \ \mathrm{cts.}$

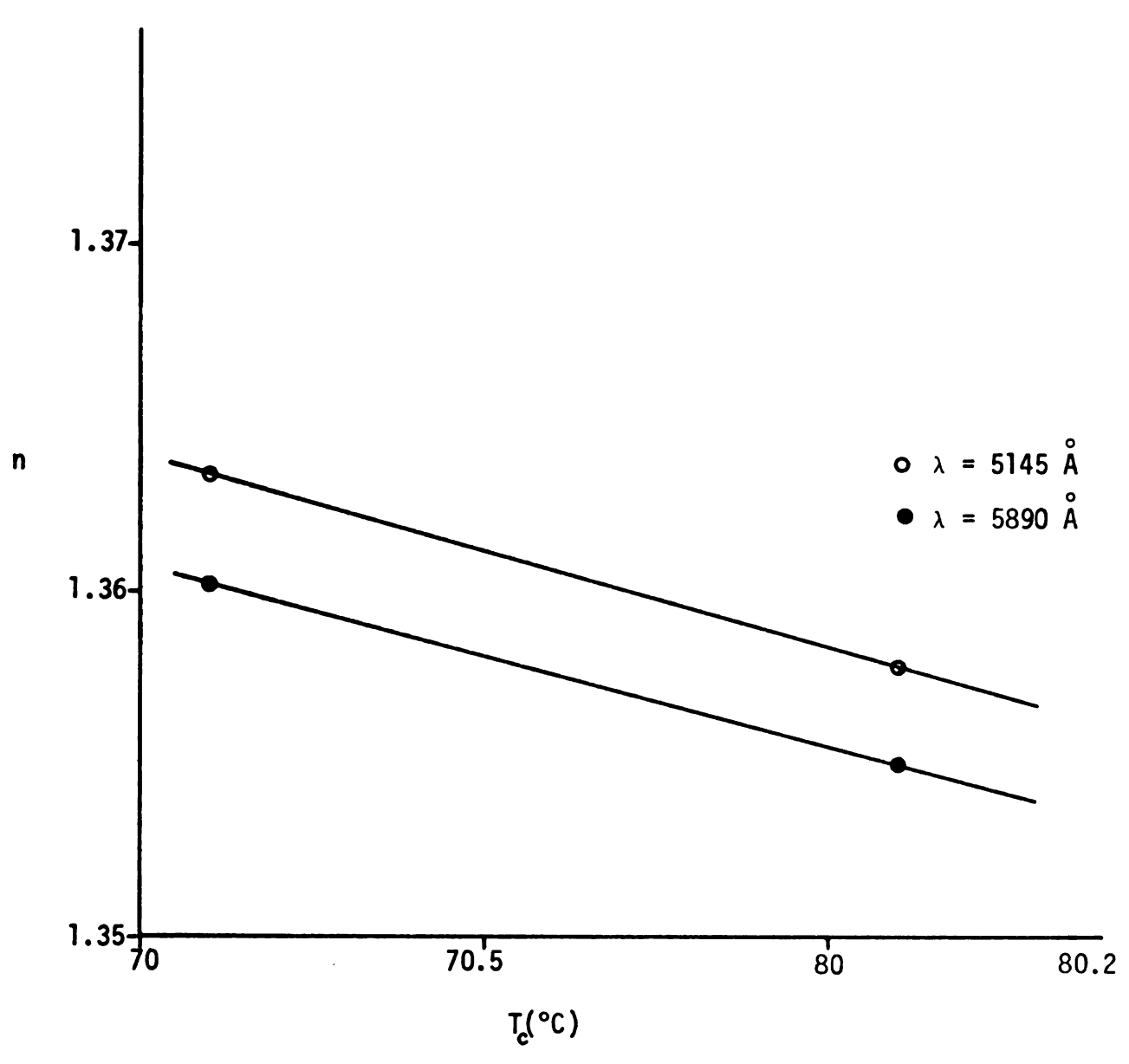


Figure A-6. Refractive Index Versus Temperature for \mathbf{D}_3 .

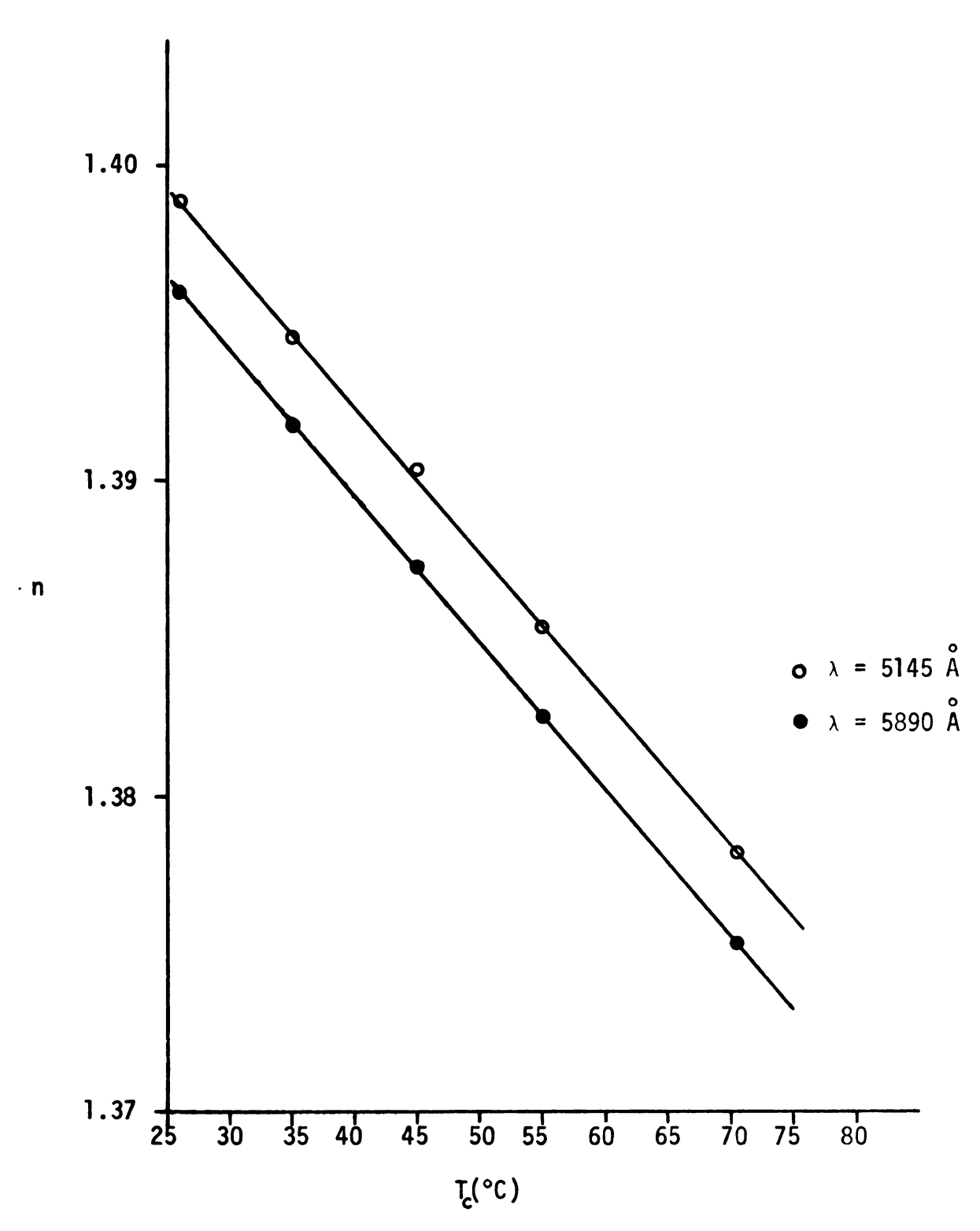


Figure A-7. Refractive Index Versus Temperature for $\mathbf{D}_5.$

		; ,
		, <u>\$</u>
		the engineering

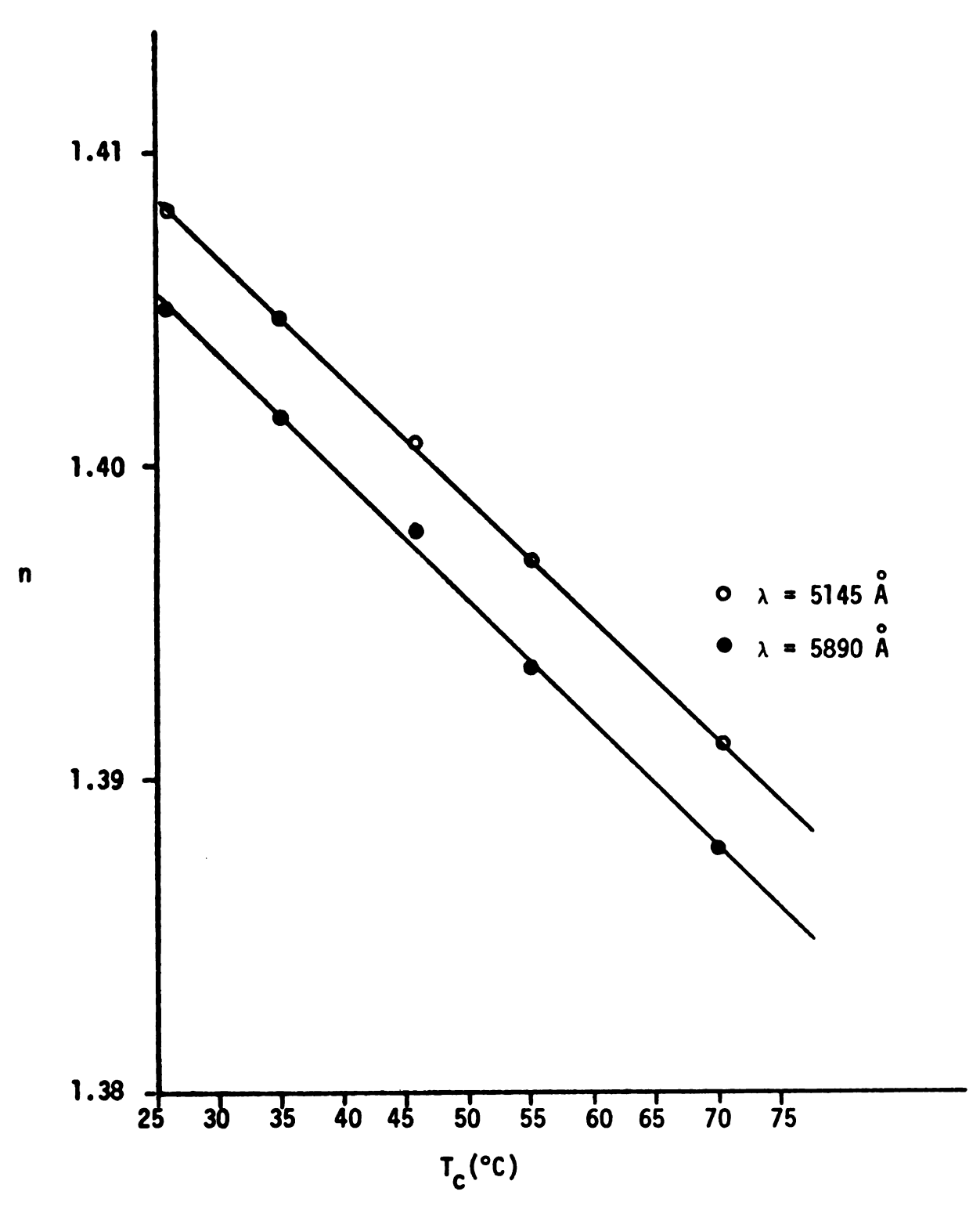


Figure A-8. Refractive Index Versus Temperature for \mathbf{D}_9 .

• . (Control of the control of the contr

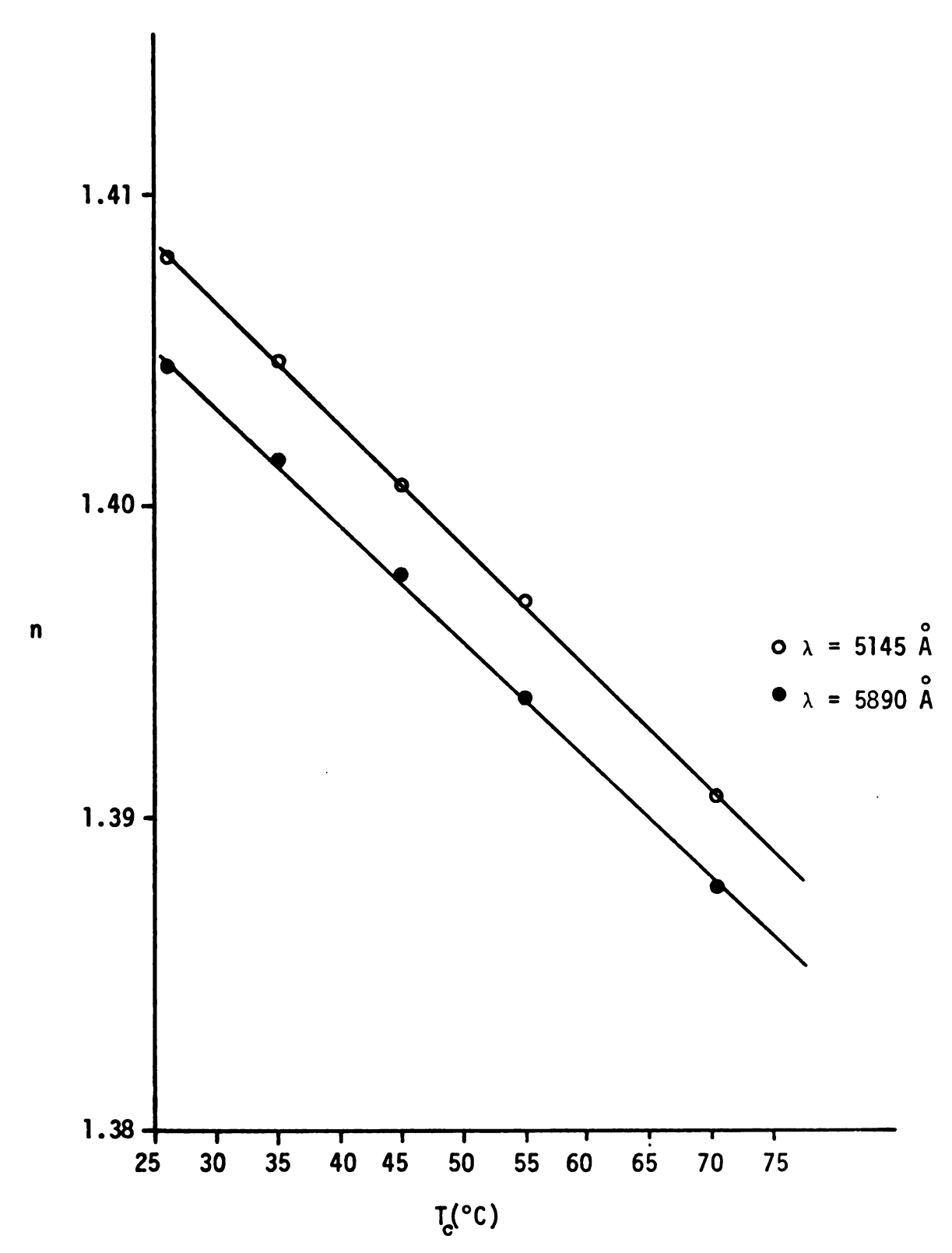


Figure A-9. Refractive Index Versus Temperature for D_{15} .

	;
	* : :
	; ;
	:
	•
	: •
	(A) (A) (A) (B) (A) (B) (B) (B) (B) (B) (B) (B) (B) (B) (B
	1
	; }
	1
	·
	i i
	State of the state
	. ****

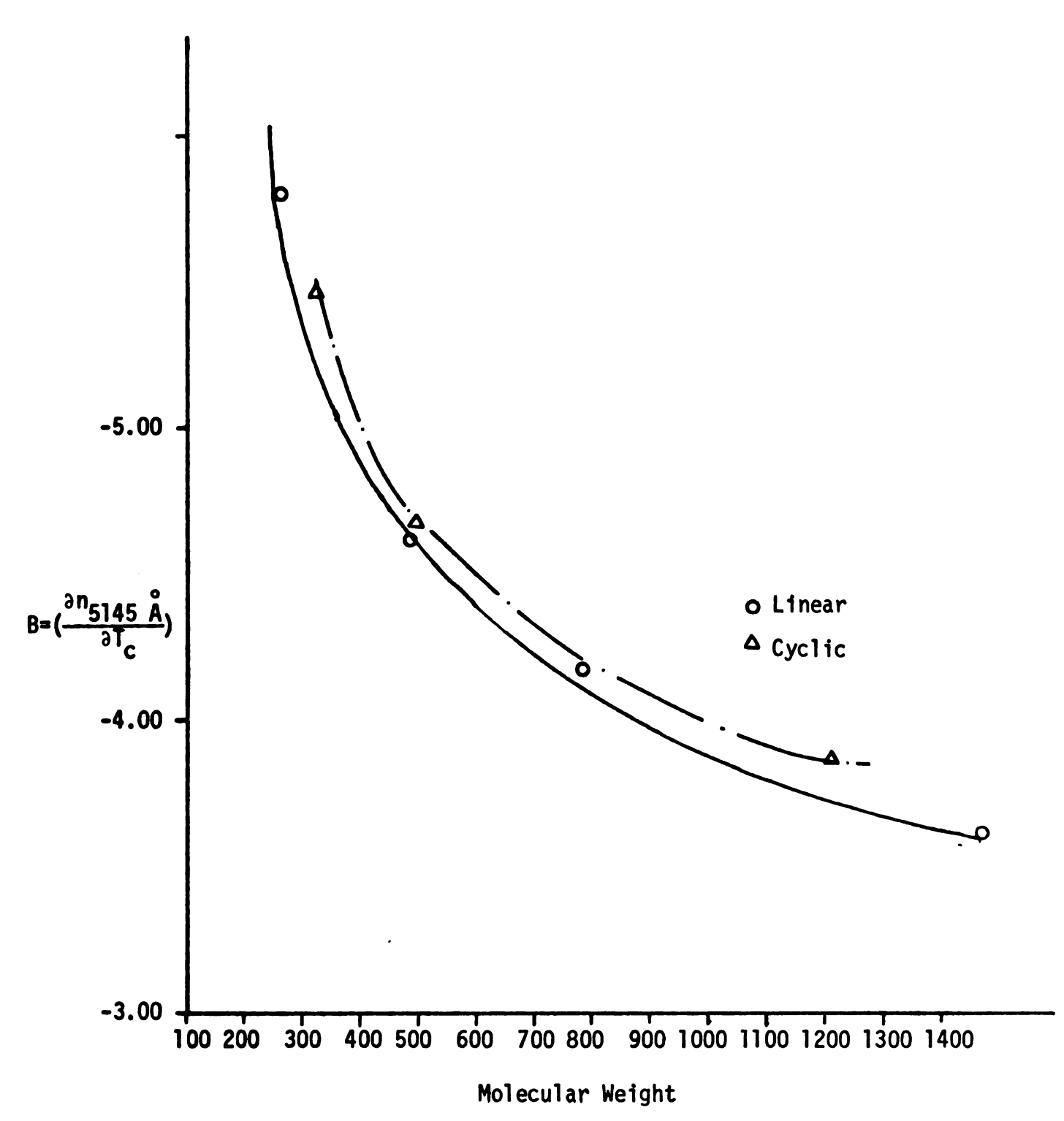


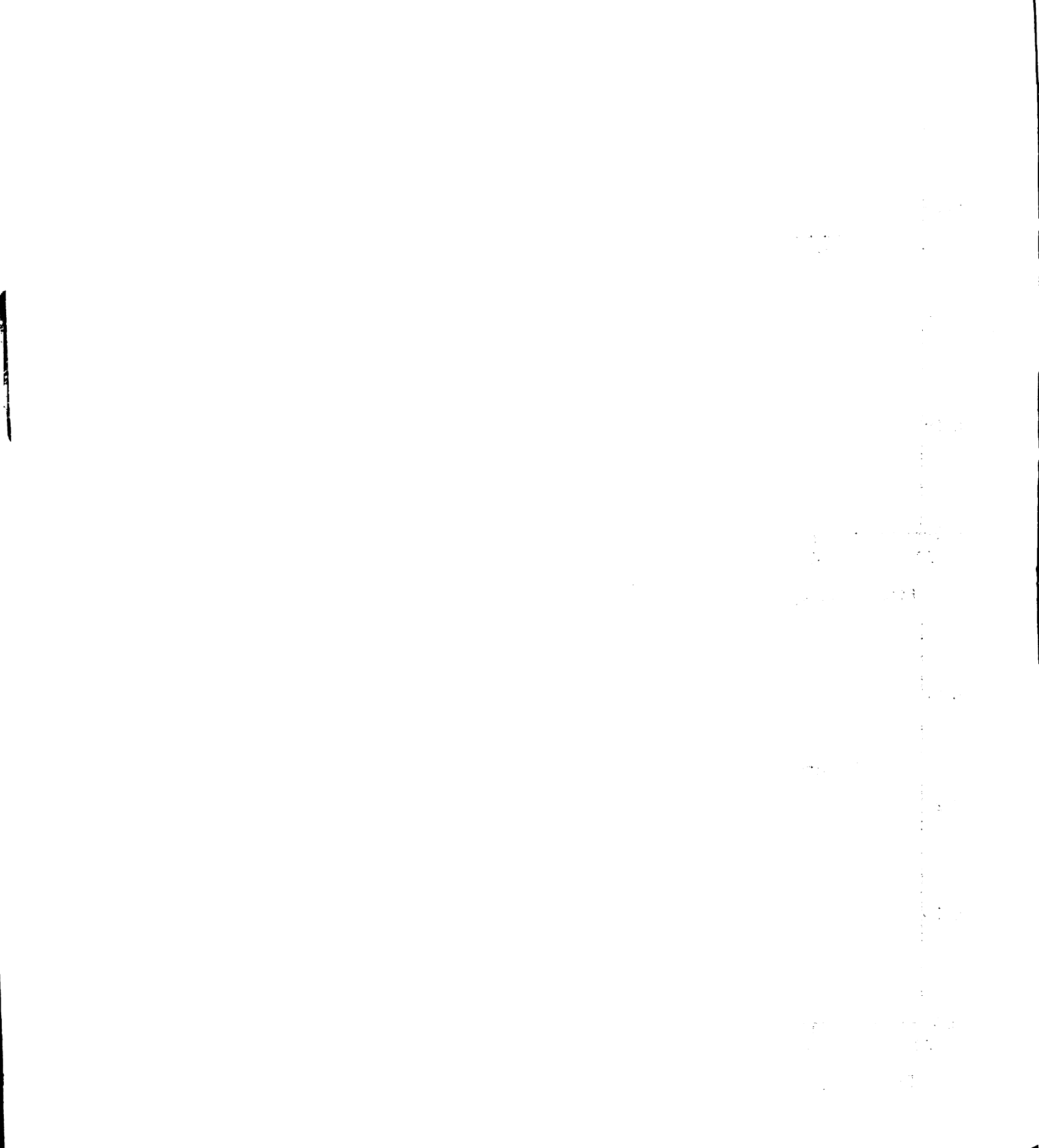
Figure A-10. Variation of the Temperature Derivative of the Refractive Index with Molecular Weight for Linear and Cyclic Compounds.

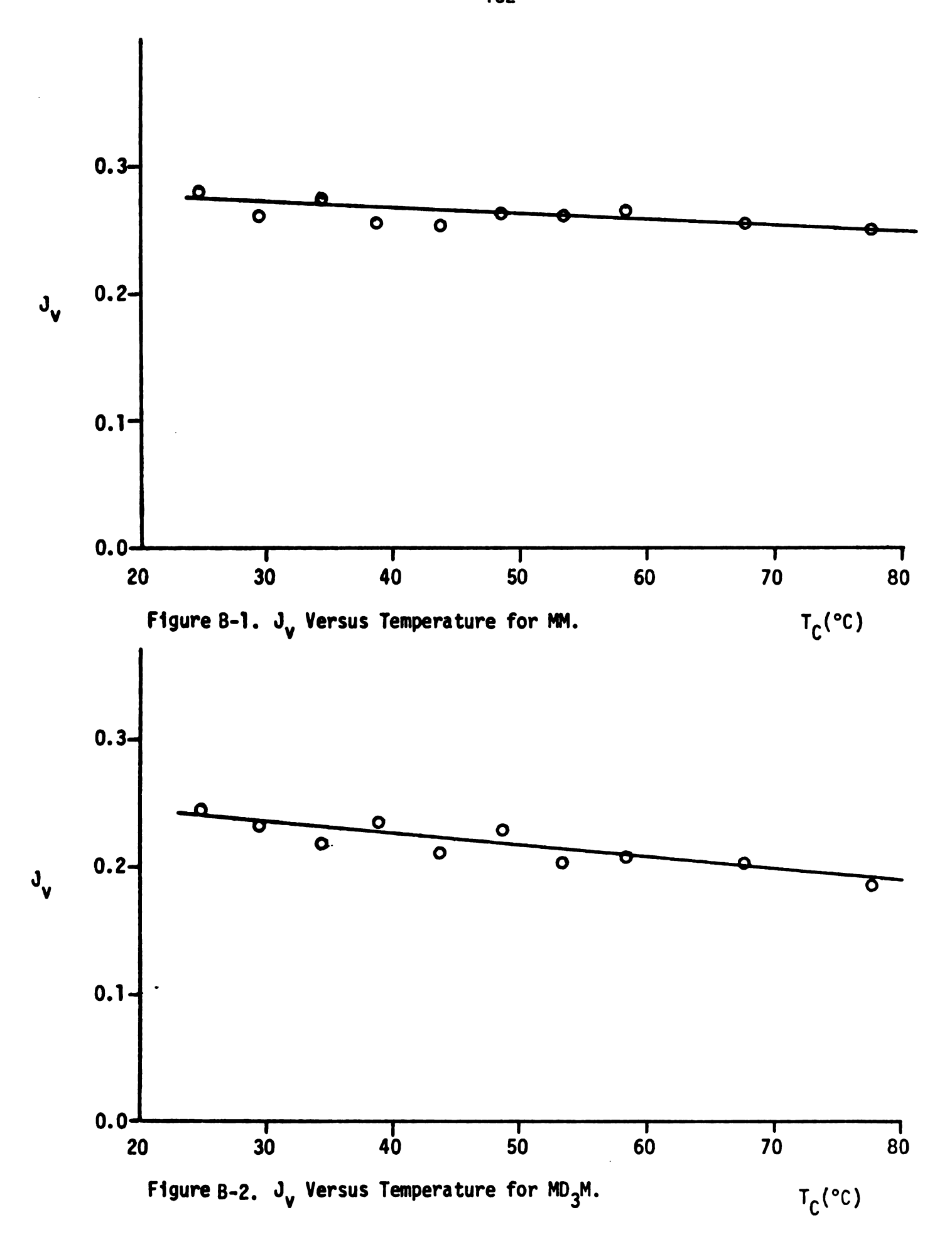
3 - 1 $=\{\star_1,\ldots,\star_n\}$

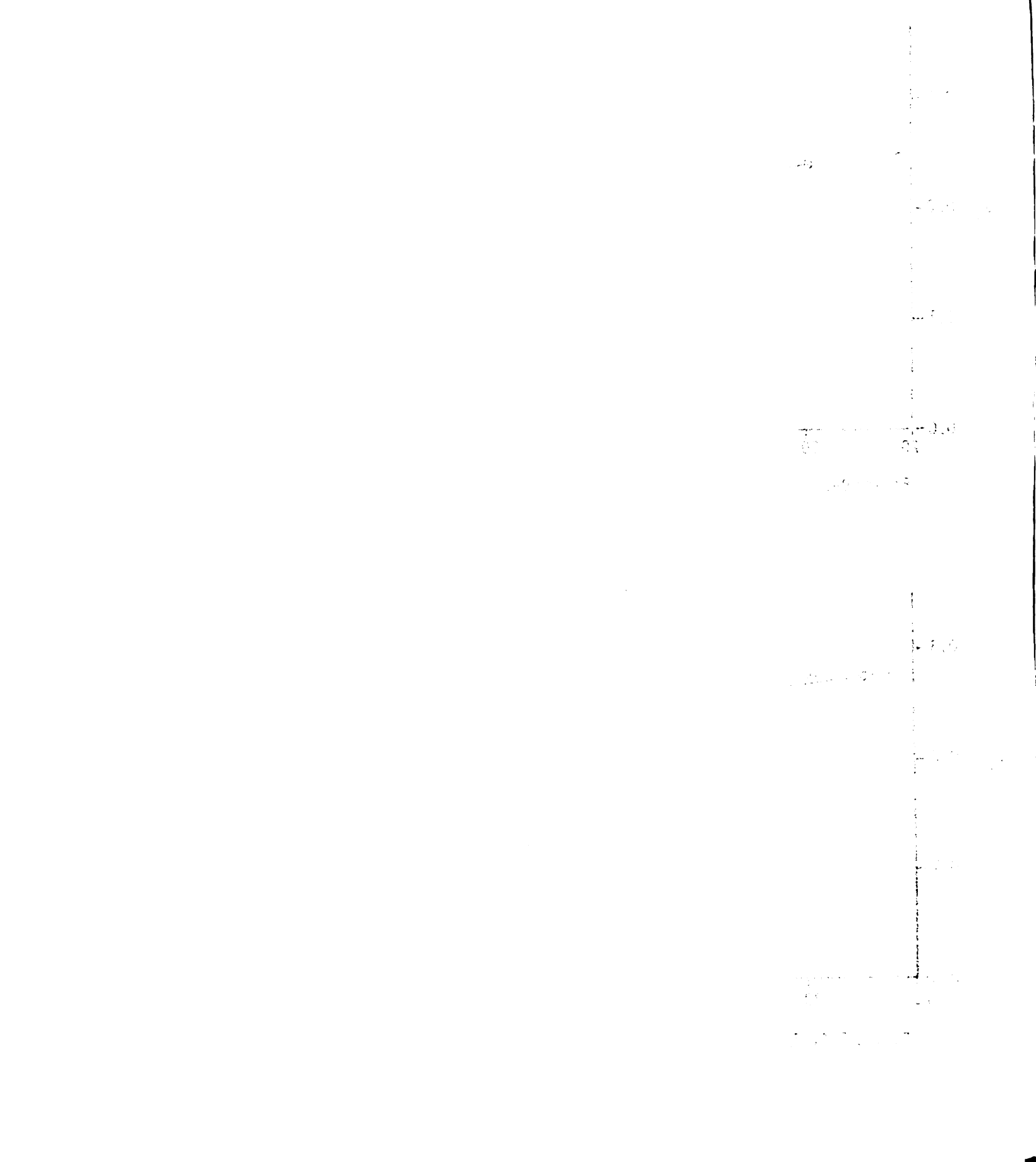
APPENDIX B

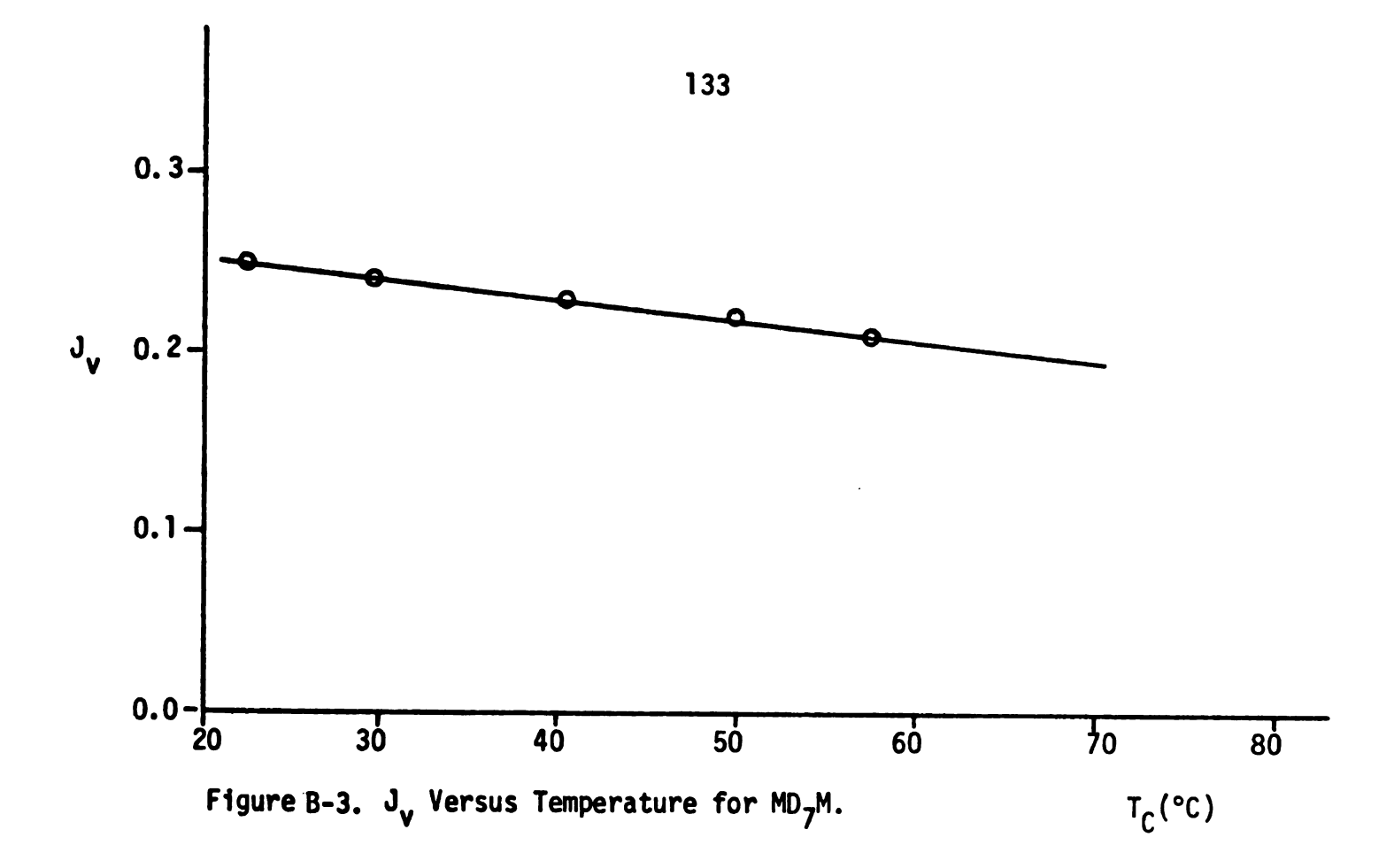
VARIATION OF J_V WITH TEMPERATURE T_C

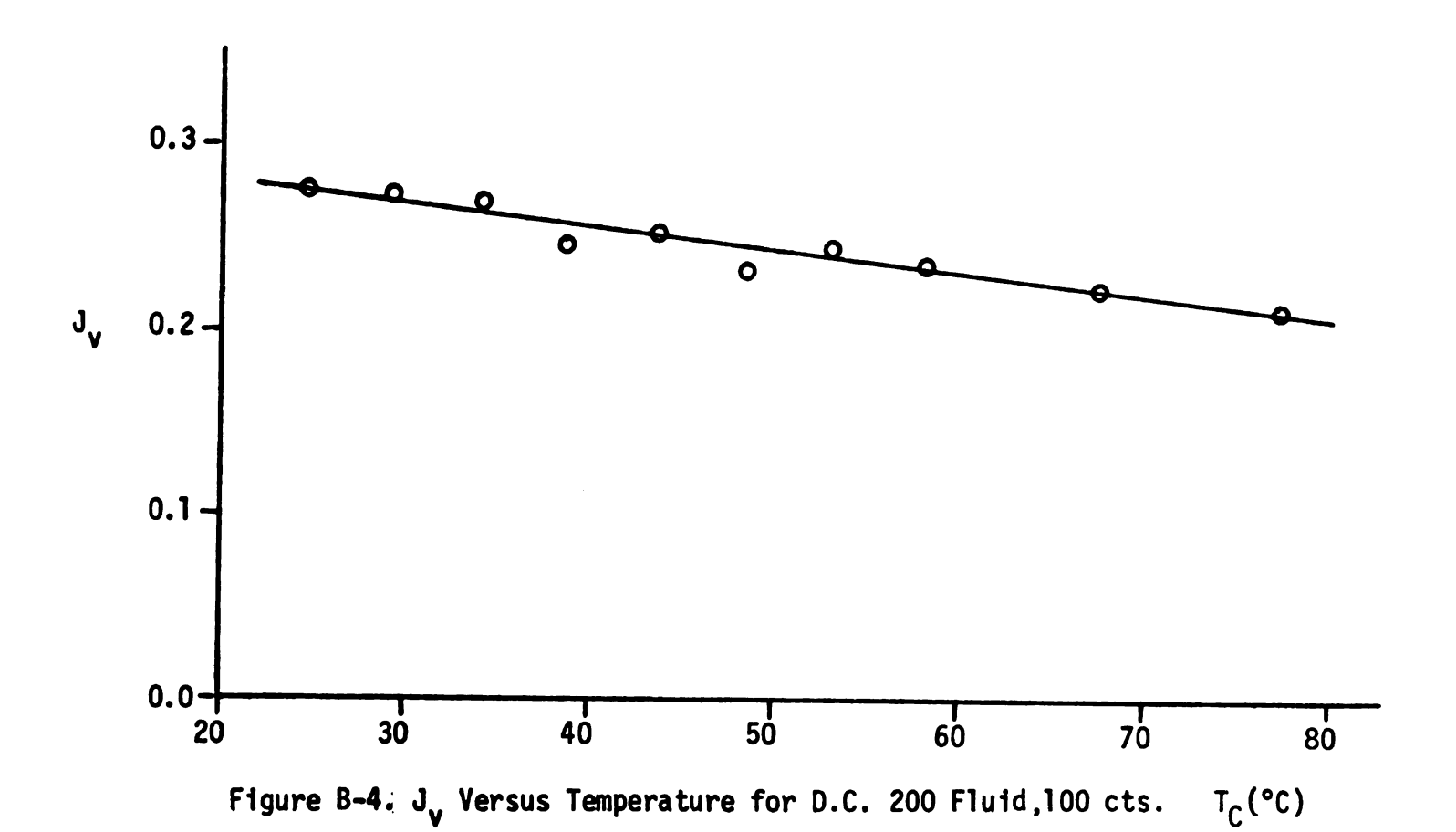
The ratio J_V , of the intensity of the central Rayleigh component to the intensity of the Brillouin doublet, was calculated for all silicones at various temperatures ranging from 20°C to 80°C. J_V was found to decrease monotonically with temperature for all silicones, as established in Figures B-1 to B-9. Figures B-5 and B-9 show some scattered points, which may be the consequence of sample contamination. D_3 was solid at room temperature, its melting point being close to 63°C; hence it was very hard to remove all dust particles.











	, i)
	<u></u> ,	
		- ्यू प त्रु -
		· : : : a .{ :
		1 1.C
	Ç	î

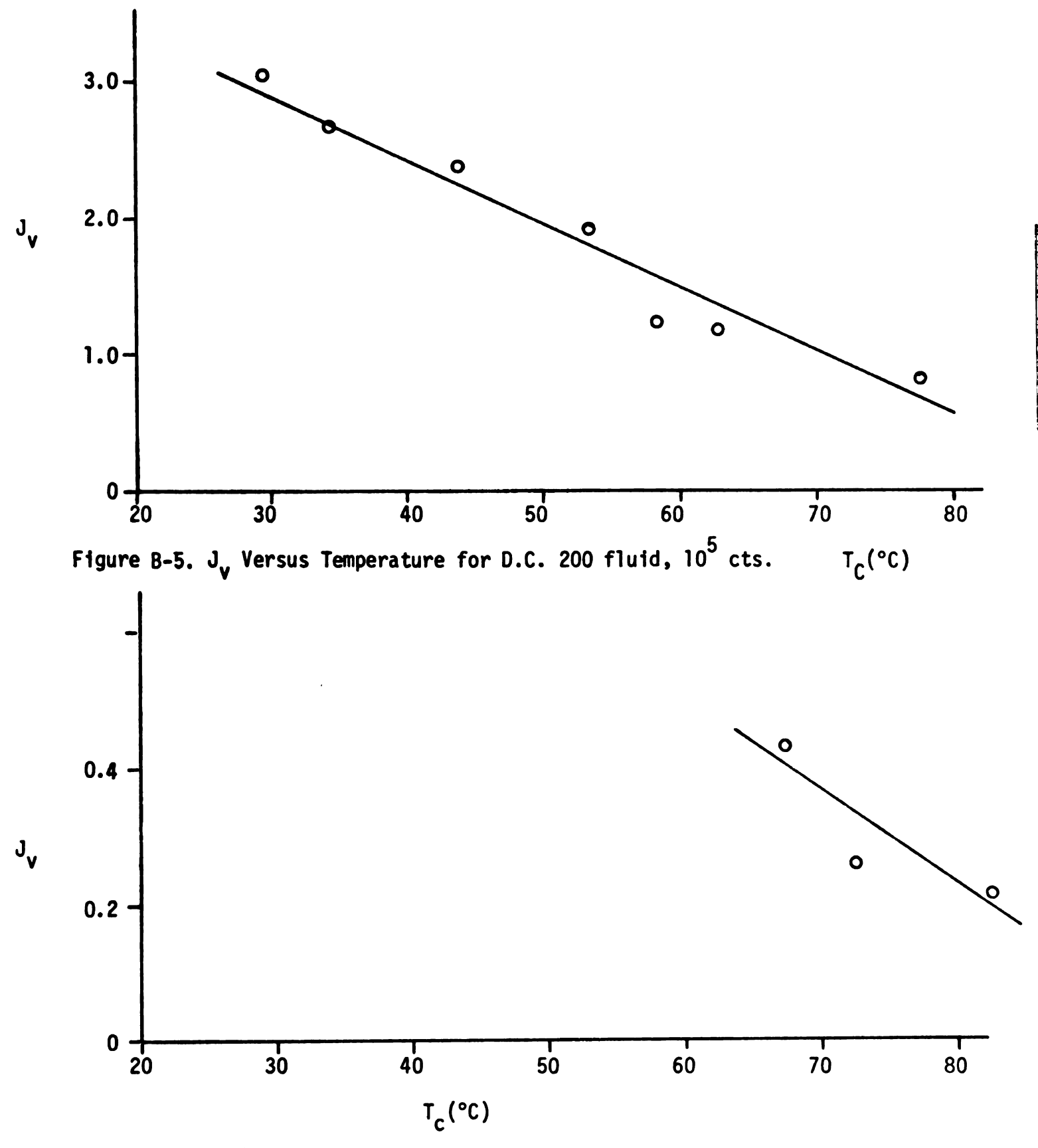


Figure B-6. J_{v} Versus Temperature for D_{3} .

... S....

£...?

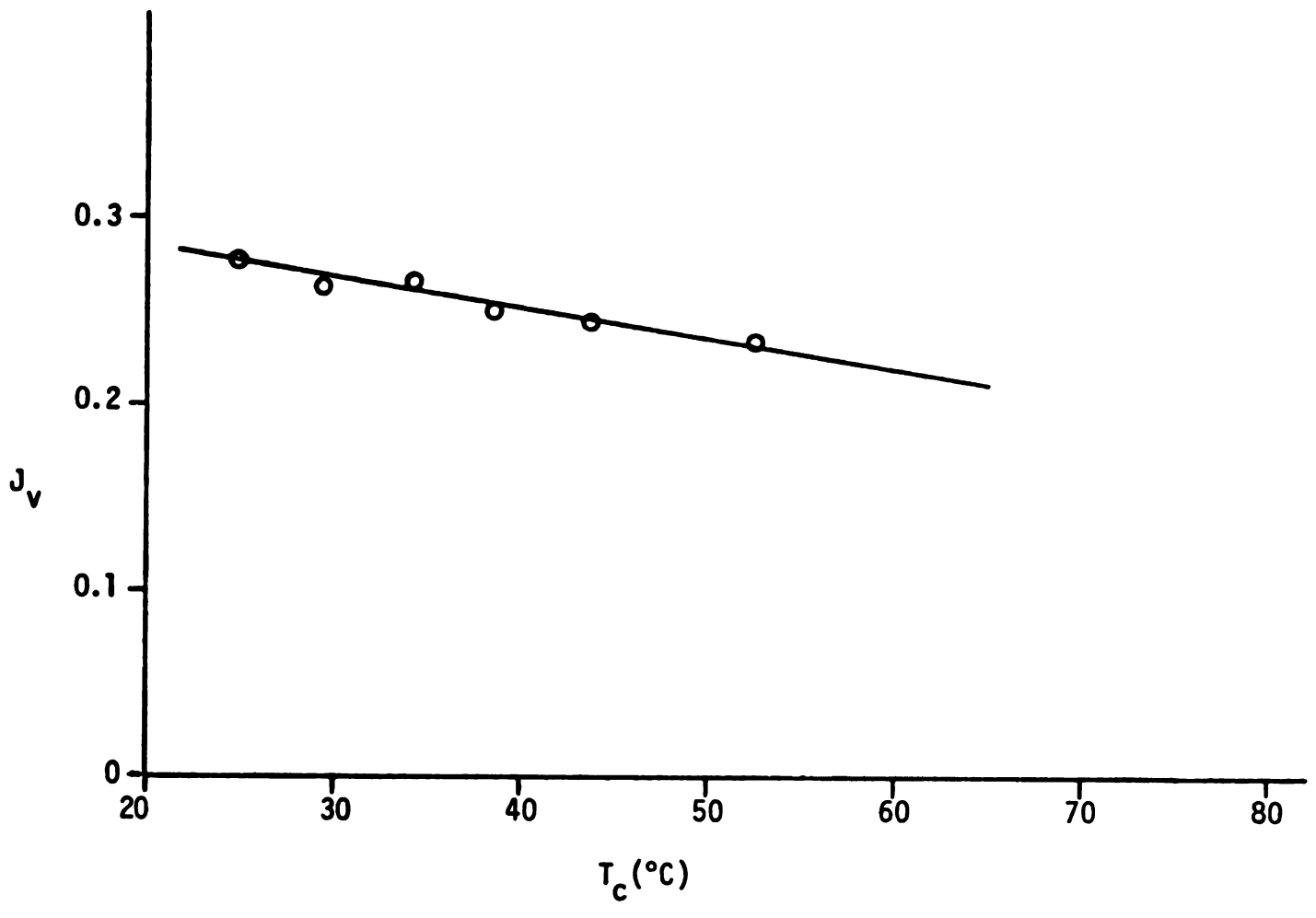


Figure B-7. J_{v} Versus Temperature for D_{5} .

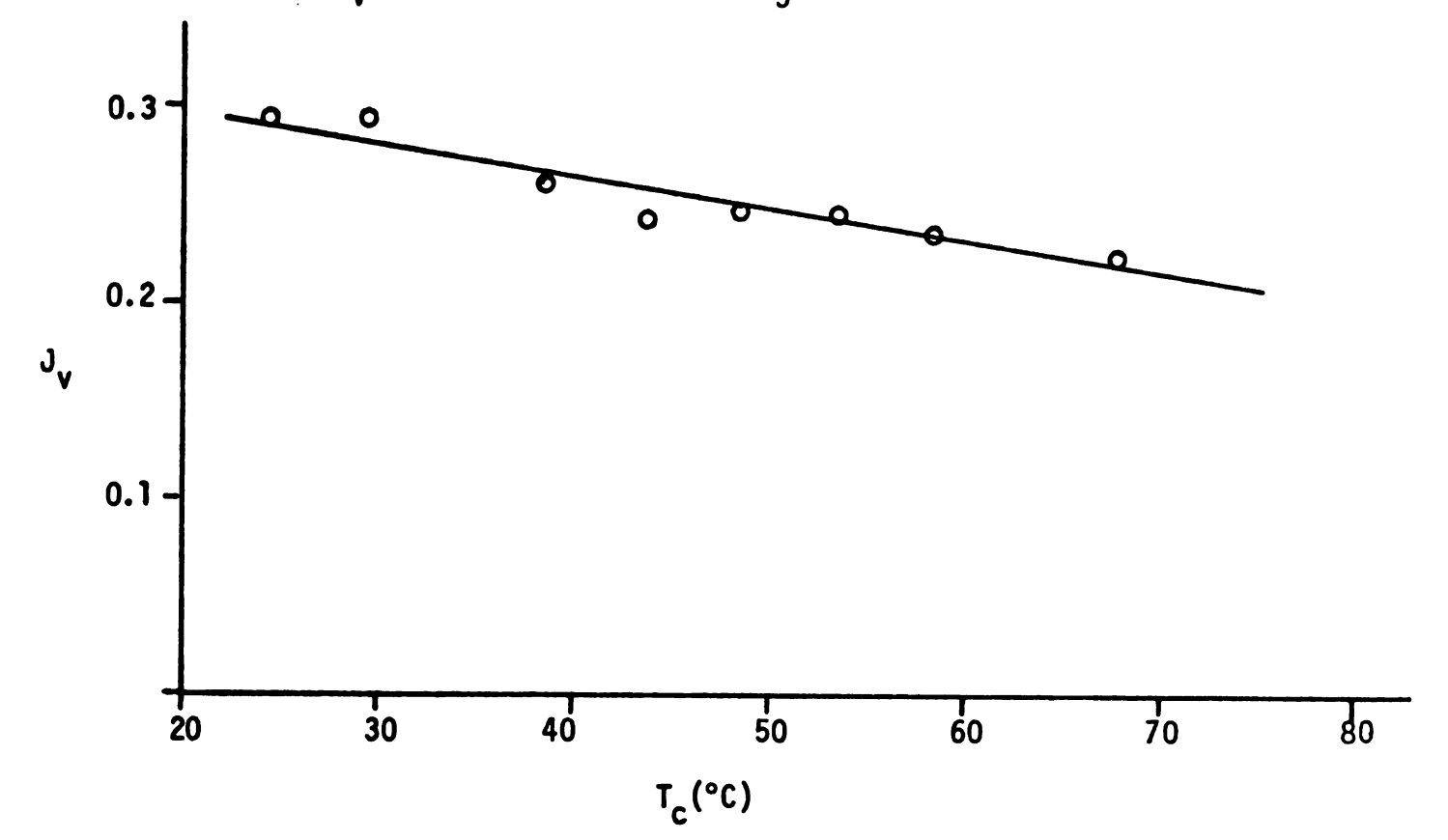
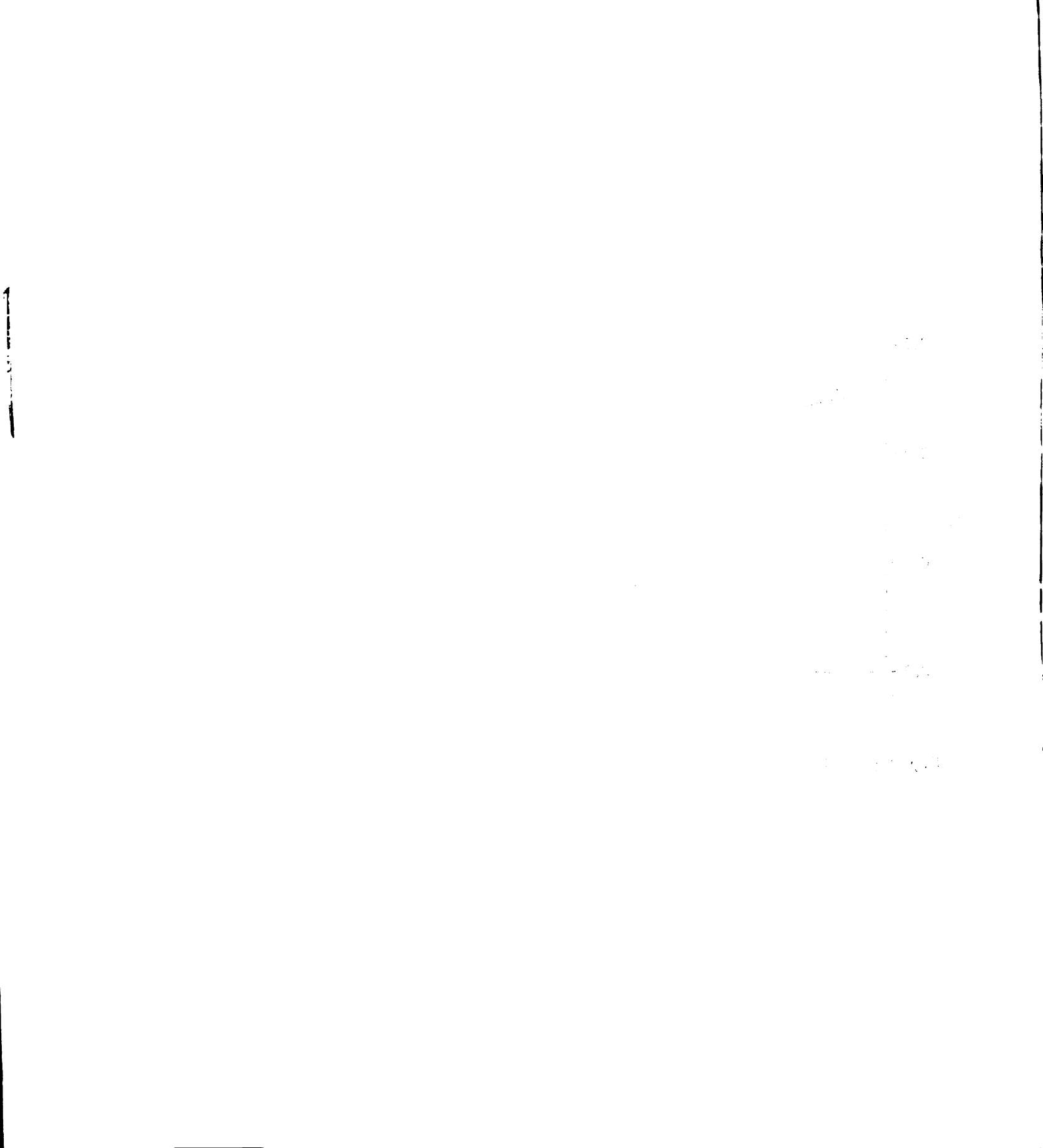


Figure B-8. J_V Versus Temperature for D_9 .



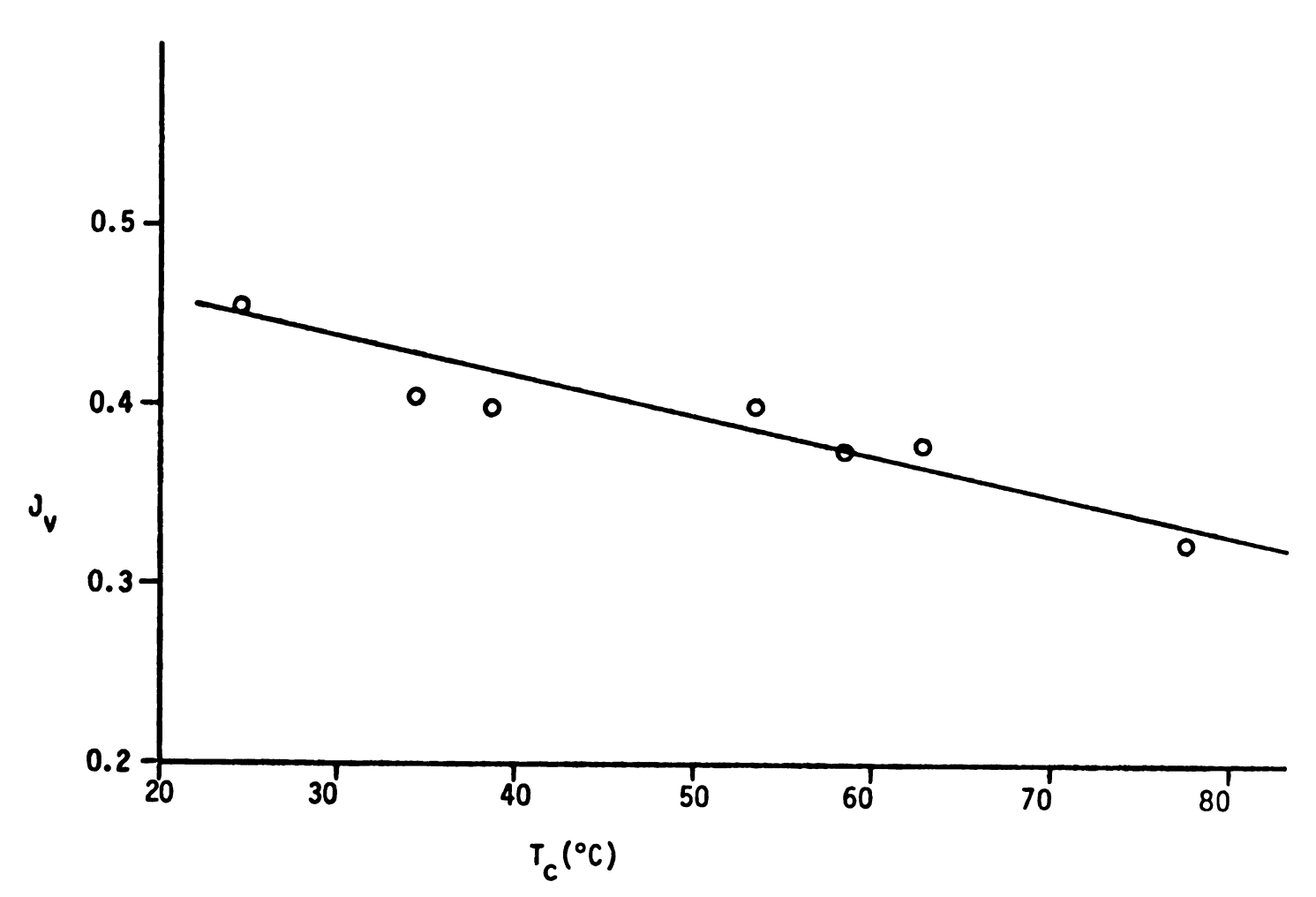


Figure 8-9. J_{v} Versus Temperature for D_{15} .

APPENDIX C

LASER-BRILLOUIN-VELOCIMETER

Static fluid properties can be measured by Brillouin scattering.

Possibly certain dynamic fluid properties such as boundary layer thickness and flow velocity^[55] can also be measured by this technique.

The Doppler-shifted frequency v_D , caused by the fluid velocity v can be expressed by the equation [56,57, 8]

$$v_{D} = \frac{n}{\lambda_{O}} \left[\vec{v} \cdot (\vec{n}_{SC} - \vec{n}_{i}) \right] , \qquad (C-1)$$

where n is the index of refraction of the fluid, λ_0 is the wavelength of the incident radiation in a direction specified by the unit vector \vec{n}_i and \vec{n}_{sc} is the unit vector of the scattered radiation. Eq. C-1 can be rewritten in terms of angles as (see Figure C-1)

$$v_{D} = \frac{2nv}{\lambda_{O}} \sin(\theta/2)\cos \left[90^{\circ} - (\phi + \theta/2)\right] , \qquad (C-2)$$

where θ is the angle between the scattered and incident radiation and ϕ is the angle between the incident radiation and the velocity vector \vec{v} . In our experimental arrangement ϕ is equal to 180° ;

11

4.

hence,

$$v_{D} = \frac{2nv}{\lambda_{O}} \sin(\theta/2)\sin(180 + \theta/2)$$
 (C-3)

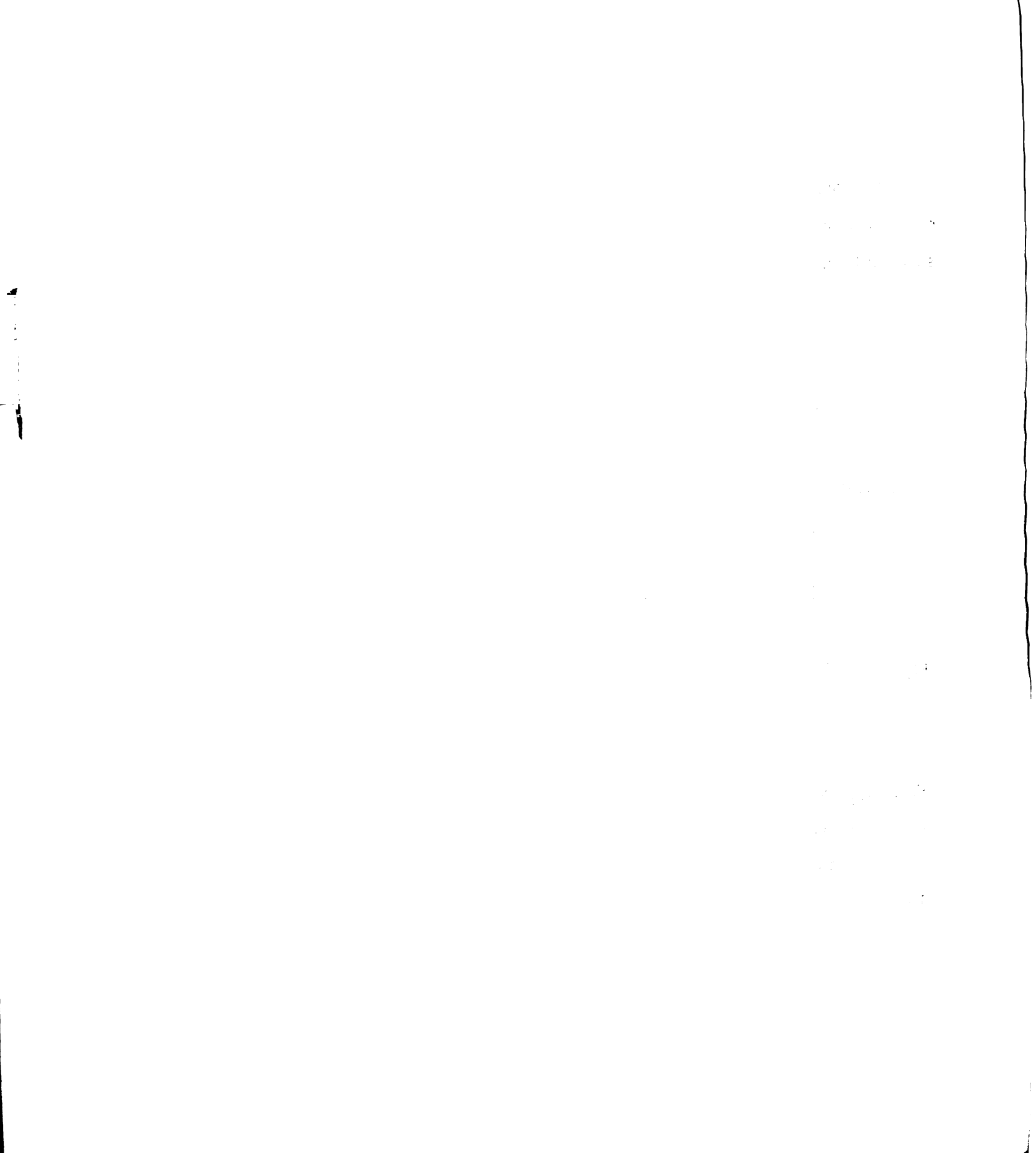
or

$$v_{\rm D} = \frac{2nv}{\lambda_{\rm O}} \sin^2 \theta/2 \qquad . \tag{C-4}$$

THE EXPERIMENTAL SET-UP

The experimental set-up for velocity measurements is shown in Figure C-1. A laser beam is passed through the tube in a direction opposite to the velocity of the flowing fluid. After the fluid (200-proof ethyl alcohol) comes to Reservoir 1, a variable-speed pump circulates it to Reservoir 2 then returns it through the system. The reservoirs are specially designed to smooth the pulsating flow from the pump and eliminate all bubbles generated by the pump's rotary motion.

The tube is scanned at a distance of 35 inches $(\frac{d}{L} \ge 1/40)$ from the end where the fluid enters. Such a clearance is required to assure a developed flow in the test section. Light scattered from the test section is then collimated and passed through the optical and detection system described in Chapter III.



DISCUSSION

The frequency spectrum obtained exhibits one Rayleigh peak at the center and two Brillouin doublets, as in the static case. Figure C-3 shows the Rayleigh peaks for the static and dynamic cases superimposed.

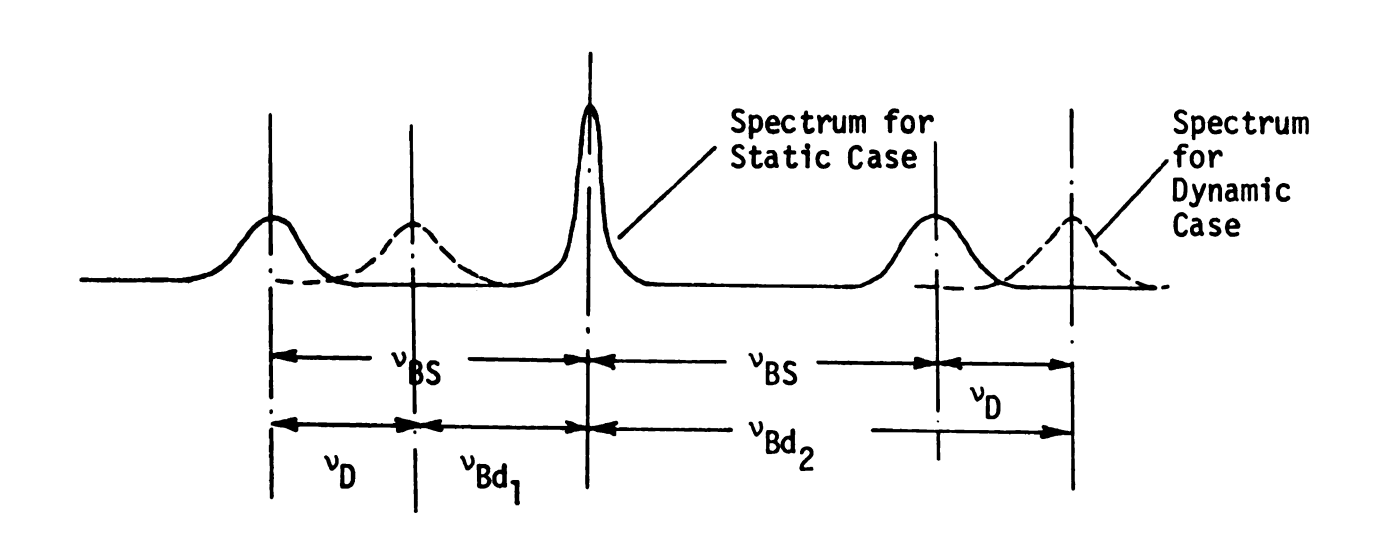


Fig. C-3. Static and Dynamic Brillouin Spectra.

Here, ν_{BS} is the Brillouin frequency shift in the static case, ν_{Bd} is the Brillouin frequency shift in the dynamic case, and ν_D is the frequency shift due to Doppler effect.

Then,

$$v_{Bd_1} = v_{BS} - v_{D}$$
 (C-5)

$$v_{Bd_2} = v_{BS} + v_{D}$$
 (C-6)

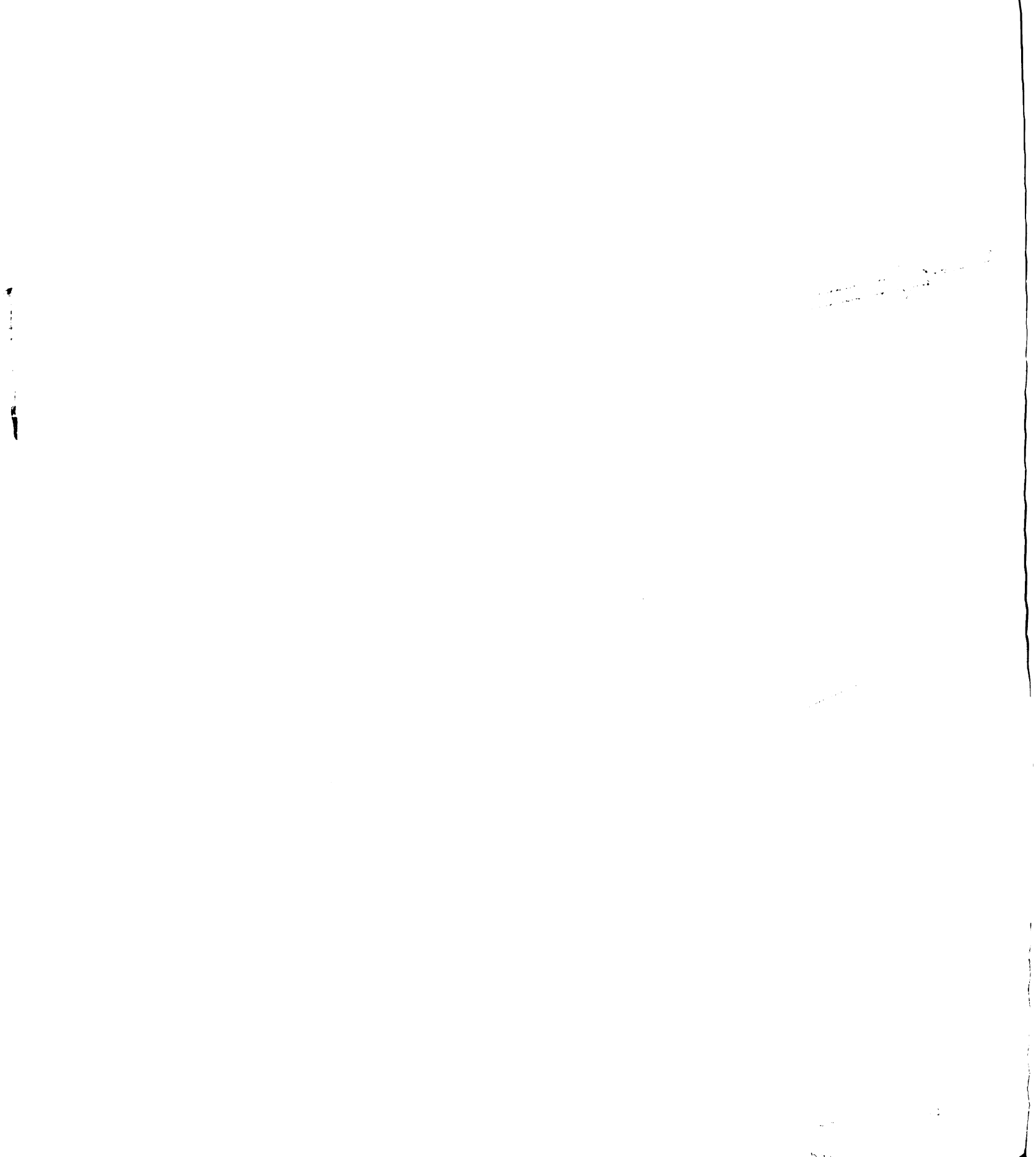
I was a second of the second 43

SO,

$$v_D = (1/2)(v_{Bd_2} - v_{Bd_1})$$
 (C-7)

Measurements were made with green light of wavelengths $\lambda_0 = 5145~\text{Å}$, or frequency $\nu_0 = 5.83 \times 10^{14}~\text{Hz}$. Then, for $\theta = 45^\circ$, $\nu_D^=3.3 \times 10^5~\text{Vsec}^{-1}$ and for $\theta = 135^\circ$, $\nu_D^=3.3 \times 10^5~\text{Vsec}^{-1}$. $\theta = 45^\circ$ and 135° are the minimum and maximum scattering angles available on the instrument. Therefore, in the present case it was only possible to vary ν_D in the range from $10^3~\text{to}$ $10^5~\text{V}~\text{Sec}^{-1}$, where V is expressed in cm/sec. Hence to measure velocities in the range of 1 cm/sec to 100~cm/sec, the Doppler frequency shift would have had to be in the range from $10^3~\text{Hz}$ to $10^7~\text{Hz}$, and a detection technique with very high resolving power would have been required. Therefore spectral range of the instrument utilized in the measurements described above is in GHz range and it would have been nearly impossible to measure shifts falling in the MHz range.

There are other heterodyning techniques which have very high resolving power and are being used for Doppler-shifted frequency measurements [6, 7,58, 59,60,61). However, the Laser-Doppler-Velocimeter requires that some foreign particles be present to effect light scattering. No such particles are needed for the Laser-Brillouin Velocimeter.



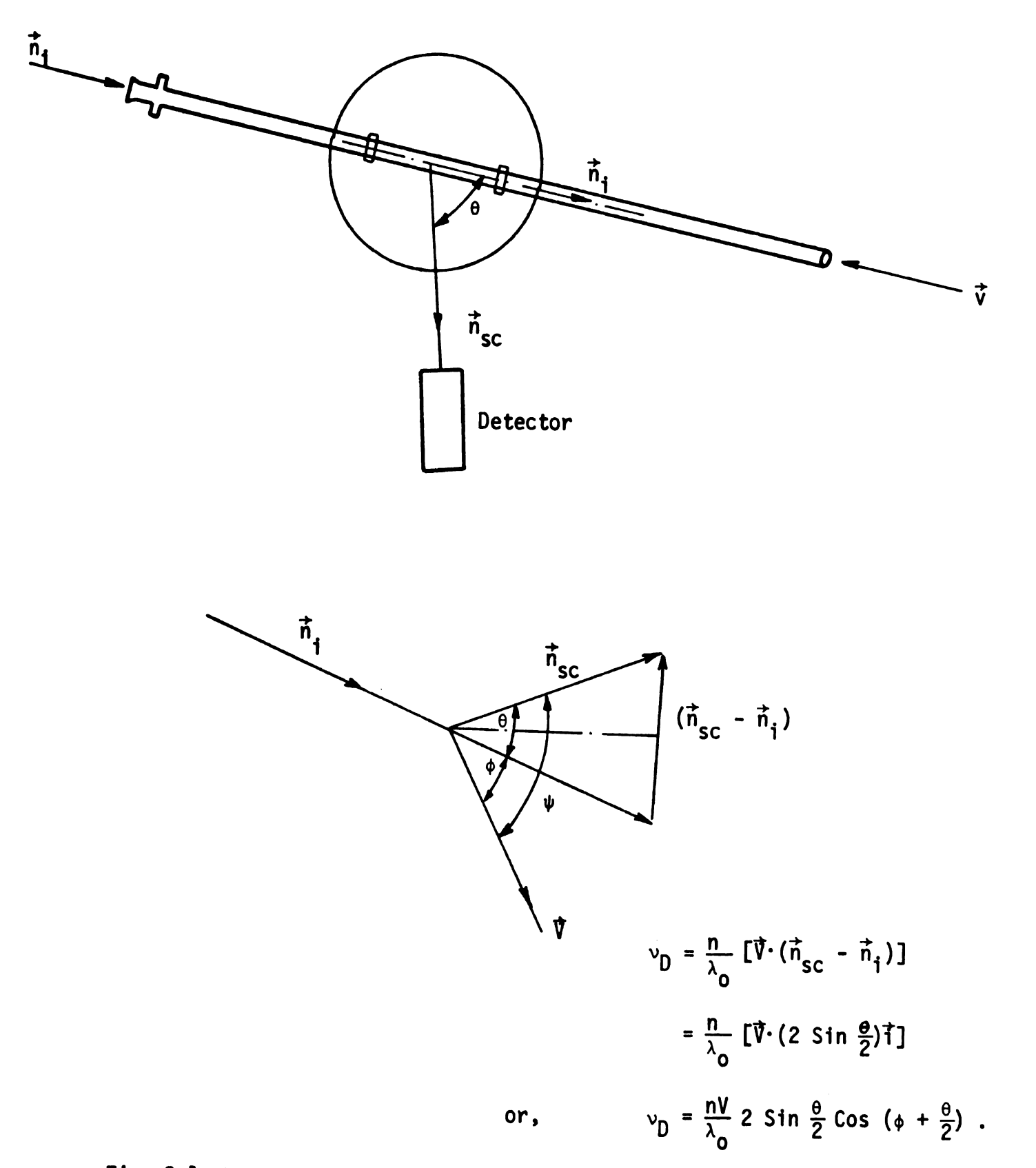
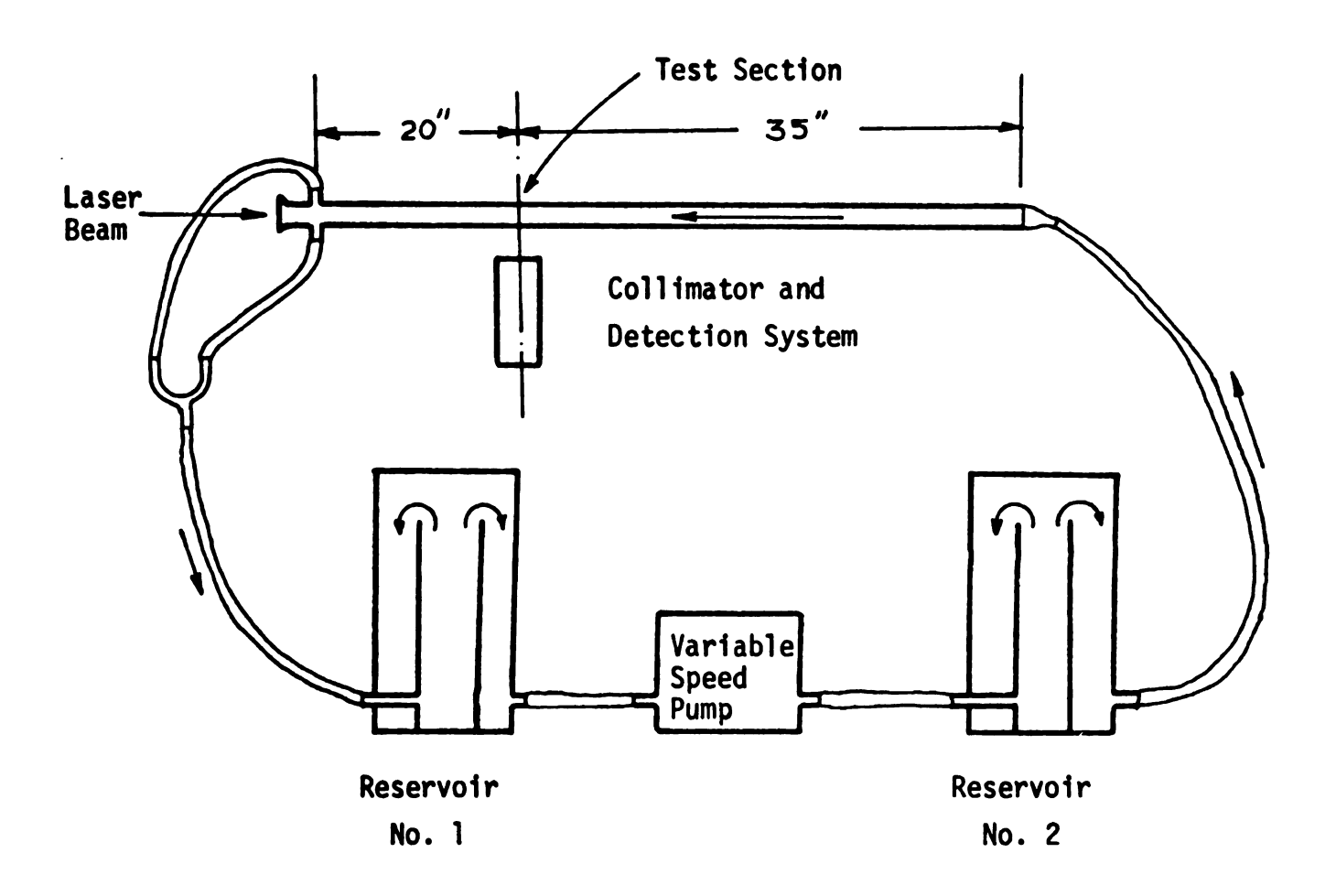


Fig. C-1. Vectorial Representation of Incident Light, Scattered Light



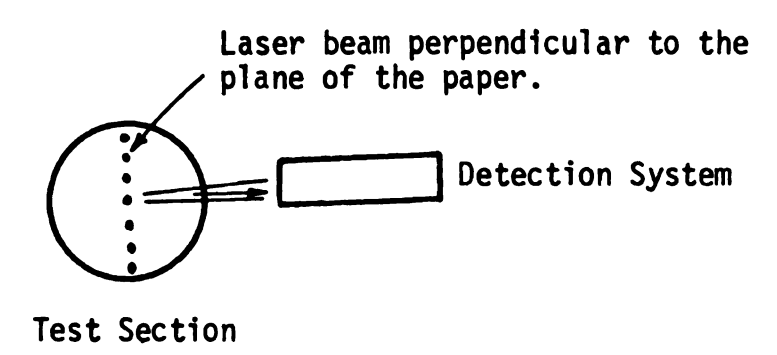


Fig. C-2. Experimental Set-up for Velocity Measurements.

